Real Time PMU-Based Stability Monitoring

Final Project Report

Power Systems Engineering Research Center

Empowering Minds to Engineer
the Future Electric Energy System

Real Time PMU-Based Stability Monitoring

Final Project Report

Project Team

Chen-Ching Liu, Project Leader
Washington State University

Umesh Vaidya
Iowa State University

A. P. Sakis Meliopoulos
Georgia Institute of Technology

PSERC Publication 14-11

October 2014

For information about this project, contact

Chen-Ching Liu
School of Electrical Engineering and Computer Science
Washington State University
Pullman, WA, 99164-2752
Email: liu@eecs.wsu.edu
Phone: 509-335-1150

Power Systems Engineering Research Center

The Power Systems Engineering Research Center (PSERC) is a multi-university Center conducting research on challenges facing the electric power industry and educating the next generation of power engineers. More information about PSERC can be found at the Center's website: http://www.pserc.org.

For additional information, contact:

Power Systems Engineering Research Center
Arizona State University
527 Engineering Research Center
Tempe, Arizona 85287-5706
Phone: 480-965-1643
Fax: 480-965-0745

Notice Concerning Copyright Material

PSERC members are given permission to copy without fee all or part of this publication for internal use if appropriate attribution is given to this document as the source material. This report is available for downloading from the PSERC website.

© 2014 Washington State University. All rights reserved.

Acknowledgements

This is the final report for the Power Systems Engineering Research Center (PSERC) research project titled "Real Time PMU-based Stability Monitoring" (project S-50). We would like to express our appreciation for the support provided by PSERC's industry members and the National Science Foundation under the Industry / University Cooperative Research Center program.

We thank Bonneville Power Administration (BPA) for the test data, and the support in part by National Science Foundation CAREER grant ECCS 1150405. The project team is very grateful to the industry advisors of the project for their contributions:

Alan Engelmann, Exelon/Commonwealth Edison
Bill Timmons, Western Area Power Administration
Clifton Black, Southern Company
David Schooley, Exelon/Commonwealth Edison
Dmitry Kosterev, Bonneville Power Administration
Eugene Litinov, ISO New England
Evangelos Farantatos, Electrical Power Research Institute
George Stefopoulos, New York Power Authority
Guiseppe Stanciulescu, BC Hydro
Jay Giri, ALSTOM Grid
Jinan Huang, Hydro-Québec Reseach Institute
Liang Min. Lawrence Livermore National Lab
Manu Parashar, ALSTOM Grid
Patrick Panciatici, Raidió Teilifís Éireann
Sanjoy Sarawgi, American Electric Power
Steven Hedden, Exelon/Commonwealth Edison
Xiaochuan Luo, ISO New England

Executive Summary

The purpose of this project is to develop PMU-based, real-time, wide area stability monitoring algorithms for the power grids using different methods and approaches. Phasor Measurement Units (PMUs) are increasingly available on power grids due to the significant investment in recent years, e.g., North America SynchroPhasor Initiative (NASPI) and the introduction of PMU functionality in relays and fault recorders. As a result, a priority in industry is to extract critical information from the increasing amount of PMU data for operation, planning, protection, and control.

This research proposes new algorithms for real time stability monitoring in a control center environment. Two distinct but complementary methods are proposed for PMU-based stability monitoring: (a) waveform analysis to extract the "trending" information of system dynamics embedded in Lyapunov exponents – Is the system approaching instability?, and (b) a real time stability analysis based on energy functions for a faulted system – Will the system remain stable following the fault? The combination of these approaches provide a comprehensive and predictive stability monitoring system that help to avoid cascading failures and enhance system security.

Part I: Real Time PMU-Based Stability Monitoring

A PMU-based online waveform stability monitoring technique is proposed based on the Maximum Lyapunov Exponent (MLE). The main idea of the MLE technique is to calculate MLE as an index over a finite time window in order to predict unstable trending of the operating conditions. Significant progress has been made to improve the accuracy of MLE technique. First, the dynamic model of the power system is greatly improved by adopting a structure preserving model taking into account the dynamics of P and Q load with respect to the frequency/voltage variations. The purpose is to extend the MLE technique to voltage stability analysis as well as rotor angle stability. Based on this model, the system can be represented by a set of differential equations, which is suitable for MLE calculation. The power network topology is preserved. Parameters for the model are identified from the results of time domain simulation. Secondly, a new method has been proposed to determine the proper time window of MLE in an online environment. This method increases the accuracy of prediction given by MLE. At the same time, the computational burden does not increase significantly and, therefore, make the MLE technique more reliable for online monitoring. The proposed methods are validated by time-domain simulation of 122-bus mini-WECC system.

Part II: Date-Driven Model-Free Approach for Real-Time Stability Monitoring

A data-driven model-free approach is developed for short-term voltage and rotor angle stability monitoring of power systems. The approach is developed with regard to its application for real-time PMU-based stability monitoring of power systems. The theory behind the proposed approach is adopted from ergodic theory of dynamical systems. In particular, Lyapunov exponent is utilized as an indicator of stability to measure the exponential rate of convergence and divergence of nearby system trajectories following a

fault or disturbance. The positive (negative) value of Maximum Lyapunov Exponent implies exponential divergence (convergence) of nearby system trajectories and hence unstable (stable) system dynamics. An algorithm is provided for the computation of Maximum Lyapunov Exponent for the time-series data. The proposed algorithm can be implemented in real-time. The proposed Lyapunov exponent-based stability approach is also used to determine the stability/instability contributions of the individual buses to the overall system stability and for computation of the critical clearing time. Various practical issues are addressed with regard to the implementation of the proposed method, such as phasor measurement noise, communication delay, and the finite window size for prediction. Simulation results for rotor angle and voltage stability monitoring are provided for IEEE 162 bus system to demonstrate the application of the developed method. Finally, preliminary results on the implementation of the algorithm on a Real Time Digital Simulator (RTDS) test bed are provided.

Part III: Predictive Transient Stability Monitoring

The objective of this task is to develop a predictive transient stability monitoring scheme that utilizes the information given by the dynamic state estimation. The developed method monitors the transient swings of the system and characterizes in real time the stability of the system. It is capable of predicting whether the generator will reach an out-of-step condition. The developed method can be utilized as a predictive out of step protection scheme capable of detecting potential generator loss of synchronism before the condition has occurred. As such it is an improvement over present day out of step protection schemes.

This novel, predictive, transient stability monitoring scheme with an application to generator out-of-step protection is presented in this report. In particular, the real-time dynamic model of the system (as computed with the distributed state estimator) is utilized to evaluate the system's energy function based on Lyapunov's direct method and monitors the energy of the generator continuously in real time, in order to characterize the stability of the generator. The two major components of the scheme are a) the calculation of the center of oscillations of the system and b) the derivation of an equivalent, reduced sized model which is used for the calculation of the potential and kinetic energy of the generator. The total energy of the generator is tracked in real time as the sum of the potential energy plus the kinetic energy. The total energy is compared to the boundaries of the potential energy to determine the stability of the generator. Finally an application of this scheme is described, a novel predictive generator out-of-step protection scheme.

The report describes implementation details of the predictive stability monitoring system. To predict generator stability accurately, the up-to-date system topology is needed during the process of creating the equivalent system in the stability monitoring scheme. A novel dynamic state estimation based protection scheme, aka setting-less protection, is presented which detects faults and provides the system topology evolution whenever a protection function acts and alters the topology of the system by tripping breaker(s). The integration and coordination of the setting-less protection and the purposed stability

monitoring scheme is described in the report. Together, they provide a completed, real-time, predictive generator out-of-step protection. The developed scheme is compared with the state-of-the art technology for generator out-of-step protection, which is based on impedance relays that monitor the impedance trajectory at the terminals of the generator. The major advantage of the proposed scheme is that it predicts the out-of-step condition before its occurrence and therefore relays can act much faster than today's state of art technology.

Project Publications:

1. H. Guo, C. -C. Liu, and G. Wang, "Lyapunov Exponents over Variable Window Sizes for Prediction of Rotor Angle Stability," Accepted for North American Power Symposium, 2014.
2. S. Dasgupta, M. Paramasivam, U. Vaidya, and A. Venkataramana, "Real-Time Monitoring of Short Term Voltage Stability Using PMU Data," IEEE Trans. Power Systems, Vol 28, No 4, pp 3702-3711, 2013.
3. S. Dasgupta, M. Paramasivam, U. Vaidya, and A. Venkataramana, "PMU-Based Model-Free Approach for Real-Time Rotor Angle Monitoring," Accepted for publications in IEEE Power Engineering Letters, 2014.
4. S. Dasgupta, M. Paramasivam, U. Vaidya, and A. Venkataramana, "Entropy-Based Metric for Characterization of Delayed Voltage Recovery," Accepted for publication in IEEE Trans. Power Systems, 2014.
5. A. Reddy, K. Ekmen, V. Ajjarapu, and U. Vaidya, "PMU Based Real-Time Short Term Voltage Stability Monitoring Analysis and Implementation on a Real-Time Test Bed," Accepted for North American Power Symposium, 2014.
6. S. Dasgupta and U.Vaidya, "Theoretical Foundation for Finite Time Stability Monitoring in Power systems," Submitted to American Control Conference, 2015**.**
7. E. Farantatos, R. Huang, G. Cokkinides, and A. P. Meliopoulos, "A Transient Stability Monitoring Scheme Enabled by a Distributed Dynamic State Estimator," submitted to the IEEE Transactions – under review.
8. E. Farantatos, R. Huang, G. Cokkinides, and A. P. Meliopoulos, "A Predictive Generator Out-of-Step Protection Scheme Enabled by a Distributed Dynamic State Estimator," submitted to the IEEE Transactions – under review.

Student Theses:

1. H. Guo, "Lyapunov Exponents over Variable Window Sizes for Prediction of Rotor Angle Stability," Master Thesis, Washington State University, 2013.
2. Z. Lin, "Lyapunov Exponent Analysis for Power System Dynamic Monitoring Based on Structure Preserving Model," Master Thesis, Washington State University, Expected Dec. 2014.
3. E. Farantatos, "A Predictive Out-Of-Step Protection Scheme Based On PMU Enabled Distributed Dynamic State Estimation", PhD Thesis, Georgia Institute of Technology, December 2012.
4. L. Sun, "Rotating Electric Machine Setting-less Protection", PhD Thesis, Georgia Institute of Technology, in progress.

Part I

Real Time PMU-Based Stability Monitoring

Principal Investigator: Professor Chen-Ching Liu

Graduate Students
Guanqun Wang
Zijie Lin
Haosen Guo

Washington State University

For information about Part I, contact:

Chen-Ching Liu
School of Electrical Engineering and Computer Science
Washington State University
Pullman, WA, 99164-2752
Email: liu@eecs.wsu.edu
Phone: 509-335-1150

Power Systems Engineering Research Center

The Power Systems Engineering Research Center (PSERC) is a multi-university Center conducting research on challenges facing the electric power industry and educating the next generation of power engineers. More information about PSERC can be found at the Center's website: http://www.pserc.org.

For additional information, contact:

Power Systems Engineering Research Center
Arizona State University
527 Engineering Research Center
Tempe, Arizona 85287-5706
Phone: 480-965-1643
Fax: 480-965-0745

Notice Concerning Copyright Material

PSERC members are given permission to copy without fee all or part of this publication for internal use if appropriate attribution is given to this document as the source material. This report is available for downloading from the PSERC website.

© 2014 Washington State University. All rights reserved

Table of Contents

List of Figures

List of Tables

1. Introduction

1.1 Background

Since 1960s, the scale and complexity of interconnected power grids have increased to such an extent that large blackouts are growing in both number and severity [1]. For example, in the 90's, there were 66 blackouts in the U.S. that affected over 100MW in the first five years. However, during 2006-2010, the number of such outages reached 219, more than tripled [2]. As a result, it is critical to enhance technology for prevention of large scale power outages.

Phasor measurement units (PMUs) provide synchronized measurements of the state of the power system at a rate up to 120 samples per second [3]. Based on the IEEE standard for synchronous phasors, the basic time synchronization accuracy of PMU is ±0.2μs [4]. Since communication technology is well developed, it enables online monitoring of power systems based on PMU data. In recent years, the number of PMUs installed on the power grids increased significantly and research on the applications of PMUs in monitoring, protection, and control of power grid has made significant progress [5].

The main purpose of this work is to develop a PMU-based, real-time, wide area stability monitoring algorithm for the power grids. The proposed algorithm takes advantage of the PMU-measured waveforms and extracts the "trending" information of power system dynamics to determine if the system is approaching instability. This algorithm can be applied to real time stability monitoring as a tool to issue warning messages for system operators when a trend toward instability is detected.

1.2 Overview of the Problem

Traditionally, there are two major approaches to transient stability analysis of power systems. One is time-domain simulation methods [6-7], which is based on numerical integration of the power system dynamic equations. This method provides details of the dynamic waveforms for a large scale system if the component and network data are available. Parallel-in-time algorithms can be performed to improve the calculation speed of the time-domain simulation [8]. However, the high computational burden limits the online applicability of this method. The other approach is the energy functions based direct methods, such as relevant unstable equilibrium point (RUEP) method [9], controlling UEP (CUEP) method [10], potential energy boundary surface (PEBS) [11], BCU method [12], and extended equal area criteria (EEAC) method [13]. These methods have a relatively fast computational speed and provide quantitative indices for stability assessment. A shortcoming of direct methods is that the assessment result may not incorporate sufficient details due to simplification of the system models. There are also knowledge-based transient stability methods. In [14], decision trees are created off-line based on a large number of simulations. The results are used to predict transient stability in an on-line environment. The hybrid intelligent system proposed in [15] can be used to assess not only transient stability, but also generator tripping. In [16], on-line PMU data

are compared with trajectory patterns stored in the database. The Euclidean distance is used as an index for prediction of system stability.

In this research, a new method called Maximum Lyapunov Exponent (MLE) is proposed for monitoring of wide-area transient stability based on PMU data in an online environment. The Maximal Lyapunov Exponent (MLE), which was a tool for prediction of out-of-step conditions [17], is applied to the analysis of rotor angle stability [18-19]. Based on a nonlinear dynamic model of the power system, the MLE can be calculated based on the waveforms resulting from dynamics of the system states. It is based on a rigorous theoretical foundation and, therefore, it is able to reliably determine the stability status using PMU streaming data within a specified time window.

However, it should be noted that certain factors can have a significant effect on the accuracy of the prediction based on the MLE technique. Two problems need to be solved to improve the proposed technique:

1, System model: For a large scale power system with generator and load buses interconnected by transmission lines, the dynamic characteristics of a power system for stability analysis is represented by a differential-algebraic equation (DAE). In order to implement MLE technique, the power network needs to be reduced to generator buses only and all the loads are modeled by constant impedances. This will lead to a loss of the system topology, reducing the level of accuracy for system stability assessment. Also, it is known that there are interactions between angle and voltage dynamics. Therefore, the dynamic model of the system needs to be improved by retaining the load buses and incorporating voltage dynamics of the system.

2, Time window for the MLE calculation: In the previous work, the time window for MLE calculation is determined by offline spectrum analysis and remains constant for different outage scenarios. Such a constant window can miss critical system oscillation patterns for some fault scenarios, resulting in an inaccurate prediction [18]. Therefore, it is necessary to determine the proper time window of MLE in an online environment.

This research project addresses these critical issues by proposing new techniques. First, a structure preserving model is applied to transient stability analysis. This model retains the load buses as well as the network topology. Based on this model, the MLE can not only consider generator dynamics, but also takes into account the load dynamics. Moreover, the structure preserving model enables the MLE to predict the short-term voltage stability. Parameter identification for this model has been conducted.

Secondly, a systematic method is proposed to determine the length of the time window for MLE calculation in an online environment. Spectrum analysis is performed on the oscillation waveforms following an outage to calculate the size of time window for the MLE. The starting window size is the inverse of the most dominant frequency component, but all windows are saved for later use. The MLEs are calculated for two consecutive time windows using the same window size. The consistency of the two MLEs indicates that sufficient information has been obtained in the first time window to

characterize the system dynamics. Otherwise, an adjustment of the window size is needed. The window size can be increased by choosing the next smallest window saved earlier. This method increases the accuracy of prediction given by MLE. At the same time, the computational burden does not increase significantly and, therefore, it does not compromise the effectiveness of this method.

The methods proposed in this research have been validated by extensive simulations.

1.3 Report Organization

The organization of the remaining chapters is as follows: Chapter 2 is a summary of the theoretical basis of the MLE technique. Chapter 3 describes the structure-preserving model and load recovery model for the MLE calculation. The method to determine an adjustable MLE window size is proposed in Chapter 4. In Chapter 5, a 122-bus mini-WECC system is utilized to validate the proposed methods. Numerous time-domain simulations of this system are performed in order to validate the MLE method. The conclusion is provided in Chapter 6.

2. Lyapunov Exponent Theory

2.1 Maximum Lyapunov Exponent

In ergodic theory [20], Lyapunov Exponent is used to characterize whether a given system is "chaotic" and how chaotic it is. For a trajectory $x(t) \in \mathbb{R}^n$ with an initial value x_0 all trajectories that start out in a neighbourhood of x_0 will converge toward $x(t)$, or diverge as time goes on. Sensitivity of the system trajectory with respect to a perturbation of the initial state can be quantified by:

$$\|\Delta x(t)\| \approx e^{\lambda t} \|\Delta x_0\| \tag{2.1}$$

as shown in Figure. 2.1.

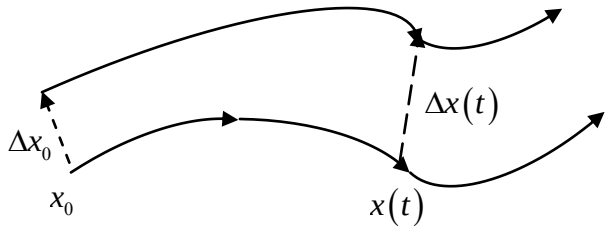

Figure 2.1 Perturbation of Trajectories of a Dynamical System

Equation (2.1) describes the exponential behaviour of nearby trajectories in a short time interval. The trajectory over a long time period may converge or diverge as time goes on. Therefore, the time average is used to measure the rate of divergence (convergence) of trajectories resulting from infinitesimal perturbations of the initial state.

Assume the system trajectory is defined by differential equations

$$\dot{x} = f(x) \tag{2.2}$$

From (2.1)

$$\lambda = \ln\left(\|\Delta x(t)\| / \|\Delta x_0\|\right) \tag{2.3}$$

By taking the limit as t→∞, the Lyapunov exponent is given by

$$\lambda = \lim_{t\to\infty} \frac{1}{t} \ln\left(\|\Delta x(t)\| / \|\Delta x_0\|\right) \tag{2.4}$$

representing the mean growth rate of the distance $\|\Delta x(t)\| / \|\Delta x_0\|$ between neighboring trajectories.

Assume $x(t) = \phi(t, x_0)$ to be the solution at time t starting from an initial condition x_0. First, consider the 1-dimensional case, i.e., $x \in \mathbb{R}^n$. For an infinitesimal perturbation of the initial state, Δx_0,

$$\lim_{\Delta x_0 \to 0} \|\Delta x(t)\| / \|\Delta x_0\| = \frac{dx(t)}{dx(0)} = \phi'(t, x_0) \tag{2.5}$$

The Lyapunov exponent can be computed by a linear approximation

$$\lambda = \lim_{t \to \infty} \frac{1}{t} \ln\left(\phi'(t, x_0)\right) \tag{2.6}$$

For an N-dimensional continuous-time dynamical system, i.e., $x \in \mathbb{R}^n$ it has N Lyapunov exponents that can also be computed in a similar way. The Lyapunov exponents λ_i for $i = 1, 2, ..., N$ are defined as the eigenvalues of a matrix as time goes to infinity, i.e.,

$$\begin{aligned} \Lambda(x_0) &= \lim_{t \to \infty} \left[J^T(t, x_0) J(t, x_0) \right]^{1/2t} \\ \lambda_i(x_0) &= \ln\left[\overline{\lambda}_i(x_0) \right] \end{aligned} \tag{2.7}$$

in which $J(t, x_0)$ is the Jacobian matrix

$$J(t, x_0) = \partial \phi(t, x_0) / \partial x \tag{2.8}$$

and $\overline{\lambda}_i$ is the i-th eigenvalue of matrix Λ.

Assume $\lambda_1 \geq \lambda_2 \geq ... \geq \lambda_N$. The Maximum Lyapunov Exponent (MLE) λ_1 dominates the system's long-term performance. A negative (positive) value of λ_1 indicates exponential convergence (or divergence, respectively) of nearby system trajectories.

2.2 Gram-Schmidt Reorthonormalization Method

The limit in (2.7) is based on the Oseledec multiplicative ergodic theorem [20]. However, it is unrealistic to consider the trajectory at an infinite time. There are different methods to estimate the MLE in a finite time window. A standard method is the Gram-Schmidt Reorthonormalization (GSR) [21], by computing the average rate of trajectory separation

in a set of discrete time interval. As shown in Fig. 2.1, let the initial perturbation be $\delta x(0) = (1,0,0,...,0)^T$. The separation $\delta x(\Delta t)$ at Δt is

$$\begin{aligned} \delta x(\Delta t) &= x_s(\Delta t) - x(\Delta t) \\ &\approx x_s(0) + f(x_s(0))\Delta t - [x(0) + f(x(0))\Delta t] \\ &= \delta x(0) + [f(x_s(0)) - f(x(0))]\Delta t \end{aligned} \tag{2.9}$$

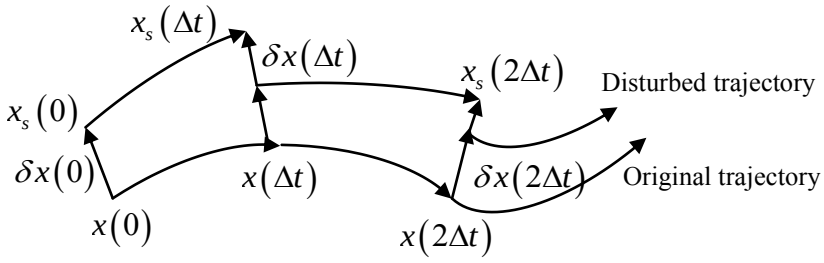

Figure 2.2 GSR Method

By Taylor's series,

$$f(x_s(0)) = f(x(0)) + J(x(0))(x_s(0) - x(0)) = f(x(0)) + J(x(0))\delta x(0) \tag{2.10}$$

Therefore,

$$\delta x(\Delta t) = [I + J(x(0))\Delta t]\delta x(0) \tag{2.11}$$

The rate of separation $\eta(0)$ at that moment is

$$\eta(0) = \ln\left(\frac{\| \delta x(\Delta t) \|}{\| \delta x(0) \|}\right) \tag{2.12}$$

Reorthonormalize the separation $\delta x(\Delta t)$ and the MLE over time window T can be computed recursively as

$$\lambda_T = \frac{[\eta(0) + \eta(1) + ... + \eta(n)]}{(n+1)\Delta t} \tag{2.13}$$

2.3 MLE Stability Criterion

A negative MLE implies that the nearby trajectories will converge to the reference trajectory exponentially. The theorem of continuous-time fixed point [22] established the relationship between the MLE and the asymptotic behavior of the dynamical system.

Consider a continuous-time dynamical system and assume that all the Lyapunov exponents are non-zero. Then the steady state behavior of the system consists of a fixed point. In particular, if all Lyapunov exponents are negative, i.e., MLE is negative, this fixed point is an attracting fixed point.

The proof of the theorem is outlined as followings. Consider the trajectory $\dot{y} = f(y)$ as a nearby trajectory of (2.2), with an initial value $y(0)$, as shown in Fig. 2.3. According to the definition of Lyapunov exponent, if the MLE of $x(t)$ is negative, there exists an $\varepsilon_1 > 0$ such that, for any $\|y(0) - x(0)\| < \varepsilon_1$,

$$\lim_{t\to\infty} \|y(t) - x(t)\| = 0$$

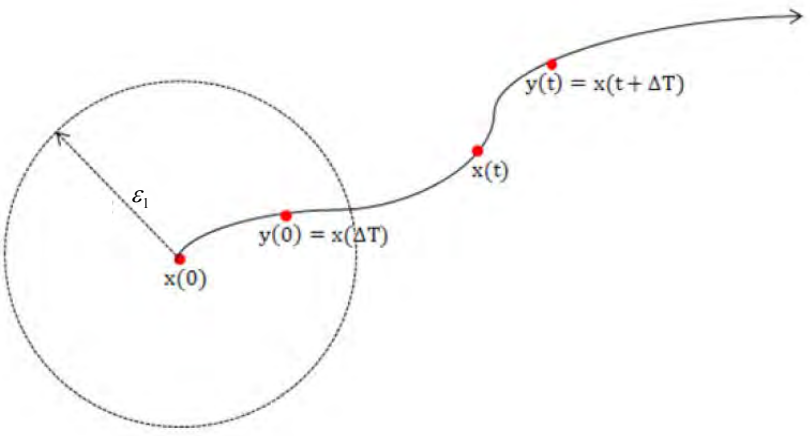

Figure 2.3 Stability of a nonlinear dynamical system

Since $x(t)$ is continuous, there must exist a $\Delta T > 0$, such that $\|x(\Delta t) - x(0)\| < \varepsilon_1$. Let $y(0) = x(\Delta t)$, then $y(t) = x(t + \Delta t)$ since the system (2.2) is autonomous. Since

$$\|y(0) - x(0)\| = \|x(\Delta t) - x(0)\| < \varepsilon_1$$

it is obtained that

$$\lim_{t\to\infty} \|y(t) - x(t)\| = \lim_{t\to\infty} \|x(t + \Delta t) - x(t)\| \approx \lim_{t\to\infty} \|f(x(t))\Delta T\| = 0$$

Since $\Delta T > 0$, it follows that

$$\lim_{t\to\infty} \|f(x(t))\| = 0$$

It means when t tends to infinity, $x(t)$ will approach an equilibrium point x_{eq}. The point x_{eq} can be viewed as a special trajectory: it starts at x_{eq} and stays at x_{eq}. Since the MLE calculation accounts for an infinite time, the x_{eq} 'trajectory' and $x(t)$ must have the same MLE. Thus there exists $\varepsilon_2 > 0$. For any $\|y(0) - x_{eq}\| < \varepsilon_2$, such that

$$\lim_{t\to\infty} \|y(t) - x_{eq}\| = 0$$

which indicates that x_{eq} is an asymptotic equilibrium point.

2.4 MLE Calculation Window

In applying the MLE method to detect system instability, it is impractical to set the time as infinity. Instead, MLE is calculated within a specified time window T. When T goes to infinity, the windowed MLE λ is equivalent to the MLE of the system λ [17]. Windowed MLE is an approximate version of the stability index for the system. Choosing a suitable time window size involves trade-offs between efficiency and accuracy. It would be better if problems can be detected as fast as possible. On the other hand, if the length of a time window is too short, inadequate measurements will lead to an inaccurate prediction. For example, if there is a large fluctuation right outside the chosen time window, it is likely to miss the instability phenomenon.

It is proposed in [23] that when the MLE is used to predict the stability of a system, it is better to choose a sliding time window rather than a static time window. This is due to the fact that a windowed MLE represents the mean rate of divergence or convergence of a trajectory within the time window. Using a sliding window can not only include more information, but also indicate the potential change of the MLE. Consistency of the MLEs in two consecutive windows indicates that no such large fluctuation exists right outside the chosen time window. Then sufficient information has been included in the first time window for characterization of the system dynamics.

2.5 Summary

The MLE can be applied to analyze transient stability of a nonlinear dynamic system. It extracts the "trending" information from the system trajectory and does not require the knowledge of the equilibrium points of the system. When the dynamical system model is known, the MLE can achieve an accurate prediction of the transient behaviour. However, several factors, such as the model of the system and the window size, will affect the accuracy of MLE calculation. These issues will be addressed in the following chapters.

3. Dynamic Load Model for MLE Calculation

The dynamic model of a power system can be formulated as a set of differential-algebraic equations (DAEs) [24]. Differential equations represent the dynamic characteristics of power system components, such as generators, governors and exciters. Algebraic equations model the steady state power flow on the network. In the previous work, the MLE technique is applied to the assessment of rotor angle stability. The system needs to be reduced to retain only the generator buses and, consequently, DAE is reduced to a set of ordinary differential equations (ODEs). The disadvantage of this method is that load bus information as well as the system topology is implicit and sometimes it causes errors in the stability assessment. Moreover, it is known that there are interactions between angle and voltage dynamics. In this project, a structure-preserving model is proposed for the MLE computation taking into account both generator and load dynamics.

3.1 Reduced Dynamic Model

Consider a power system with a total of n_0 buses with generators at m buses. Hence there are $n_0 - m$ load buses. The classical 2nd-order swing equations are used to represent the synchronous generators. Such generators are modeled as a constant voltage source in series with the transient reactance x_d'. Therefore, the power system can be augmented by m fictitious buses representing the generator internal buses. The total number of buses in the augmented network is n, which is $n_0 + m$.

The swing equations of the system are given by

$$\begin{aligned} \dot{\delta}_i &= \omega_i \\ \dot{\omega}_i &= \frac{1}{2H_i}\left(P_{M_i} - P_{e_i} - D_i\omega_i\right), \quad i = 1,...,m \end{aligned} \tag{3.1}$$

The algebraic equations of the system are the power flow relationship, i.e.,

$$\begin{aligned} P_i &= V_i \sum_{j=1}^{n} V_j Y_{ij} \cos\left(\theta_i - \theta_j - \delta_{ij}\right) \quad i = 1,...,n \\ Q_i &= V_i \sum_{j=1}^{n} V_j Y_{ij} \sin\left(\theta_i - \theta_j - \delta_{ij}\right) \quad i = 1,...,n \end{aligned} \tag{3.2}$$

Since the MLE can only be applied to ODEs, the algebraic equations at load buses need to be reduced. An example of a 3-bus system is used to illustrate the Ward equivalent.

A 3-bus system with two generator buses and one load bus is shown in Figure 3.1. Parameters of a three-bus system are listed in Figure 3.1.

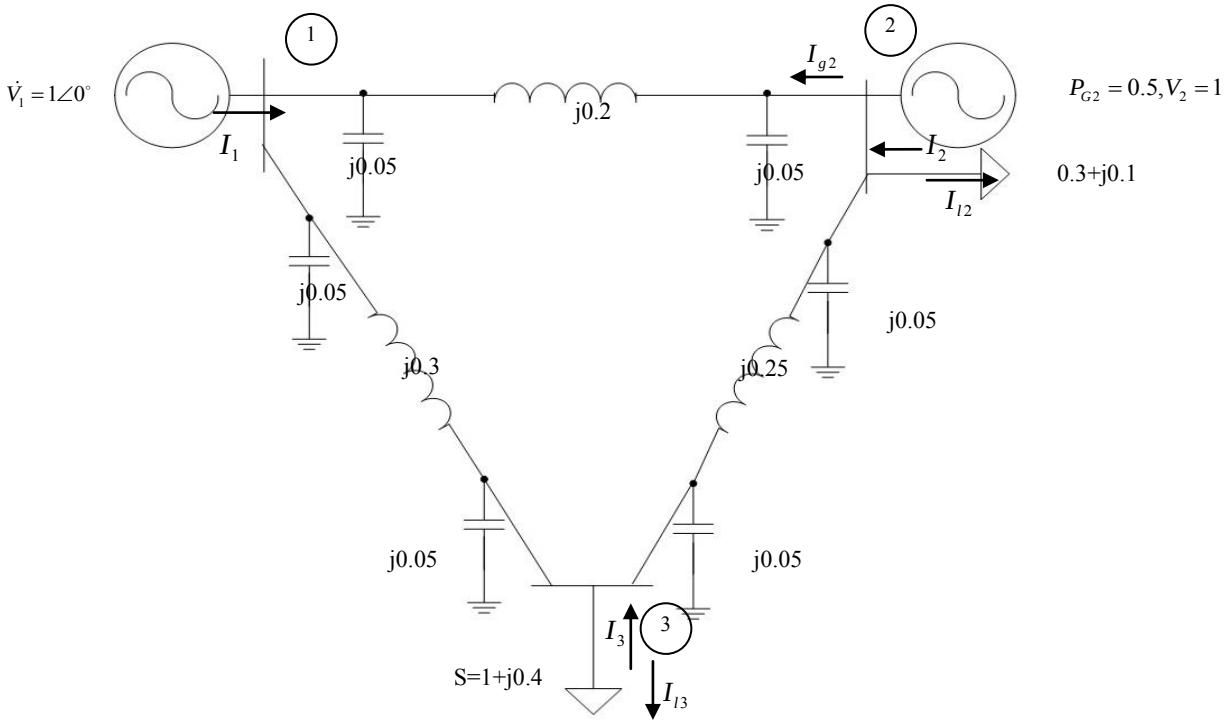

Figure 3.1 Parameters of a Three-bus System

The admittance matrix of the system is

$$\mathrm{Y} = \begin{bmatrix} y_{11} & y_{12} & y_{13} \\ y_{21} & y_{22} & y_{23} \\ y_{31} & y_{32} & y_{33} \end{bmatrix} = \begin{bmatrix} -j8.23 & j5 & j3.33 \\ j5 & -j8.9 & j4 \\ j3.33 & j4 & -j7.23 \end{bmatrix}$$

The power flow is computed by the Newton-Raphson algorithm

$$\dot{\mathrm{V}} = \begin{bmatrix} 1\angle 0 \\ 1\angle -0.052 \\ 0.944\angle -0.172 \end{bmatrix} = \begin{bmatrix} 1.0000 + j0.0000 \\ 0.9986 - j0.0522 \\ 0.9301 - j0.1616 \end{bmatrix}$$

Based on the node analysis, the current injections at each bus are:

$$\dot{\mathrm{I}} = \begin{bmatrix} \dot{I}_1 \\ \dot{I}_2 \\ \dot{I}_3 \end{bmatrix} = \mathrm{Y}\dot{\mathrm{V}} = \begin{bmatrix} 0.7989 - j0.1397 \\ 0.1819 - j0.1676 \\ -0.9594 + j0.6001 \end{bmatrix}$$

Based on the current direction noted in Figure 3.1, it is seen that

$$\dot{I}_2 = \dot{I}_{g2} + \dot{I}_{l2}$$

$$\dot{I}_{l2} = \frac{S_{l2}^{\ *}}{\dot{V}_2^{\ *}} = \frac{0.3 - j0.1}{0.9986 + j0.0522} = 0.2944 - j0.1155$$

$$\dot{I}_{g2} = \dot{I}_2 - \dot{I}_{l2} = 0.4763 - j0.2831$$

$$\dot{I}_{l3} = \dot{I}_3$$

When the internal admittance of the generators is considered, two more buses are added to the system. Therefore, the structure of the five-bus system is shown in Figure 3.2.

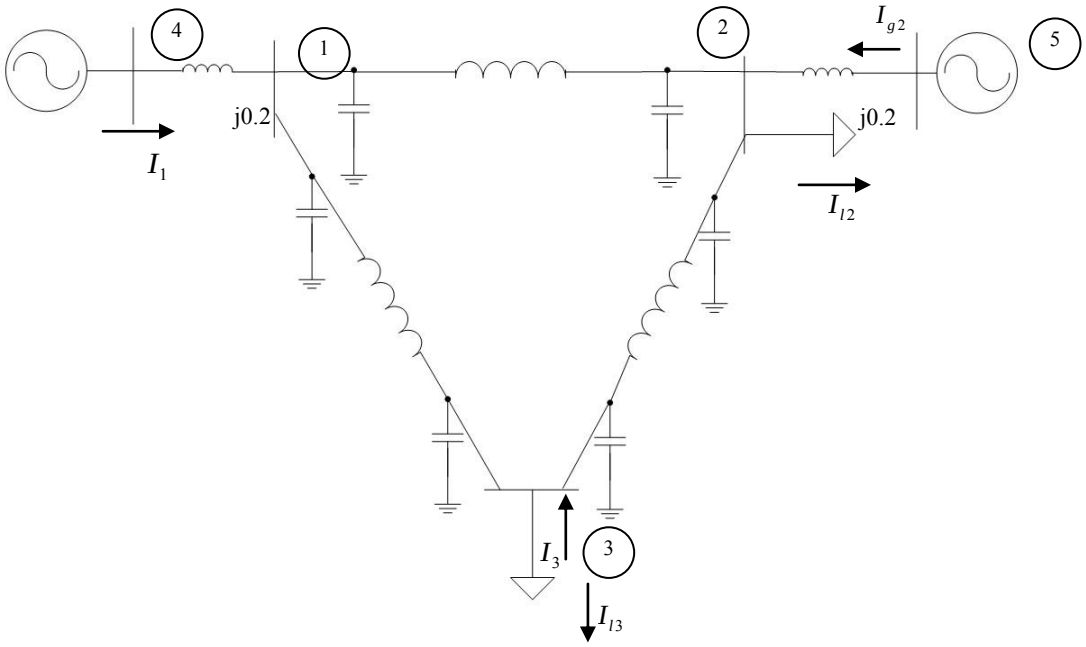

Figure 3.2 Structure of the Five-node system

The internal voltage of the two generator buses are

$$\dot{V}_4 = \dot{V}_1 + \dot{I}_1 * j0.2 = 1.0279 + j0.1598$$

$$\dot{V}_5 = \dot{V}_2 + \dot{I}_{g2} * j0.2 = 1.0553 + j0.0431$$

The internal admittance of generator is

$$y_d = \frac{1}{j0.2} = -j5$$

While performing the network reduction of a power system, load buses can be treated as either current sources or admittances.

3.1.1 Constant Current Load

The admittance matrix of the five-system is

$$Y_{5*5}=\left[\begin{array}{ccc:cc} -j8.23+y_d & j5 & j3.33 & -y_d & 0 \\ j5 & -j8.9+y_d & j4 & 0 & -y_d \\ j3.33 & j4 & -j7.23 & 0 & 0 \\ \hdashline -y_d & 0 & 0 & y_d & 0 \\ 0 & -y_d & 0 & 0 & y_d \end{array}\right]=\left[\begin{array}{cc} a & b \\ c & d \end{array}\right]$$

Based on the node analysis, current injections at each bus are

$$\dot{I}_{5*1}=Y_{5*5}*\dot{V}_{5*1}=\left[\begin{array}{c} 0 \\ -0.2944+j0.1155 \\ -0.9594+j0.6001 \\ \hdashline 0.7989-j0.1397 \\ 0.4763-j0.2831 \end{array}\right]=\left[\begin{array}{c} 0 \\ -\dot{I}_{2l} \\ \dot{I}_3 \\ \hdashline \dot{I}_1 \\ \dot{I}_{g2} \end{array}\right]=\left[\begin{array}{c} \dot{I}_i \\ \dot{I}_e \end{array}\right]$$

Take $\dot{I}_{5*1}(1)$ as an example:

$$\dot{I}_1=y_{11}*\dot{V}_1+y_{12}*\dot{V}_2+y_{13}*\dot{V}_3$$
$$\dot{I}_{5*1}(1)=y_{11}*\dot{V}_1+y_d*\dot{V}_1+y_{12}*\dot{V}_2+y_{13}*\dot{V}_3-y_d*\dot{V}_4=\dot{I}_1+y_d*\dot{V}_1-y_d*\dot{V}_4=0$$

Perform the network reduction and one obtains

$$Y_{2*2}=d-\left(c/a\right)*b=\left[\begin{array}{cc} 0.0000-j1.7492 & 0.0000+j1.9032 \\ 0.0000+1.9032 & 0.0000-j1.7466 \end{array}\right]$$
$$\dot{I}_{eq}=-c/a*\dot{I}_i=\left[\begin{array}{c} -0.6014+j0.3501 \\ -0.7051+j0.3964 \end{array}\right]$$
$$\dot{I}_{reduce}=\dot{I}_e+\dot{I}_{eq}=\left[\begin{array}{c} 0.1975+j0.2104 \\ -0.2289+j0.1133 \end{array}\right]=Y_{2*2}*\left[\begin{array}{c} \dot{V}_4 \\ \dot{V}_5 \end{array}\right]$$

$\dot{I}_{eq}$ is the equivalent current sources of the two loads in the previous system. Figure 3.3 shows the structure of the system after the network reduction.

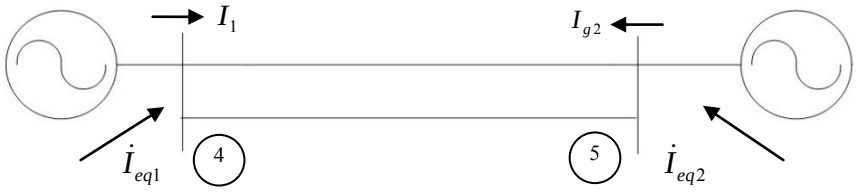

Figure 3.3 Structure of the System after Reduction (Current Source Load)

3.1.2 Constant Impedance Load

The Y matrix of the 5-node system is

$$Y_{5*5}=\left[\begin{array}{ccc:cc} -j8.23+y_d & j5 & j3.33 & -y_d & 0 \\ j5 & -j8.9+y_{l2}+y_d & j4 & 0 & -y_d \\ j3.33 & j4 & -j7.23+y_{l3} & 0 & 0 \\ \hdashline -y_d & 0 & 0 & y_d & 0 \\ 0 & -y_d & 0 & 0 & y_d \end{array}\right]=\left[\begin{array}{cc} a & b \\ c & d \end{array}\right]$$

The equivalent admittance of the two loads are

$$y_{l2}=\frac{\dot{I}_{l2}}{\dot{V}_2}=0.3000-j0.1000$$

$$y_{l3}=\frac{\dot{I}_{l3}}{\dot{V}_3}=1.1102-j0.4524$$

Based on the node analysis, current injections at the buses are

$$\dot{I}_{5*1}=Y_{5*5}*\dot{V}_{5*1}=\left[\begin{array}{c} 0 \\ 0 \\ 0 \\ \hdashline 0.7989-j0.1397 \\ 0.4763-j0.2831 \end{array}\right]=\left[\begin{array}{c} 0 \\ 0 \\ 0 \\ \hdashline \dot{I}_1 \\ \dot{I}_{g2} \end{array}\right]=\left[\begin{array}{c} \dot{I}_e \\ \dot{I}_i \end{array}\right]$$

Take $\dot{I}_{5*1}(2)$ as an example

$$\dot{I}_2=y_{21}*\dot{V}_1+y_{22}*\dot{V}_2+y_{33}*\dot{V}_3$$

$$\dot{I}_{5*1}(2)=y_{21}*\dot{V}_1+y_{22}*\dot{V}_2+y_{l2}*\dot{V}_2+y_d*\dot{V}_2+y_{23}*\dot{V}_3-y_d*\dot{V}_5$$

$$=\dot{I}_2+y_{l2}*\dot{V}_2+y_d*\dot{V}_2-y_d*\dot{V}_5=\dot{I}_{g2}-\dot{I}_{l2}+y_{l2}*\dot{V}_2+y_d*\dot{V}_2-y_d*\dot{V}_5$$

$$=\dot{I}_{g2}-\dot{I}_{l2}+\dot{I}_{l2}-\dot{I}_{g2}=0$$

Perform the network reduction to obtain

$$Y_{2*2} = d - \left(c/a\right) * b = \begin{bmatrix} 0.2519 - j1.9314 & 0.2886 + j1.6991 \\ 0.2886 + 1.6991 & 0.3466 - j1.9812 \end{bmatrix}$$

$$\dot{I}_{eq} = -c/a * \dot{I}_e = \begin{bmatrix} 0 \\ 0 \end{bmatrix}$$

In this case, loads are converted into admittances, so no equivalent current sources need to be added to the internal buses. However, the new Y matrix is different with the previous case, because the load admittance has changed the structure of the system. The structure of the system after reduction is shown in Figure 3.4.

$$\dot{I}_{reduce} = \dot{I}_i + \dot{I}_{eq} = \begin{bmatrix} 0.7989 - j0.1397 \\ 0.4763 - j0.2831 \end{bmatrix} = Y_{2*2} * \begin{bmatrix} \dot{V}_4 \\ \dot{V}_5 \end{bmatrix}$$

Figure 3.4 Structure of the System after Reduction (Admittance Load)

3.1.3 Static Load Models

Besides the constant current load and constant impedance load, there are several load models, such as the ZIP model

$$P = k_1 + m_1 v + h_1 v^2 \quad (3.3)$$

$$Q = k_2 + m_2 v + h_2 v^2 \quad (3.4)$$

These models consider the influence of voltage or frequency at load buses on the load amount. However, these models are static; they cannot represent the dynamic response of loads. A dynamic load model is required to reflect the dynamic characteristics of loads under frequency and voltage variations.

3.2 Structure Preserving Model

3.2.1 Frequency Dependent Model

The structure preserving model with frequency-dependent load is first proposed in [25]. It assumes that the real power load contains two parts: a static part and a frequency dependent part, i.e.,

$$P_D = P_D^0 + D\,\dot{\delta} \tag{3.5}$$

in which δ is the angle at the load bus and D is the damping factor describing the affect of frequency on the real power load. With this model, the original network topology is explicitly represented. The complete dynamic model of the system containing both generators and loads can be described as:

$$M_i\ddot{\delta}_i + D_i\dot{\delta}_i + \sum_{\substack{j=1 \\ j\neq i}}^{n} b_{ij}\sin\left(\delta_i - \delta_j\right) = P_{Mi}^0 - P_{Di}^0, \qquad i = 1,...,n \tag{3.6}$$

For generator buses, the parameters satisfy

$$M_i > 0, D_i > 0, P_{Di}^0 = 0$$

For load buses, the conditions on the parameters are

$$M_i = 0, D_i > 0, P_{Mi}^0 = 0$$

3.2.2 Load Recovery Model

The frequency dependent model does not consider the voltage behavior at the load buses related essentially to the reactive power load. Moreover, it does not consider the load recovery process.

Measurements in the laboratory and on power system buses indicate that a typical MW load response to a step change in voltage is of the general form in Figure 3.5. The responses for real and reactive power are similar qualitatively. Intuitively, this behavior can be interpreted as follows. A step change in voltage produces a step change in MW load. In a longer time-scale, the lower voltage tap changers and other control devices act to restore voltages and, as a result, the load also recovers. With a certain recovery time on a time-scale of a few seconds, this behavior captures the behavior of induction machines. In a time-scale of minutes, the role of tap-changers and other control devices is included. Over hours, the load recovery and possible overshoot may emanate from heating load. The importance of load models which capture the more general response in Figure 3.5 is evident. Indeed, the dynamic changes in load may substantially affect the voltage dynamics.

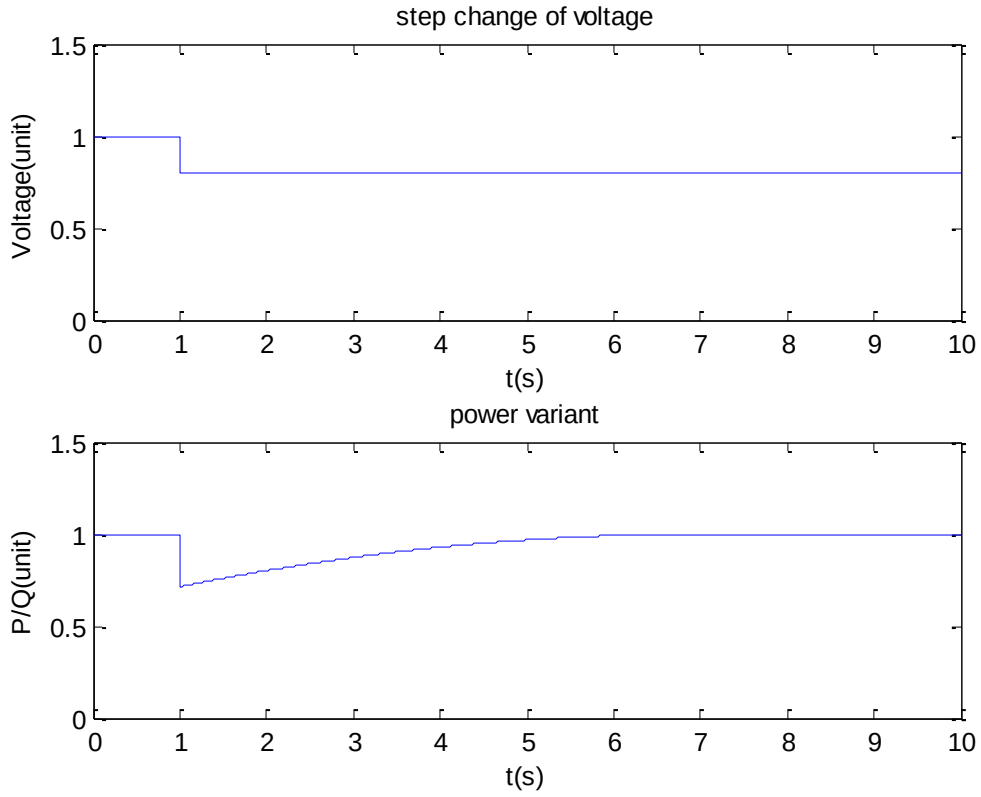

Figure 3.5 Power Recovery Process after a Step Change of Voltage

Based on the above discussion, the load recovery model is proposed in [26]. This work applies the load recovery model to reactive power load, i.e.,

$$T_q \dot{Q}_d(V,\theta) + Q_d(V,\theta) = Q_s^0 + T_q \sigma_q(V)\dot{V} \tag{3.7}$$

where T_q is a time constant that describes the recovery response of the load. This model can also be expressed as

$$T_q \dot{x}_q = -x_q + Q_s(V) - Q_t(V) \tag{3.8}$$

in which

$$x_q = Q_d - Q_t(V) \tag{3.9}$$

Q_s and Q_t represent the steady-state response and transient response respectively.

By combining (3.6) and (3.8), the structure preserving model considering reactive load recovery is formulated for MLE analysis.

3.3 Parameter Identification

In the structure preserving model, a few parameters are needed for each load bus. In order to reduce the parameter, the models of Q_s and Q_t in a single-index form [26] are used, i.e.,

$$\begin{aligned} Q_s(V) &= Q_0 \left(V / V_0\right)^{n_{qs}} \\ Q_t(V) &= Q_0 \left(V / V_0\right)^{n_{qt}} \end{aligned} \tag{3.10}$$

Hence, 4 parameters need to be identified, i.e., damping factor *D* for MW load which is relative to the frequency variation, time constant T_q for voltage recovery time, and n_{qs} and n_{qt} for static and transient voltage exponents. In the frequency dependent model, only D is needed while in the load recovery model, all four parameters are necessary.

A practical way to determine the parameters by simulations is adopted. First, waveforms are computed for each load bus. The frequency and voltage curves are viewed as inputs, and the real and reactive power load curve are outputs. For a fault scenario, record the inputs and outputs at N discrete time instants, i.e., 1, … , N.

For the damping factor *D*, since this is a linear coefficient between real power and frequency from (3.5), one can take the N points, i.e., (P_1, ω_1), (P_2, ω_2), …, (P_N, ω_N) as N samples. Then, the least square method is used to determine the slope *D*.

The parameter T_q can be estimated based on the time response of the curve. Ny linearizing (3.7), the relationship between ΔQ_d and ΔV can be derived as

$$\Delta Q_d = \left(Q_0 / V_0\right) \frac{\left(n_{qt} T_q s + n_{qs}\right)}{\left(T_q s + 1\right)} \Delta V \tag{3.11}$$

Therefore, by using the same input value ΔV, the outputs ΔQ_d produced are compared to the outputs. Typically, a least square quadratic criterion can be used to obtain the most suitable values of n_{qs} and n_{qt}.

3.4 Summary

A structure-preserving model is developed which includes the frequency dependent "P" model and load recovery "Q" model. The structure preserving model retains the load buses for MLE calculation. Previously a reduced model was used where load buses are reduced for the computation of Lyapunov Exponents. By the structure-preserving model, useful information from both generator and load buses can be obtained. The effectiveness of the three models are validated by time-domain simulations.

4. MLE Window Size Selection

In the previous work, the time window T for MLE calculation is obtained by taking a frequency range of the system response for a contingency based on off-line study. The inverse of the lower limit of the frequency band contains at least one period of all the frequency components within the frequency band. Thus, it is chosen as a fixed window size T. However, the frequency band of each contingency is different. Using a fixed time window to determine MLE may not be accurate enough. In this work, a method to select a variable window size for a specific scenario is proposed based on online spectral analysis. The increasing frequency components for that specific scenario are of interest as far as system stability is concerned. The decaying frequency components should be removed before choosing time window of MLE. With this method, a most appropriate window size will be chosen.

4.1 Spectral Analysis

Every signal has a corresponding spectrum. A signal can be sampled over time. For example, Figure 4.1 represents a periodic signal in the time domain. It is composed of three trigonometric functions shown in Figure 4.2. Applying frequency domain analysis, the results can be obtained as shown in Figure 4.3. Figure 4.3 is a one-sided spectrum, i.e., only positive frequencies are represented. It is a way to describe a signal and show that the signal contains primarily three frequencies. The coefficient of each frequency is a complex number which represents the amplitude and phase angle.

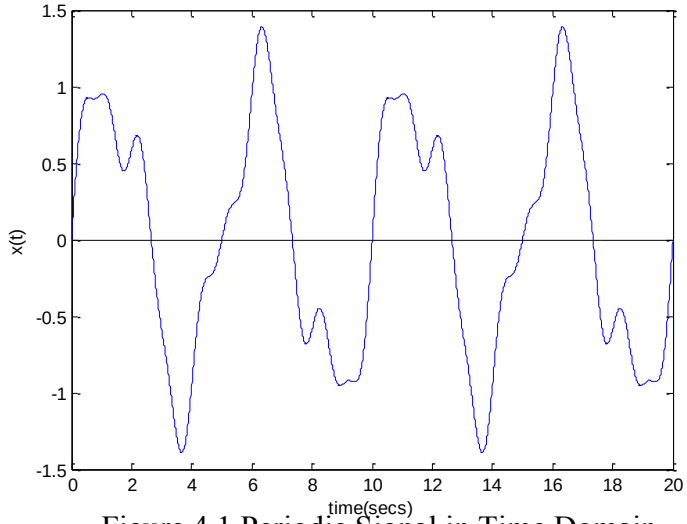

Figure 4.1 Periodic Signal in Time Domain

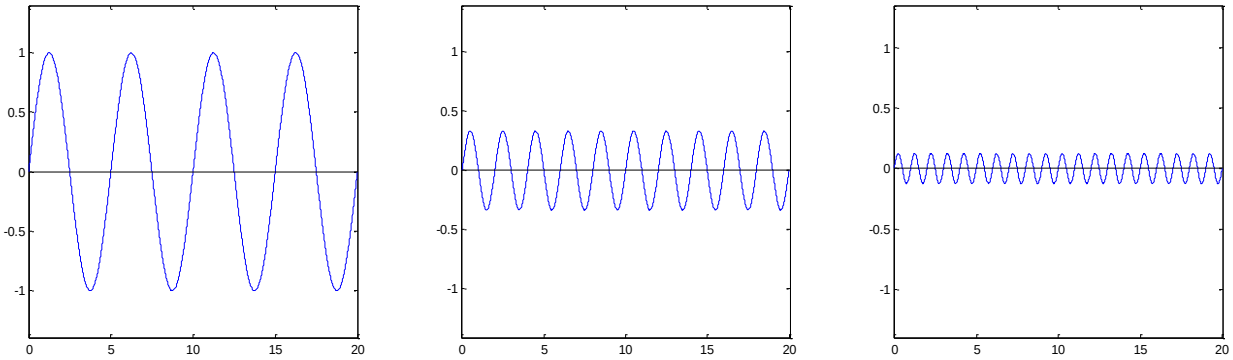

Figure 4.2 Simple Trigonometric Functions

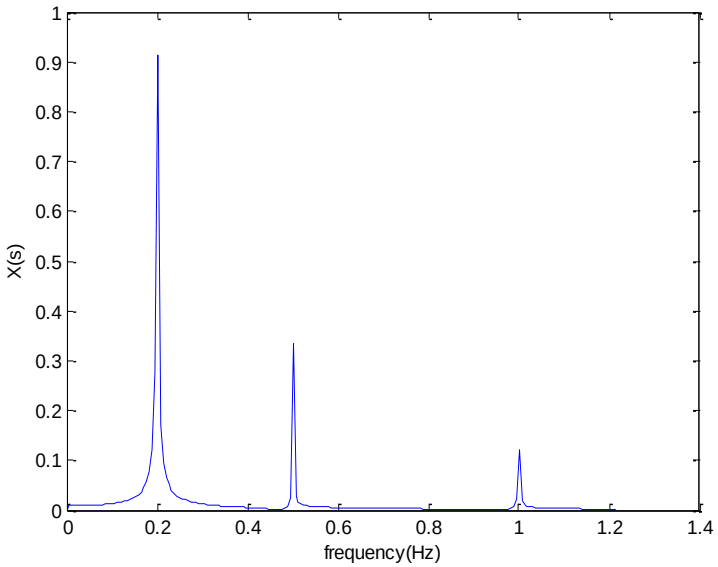

Figure 4.3 Signal Spectrum

Figure 4.4 illustrates the relationship between the time domain and frequency domain. From the perspective of the time domain, the signal is the sum of these three trigonometric waves, while from the frequency domain, the signal can be decomposed into three frequencies [27]. Spectral analysis is used to determine the time window of MLE in previous research. Power swings exhibit a strong periodic behavior.

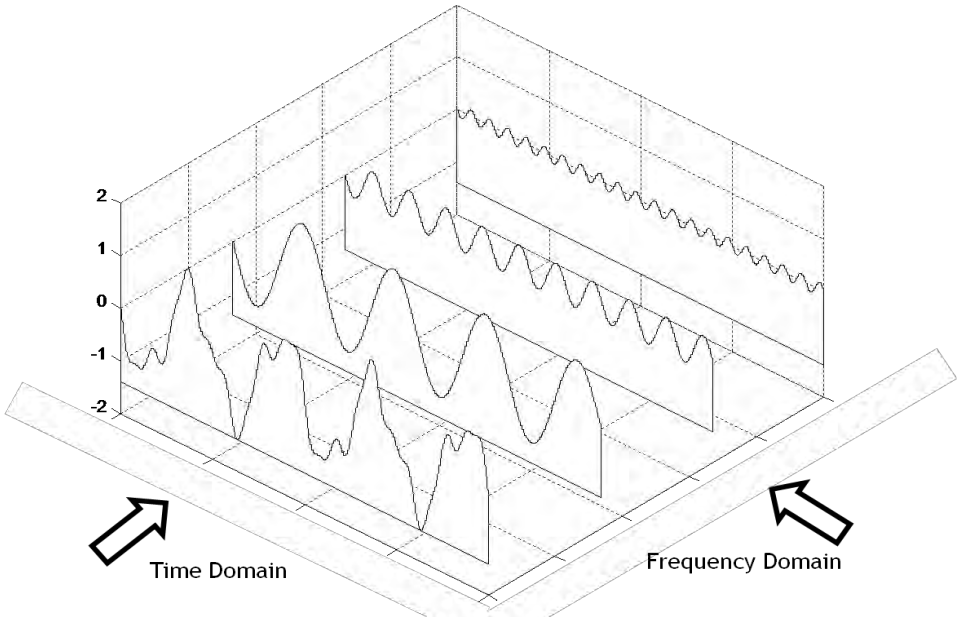

Figure 4.4 Relationship between Time Domain and Frequency Domain

4.2 Fast Fourier Transform (FFT)

FFT is widely used for conversion of a signal from the time domain into frequency domain. An assumption of FFT is that a signal is periodic in a time window and repeats for all times outside the time window. The length of the actual input is either an equal or an integer multiple of periodic length.

Figure 4.5 illustrates that a non-periodic signal can become periodic by repeating the pattern. For example, the curve is a signal, and the data from 5 seconds to 10 seconds are chosen for FFT analysis. It is assumed that the signal will look like the lower curve as an infinite signal with the repetition of the signal within the time window. Discontinuities emerge at the boundaries of the time window. It takes high frequencies to construct sharp corners. To avoid the discontinuity of an input signal when it is made repetitive, the signal should be modified to smoothly reduce to zero at the boundaries of the time window.

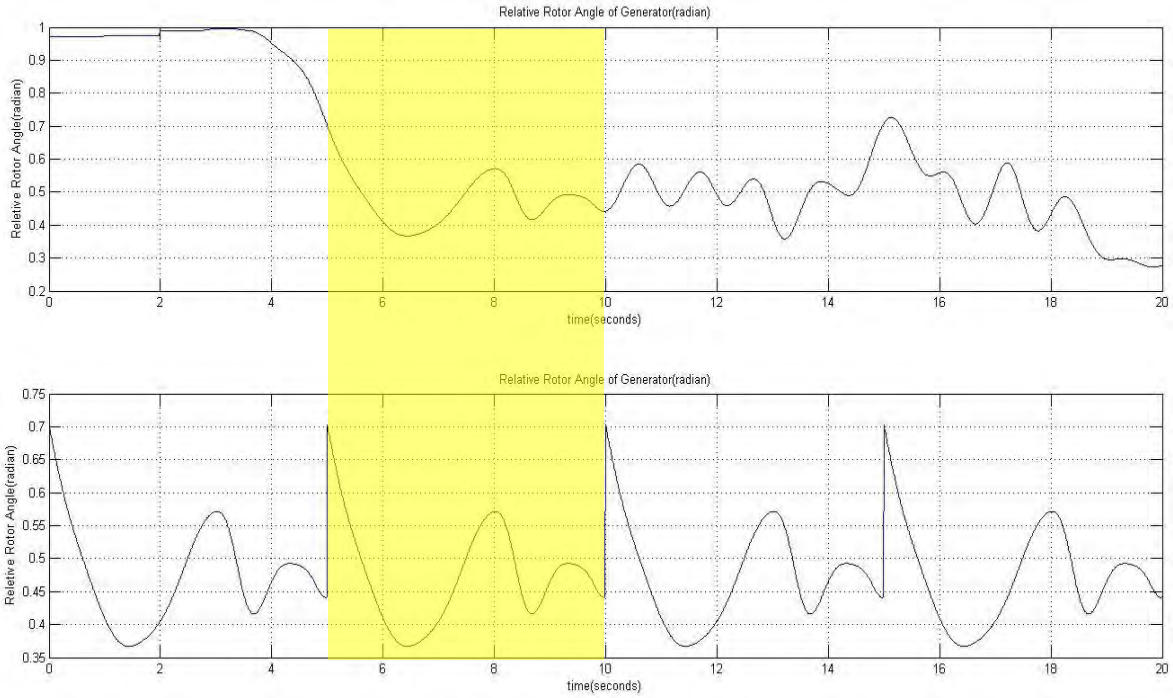

Figure 4.5 Periodization of a Signal

Window functions can be multiplied by a signal to reduce discontinuity at both ends. By centralizing the energy into the main lobe, the side lobes level is lowered and the magnitude accuracy is improved. The disadvantage of a window function is that the main lobe of frequencies is widened which will make two neighboring frequencies less distinguishable [28]. This research is focused on analyzing frequency components in the range from 0.1 Hz to 1.0 Hz. Frequency resolution is 0.1 Hz. Take 0.1 Hz and 0.2 Hz frequency components as examples. They are close to each other. When they are included in a signal, two main lobes can be observed in the frequency domain without a window function. By utilizing a window function, these two main lobes are widened. It is likely that those two main lobes overlap. Whether or not a window function should be applied depends on the purpose of research, high frequency resolution, or high magnitude accuracy. As a result, to obtain the highest frequency resolution, a rectangular window function is adopted in this study.

Definition of FFT:

$$X(k) = \sum_{j=0}^{N-1} x(j) \quad {}_N{}^{j*k} \qquad k = 0,1,2,\cdots,N-1 \tag{4.1}$$

$$x(j) = \left(\frac{1}{N}\right) \sum_{k=0}^{N-1} X(k) \quad {}_N{}^{j*k} \qquad j = 0,1,2,\cdots,N-1 \tag{4.2}$$

where ${}_N = e^{(-2\ i)/N}$, and N is the number of samples.

$X(0)$ denotes the magnitude of zero-frequency component. $X(1)$ term determines the trigonometric waveform that happens to go through one cycle during the N data samples.

In the same way, X(k) term determines the trigonometric waveform that goes through k cycles during the N data samples [28]. The coefficients of each term can be considered as the length of projection of the signal onto its frequency components'.

It is clear that only $X(1)$ term and multiples of $X(1)$ term can be presented. Frequency resolution is defined by how close two distinguishable frequency components can be [28]. Since N samples are evenly distributed over the range from zero to the sampling frequency, frequency resolution is the sampling frequency over N. For a given sampling frequency, frequency resolution is the inverse of the sampling time.

$$frequency\ resolution = \frac{f_s}{N} = \frac{1}{T} \tag{4.3}$$

References [29]-[31] propose a method of using a sliding window to apply FFT to analyze the changing magnitude of each frequency contained in the signal. An example is shown here. Suppose that a signal x_n contains two frequencies. The parameters are listed in Table.4-1. Figure 4.6 and 4.7 illustrate the signal in the time domain and frequency domain, respectively.

$$x_n(t) = x_1(t) + x_2(t)$$

$$x_1(t) = 1.5 * e^{-0.01*t} * \cos(2\pi * 0.2 * t)$$

$$x_2(t) = 1.2 * e^{0.02*t} * \cos(2\pi * 0.5 * t)$$

Table 4-1 Parameters of Signal x_n

	Frequency(Hz)	Initial Magnitude	Damping
X_1	0.2	1.5	0.01
X_2	0.5	1.2	-0.02

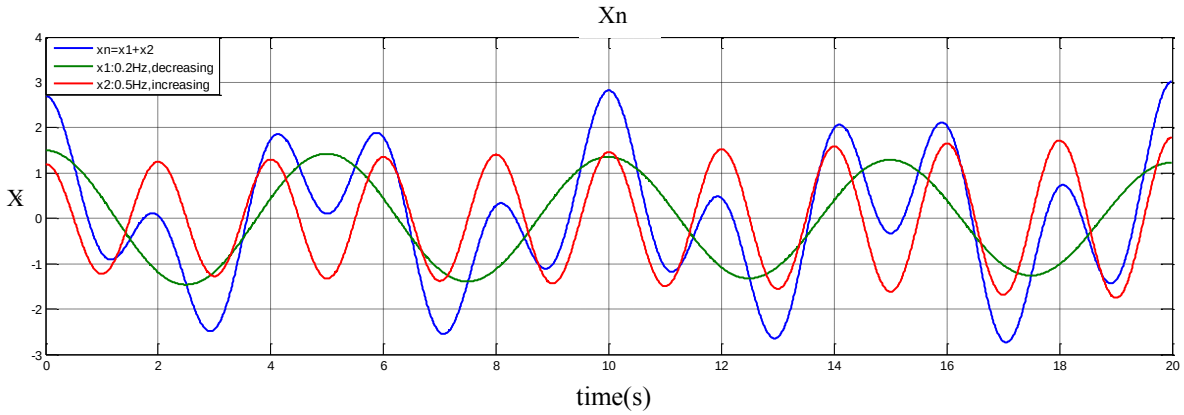

Figure 4.6 Curves of x_n, x_1, and x_2

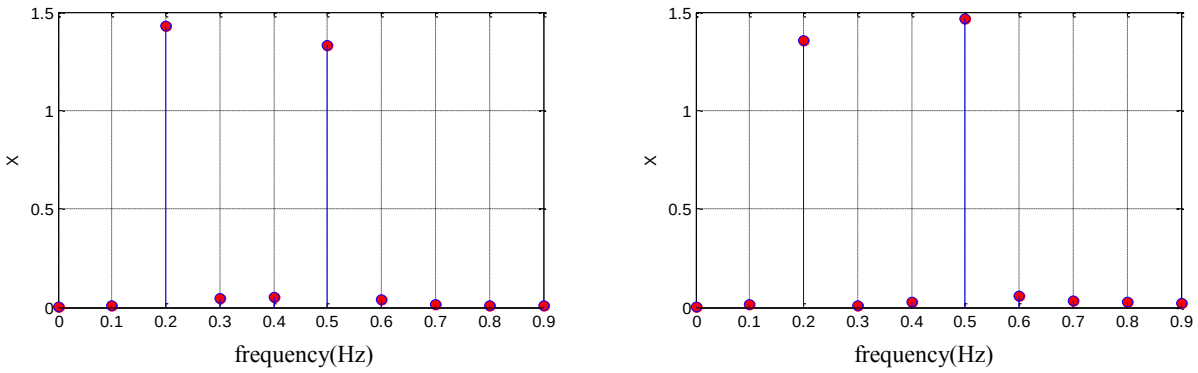

Figure 4.7 Changing of Spectrum When a Sliding Window is Applied

When FFT is applied to the samples within the first 10 second, results are shown in the left hand side spectrum in Figure 4.7. The magnitude of 0.2 Hz frequency is higher than that of 0.5 Hz's. As shown in Table 1, 0.2 Hz frequency component is negatively damped, while 0.5 Hz frequency component is positively damped. When FFT is applied to the samples from 5 seconds to 15 seconds, results are shown in the left hand side spectrum in Figure 4.7. The magnitude of 0.2 Hz frequency is lower than that of 0.5 Hz's. As a result, changes in the frequency components can be identified by FFT using a sliding window.

4.3 Method Description

The proposed method includes three main parts: (1) Apply FFT to the relative rotor angle curves and then choose dominant frequency components. (2) Compare the MLEs calculated using the same window size but 1 second later. (3) Predict the stability of the system based on the comparison of the MLEs. The detailed procedure is listed in Figure 4.8.

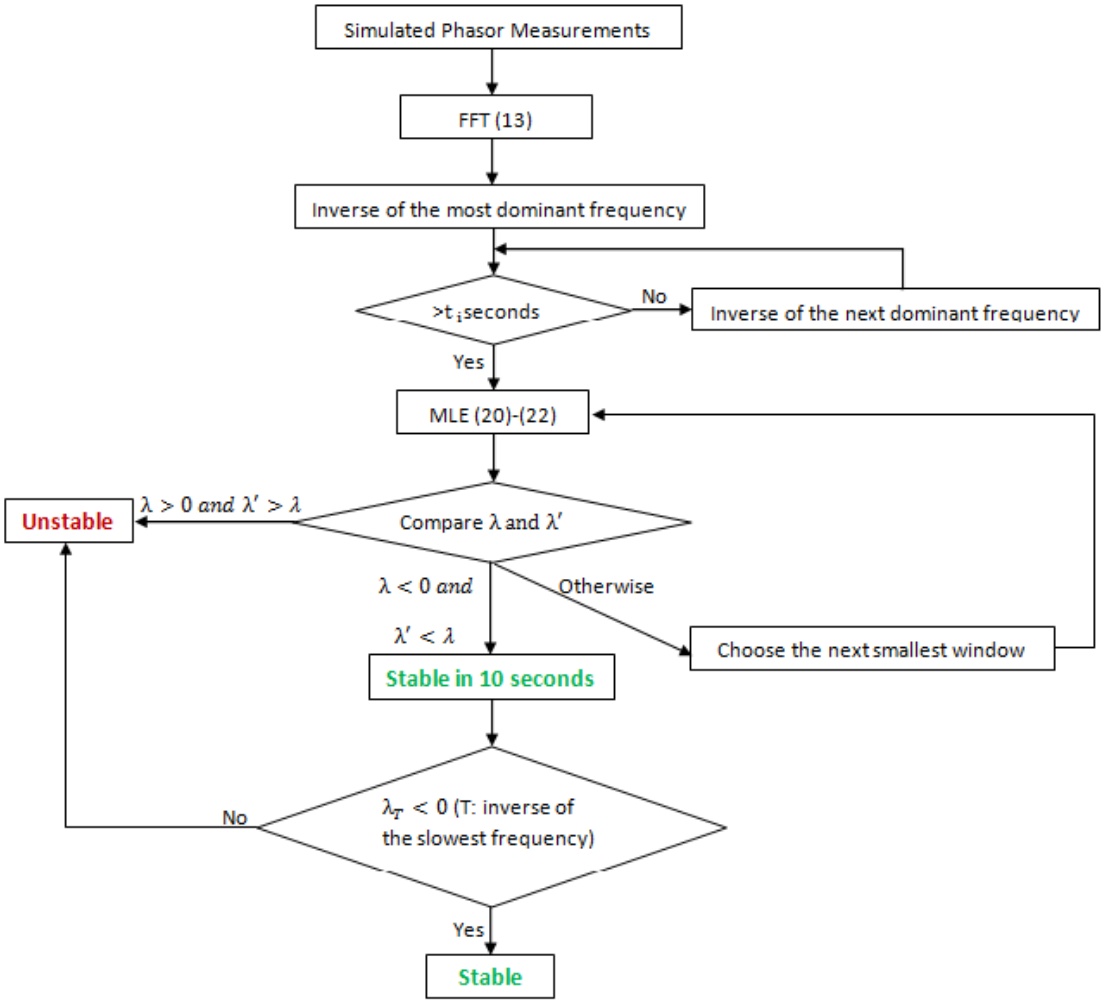

Figure 4.8 Flowchart of the MLE Method with Adjustable Window Sizes

4.3.1 Choose the Dominant Frequency

On top of the flowchart, simulated phasor measurements are voltage angles of the generator buses. They will be converted into the rotor angles of the generators by incorporating the internal admittances of generators. A reference generator is chosen to determine relative rotor angles. Relative rotor angles are the inputs of the proposed method.

A dominant frequency component is defined as the frequency component that has the largest increase in magnitude when applying FFT of the same length but some time later. There is a tradeoff between the absolute increase of magnitude M_{inc} and the increase rate R_{inc} of each frequency component.

$$M_{inc} = X'(k) - X(k) \tag{4.4}$$

$$R_{inc} = \frac{X'(k)-X(k)}{X(k)} \tag{4.5}$$

where X(k) and X'(k) are the kth frequency component when FFT of the same length is applied some time later.

If one of the frequency components has a larger percentage increase but a smaller magnitude after the growth, it still has less effect over the overall spectrum. As a result, both M_{inc} and R_{inc} are used to determine dominant frequency components. First, choose three frequency components that have the largest absolute increment Minc. Then, compare the percentage increase R_{inc} of these three frequency components and choose the one that has the largest R_{inc}.

The states of a power system include rotor angle and rotor speed of all generators. The rotor speed is the derivative of the rotor angle based on the swing equations. The rotor angle affects the stability of a power system and, therefore, FFT has been applied to all relative rotor angles of the power system following a disturbance to identify the frequency components of the system. For each relative rotor angle, a sliding window is used to determine the dominant frequency component of this state. Every state is an indicator of the stability of the power system. Some of them include different dominant frequency components. All the dominant frequency components in the power system need to be considered. Assemble all those dominant frequency components and remove the repeated ones. Sort the inverse of those frequencies in an ascending order. An array is used to save those windows for later use. At the same time, sort all these frequency components in a descending order by percentage increase, saved in f_{dom}.

Note that the first value in *win* is the period of the highest dominant frequency, while the last value is the period of the slowest dominant frequency component. The time window of the MLE starts from the inverse of the most dominant frequency, the first value in f_{dom}. In cases where this method is applied to the relative rotor angle curves, most of the frequency components are decreasing and the dominance of a higher frequency component might be amplified because of the small but faster increase. If the inverse of the most dominant frequency is less than t_i, the next dominant frequency will be chosen instead. t_i is set to 2 seconds in the case study. For a chosen window size, it will be applied twice by sliding 1 second forward. λ and λ' are the two MLEs calculated using the same window size but at different initial times, which starts at 0 and 1 second, respectively.

4.3.2 MLE Computation

MLE for a fixed window size can be calculated by GSR method described in Chapter 2.2. By using the sliding window, two MLEs can be obtained as λ and λ'. By comparison of these two values, the system stability can be further assessed.

4.4 Stability Prediction

To achieve an accurate prediction, the following requirements need to be satisfied:

1) If $\lambda < 0$ and $\lambda' < \lambda$, it means that the system is stable in the first window and will be more stable in the second window. In other words, the information included in the first window is sufficient to predict that the system is stable.

2) If $\lambda > 0$ and $\lambda' > \lambda$, it means that the system is unstable in the first window and going to be more uncertain in the second window. In other words, the first window contains enough information to conclude that the system is unstable.

3) Otherwise, even if the prediction cannot be made using the existing information, further analysis is required. The predetermined time window sizes have been saved in an array in an ascending order. Then the next smallest window in array will be used for the prediction. The above process will be repeated.

If the chosen window is the last value in the array, it is unnecessary to compare the MLEs calculated using a sliding window, since this window size is long enough to include information of all the frequency components. Prediction can be made according to λ, and this is the final prediction. However, in some cases, the system appears to be stable at around 10 seconds, but it then goes unstable after that. The requirement $\lambda < 0$ and $\lambda' < \lambda$ mentioned earlier can only conclude that the system is stable in the first 10 seconds. If the last value in the array is less than 10 seconds, a 10 seconds window is used for the final prediction. To decide whether or not further analysis is needed, two MLEs need to be computed using the last value in the array.

4.5 Summary

With an adjustable window size utilizing the proposed method, the accuracy of the prediction of system waveform stability by MLE technique has been improved. At the same time, the computational burden does not increase significantly. Combining with the dynamic load model proposed in Chapter 3, the new technique leads to a more reliable approach for prediction of system rotor angle and short-term voltage stability. Extensive computational tests have been performed to validate this method. The results are presented in the next chapter.

5. Case Study and Simulation Results

5.1 The Mini-WECC System and Simulation Model

In this research, the mini-WECC system is used to test the proposed models and algorithms. The mini-WECC system is a reduced-order model of the WECC system designed for the study of power oscillation issues. The system has 122 buses with 34 generators, 171 lines, and 25 loads. Figure 5-1 shows a one-line diagram of the system which only includes high-voltage buses. Load and generators are connected via step-up transformers.

The Matlab toolbox PSAT is used to perform time-domain simulation of this system. The detailed 6-order model is used for generators. That is,

$$\dot{\delta} = \omega_s(\omega - 1)$$

$$\dot{\omega} = \frac{Pm - Pe - D(\omega - 1)}{M}$$

$$\dot{e}'_q = (-f * (e'_q) - \left(x_d - x'_d - \frac{T''_{d0}}{T'_{d0}}\frac{x''_d}{x'_d}(x_d - x'_d)\right) i_d + \left(1 - \frac{T_{AA}}{T'_{d0}}\right) * v)/T'_{d0}$$

$$\dot{e}'_d = (-e'_d + \left(x_q - x'_q - \frac{T''_{q0}}{T'_{q0}}\frac{x''_q}{x'_q}(x_q - x'_q)\right) i_q)/T'_{q0}$$

$$\dot{e}''_q = (-e''_q + e'_q - \left(x'_d - x''_d + \frac{T''_{d0}}{T'_{d0}}\frac{x''_d}{x'_d}(x_d - x'_d)\right) i_d + \frac{T_{AA}}{T'_{d0}} * v)/T''_{d0}$$

$$\dot{e}''_d = (-e''_d + e'_d + \left(x'_q - x''_q + \frac{T''_{q0}}{T'_{q0}}\frac{x''_q}{x'_q}(x_q - x'_q)\right) i_q)/T''_{q0}$$

The loads are modeled as a generalized exponential voltage frequency dependent model [32], i.e.,

$$P = \frac{k_p}{100}(\frac{V}{V_0})^{\alpha p}(1 + \Delta\omega)^{\beta p}$$

$$Q = \frac{k_Q}{100}(\frac{V}{V_0})^{\alpha Q}(1 + \Delta\omega)^{\beta Q}$$

5.2 Parameter Identification

Consider a 3-phase fault on a transmission line with a duration of 0.1 second. The fault is cleared by opening circuit breakers on both ends of the line. By time-domain simulation, the waveforms of bus voltage, frequency, as well as real and reactive injection power can

be obtained. By using the parameter identification technique in Chapter 3.3, the parameters for structure preserving model of 25 loads are shown in Table 5.1.

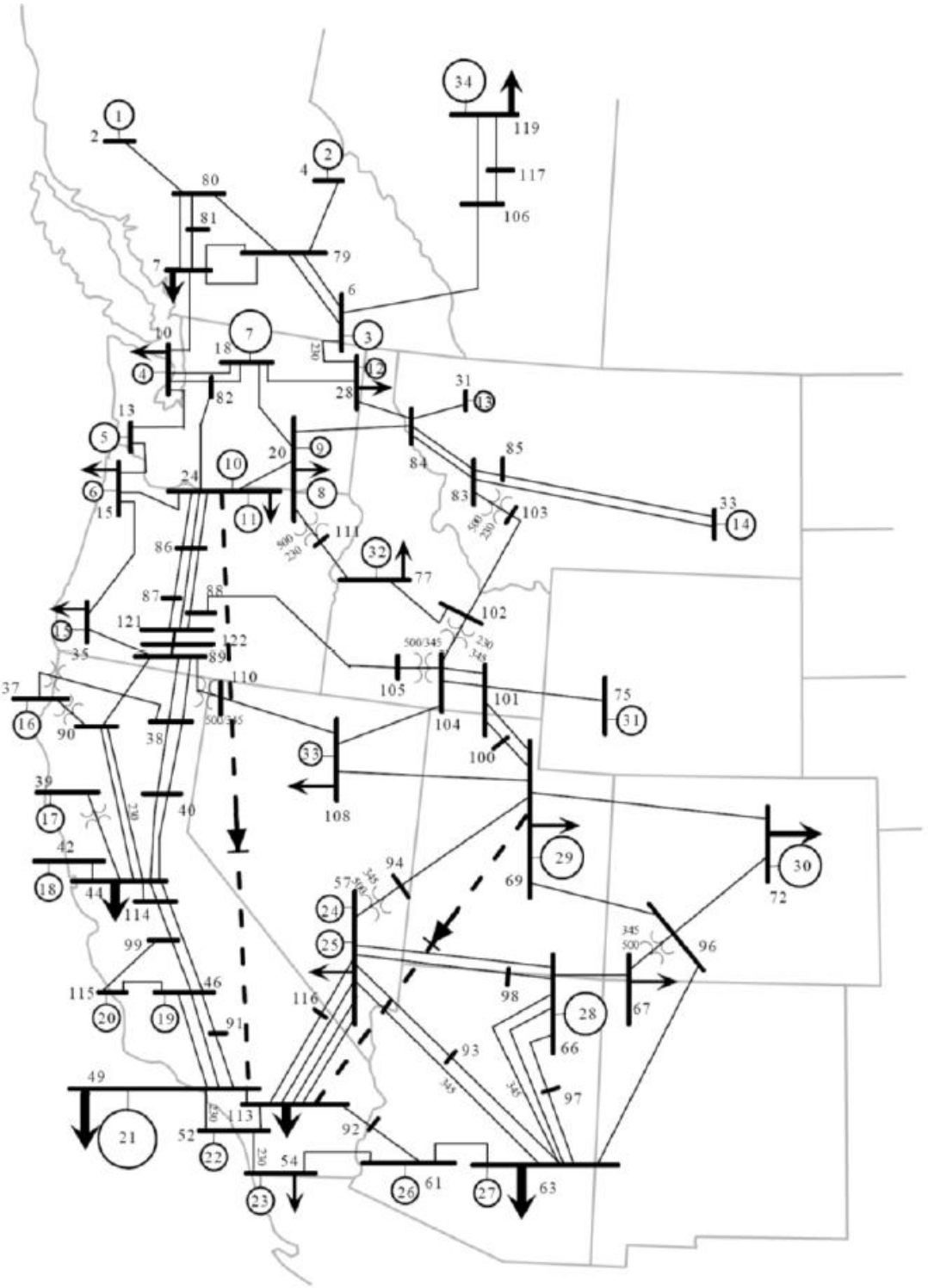

Figure 5.1 One-line Diagram of Mini-WECC System

Table 5-1 System Parameter Verification

Load Bus Number	**8**	**11**	**16**	**21**	**24**	**26**	**29**	**36**	**43**
D	1.482	0.874	1.118	0.972	1	0.144	0.862	0.489	5.31
T_q	3	5	3	3	3	3	3	3	3
n_{qs}	1.9	1.8	2	2	2	2	2	2	2
n_{qt}	2	2	2	2	2	2	2	2	2
Load Bus Number	**49**	**50**	**55**	**56**	**64**	**69**	**70**	**73**	**78**
D	1	4.313	1.127	2.626	4.237	1	1.984	2.809	0.762
T_q	3	3	3	3	3	3.5	3.5	4	4
n_{qs}	2	2	2	2	2	2	2	2	2
n_{qt}	2	2	2	2	2	1.9	1.9	2	2
Load Bus Number	**89**	**95**	**109**	**112**	**113**	**120**	**121**		
D	1	0.869	0.619	3.522	1	3.839	1		
T_q	4	4	4	4	4	4	4		
n_{qs}	2	2	2	2	2	2	2		
n_{qt}	2	2	2	2	2	1.9	2		

Take bus 8 as an example. The waveform of the bus voltage is shown in Figure. 5.2. The reactive power load from the simulation is shown in Figure. 5.3. The reactive load response of the structure preserving model under the same voltage input with different parameters is shown as Figure. 5.4. It is observed that with the parameter (T_q, n_{qt}, n_{qs}) =(3, 2, 1.9), the reactive load response is closest to the simulation result.

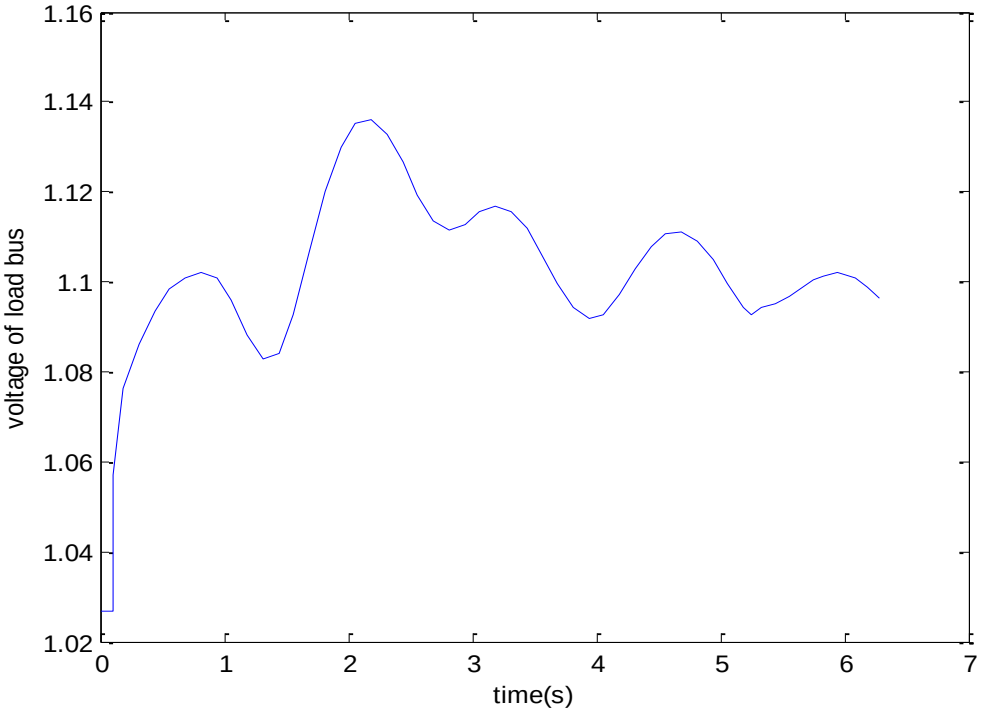

Figure 5.2 Voltage at Bus 8 from PSAT Simulation

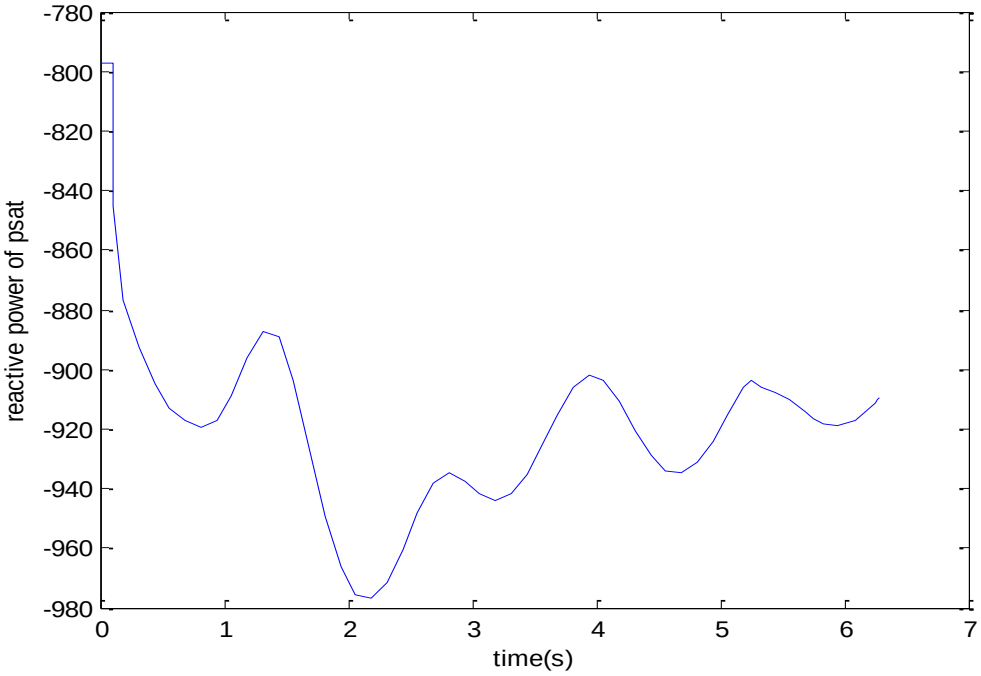

Figure 5.3 Reactive Power Load at Bus 8 from PSAT Simulation

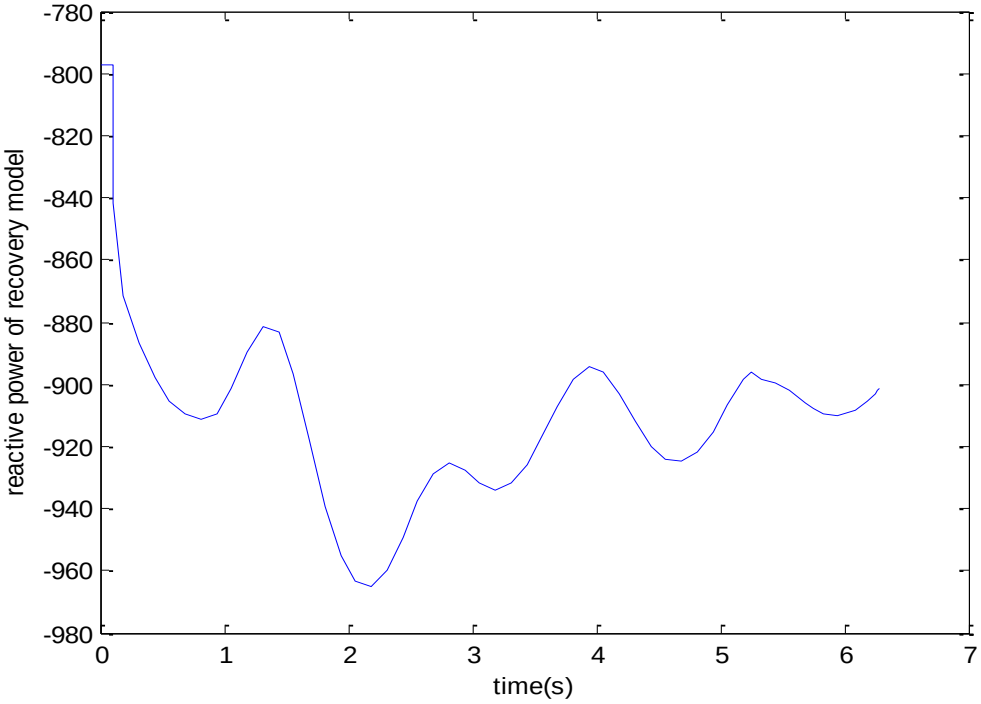

Figure 5.4 Structure Preserving Model at Bus 8 with T_q=3, n_{qt}=2, n_{qs}=1

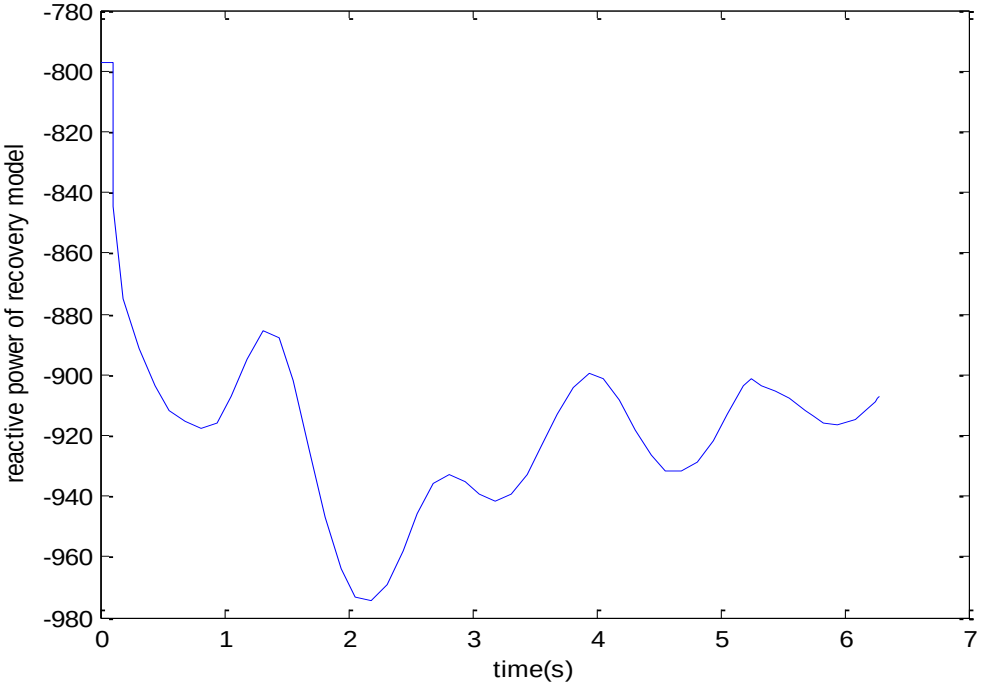

Figure 5.5 Structure Preserving Model at Bus 8 with T_q=3, n_{qt}=2, n_{qs}=1.9

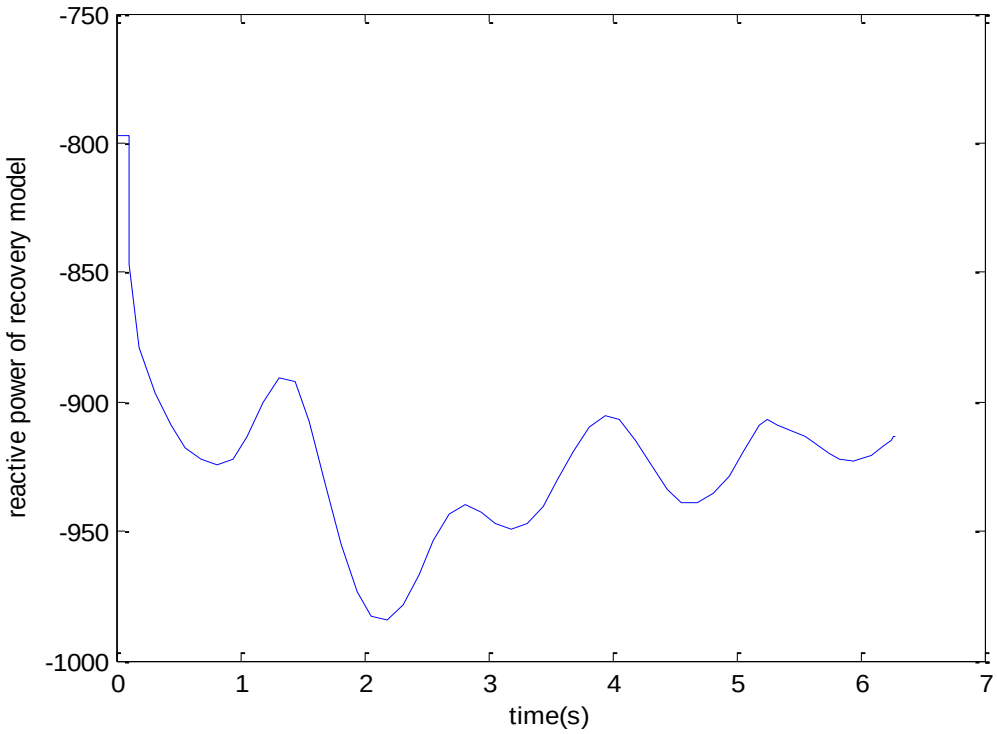

Figure 5.6 Structure Preserving Model at Bus 8 with T_q=3, n_{qt}=2.1, n_{qs}=2

5.3 Simulation Results of Different Dynamic Models

In this work, a total of 120 fault scenarios have been considered. The results of time-domain simulation, reduced dynamic model, structure preserving model with frequency dependent MW load ("P model"), and structuring preserving model with both frequency-dependent MW load and load recovery model ("PQ model") are compared for each scenarios, together with the MLE. Detailed results are shown in Appendix A.

Some typical cases are listed in Table 5.2. In this table, the green color means that the result of the model is consistent with the time-domain simulation result, while the orange color means the opposite.

Table 5-2 Typical Examples

Fault Type	Fault Location	Clear Time	Reduced Model	MLE	"P" Model	MLE	"PQ" Model	MLE	Simulation Results
Generator trip	1	0.1s	stable	-0.2408	stable	-0.2708	stable	-0.2816	stable
Generator trip	5	1s	stable	-0.1189	unstable	0.2101	unstable	2.2087	unstable
Generator trip	10	1s	stable	-0.1232	unstable	-0.1201	unstable	0.1247	unstable
Generator trip	17	1s	stable	-0.1225	stable	-0.1435	unstable	4.7173	unstable
Line Outage	19-20	0.2s	stable	-0.0599	stable	-0.1425	unstable	7.7455	unstable
Line Outage	66-67	0.5s	stable	-0.0390	unstable	1.8246	unstable	0.2894	unstable
Line Outage	89-90	0.5s	stable	-0.0464	unstable	0.693	unstable	0.2825	unstable
Line Outage	105-104	0.5s	stable	-0.0491	stable	-0.1444	stable	-0.1451	unstable

The results of these cases can be categorized into 4 types.

Type 1: All three models, i.e., load-reduced model, "P" model and "PQ" model are consistent with the results of time domain simulation. Specifically, the assessment of the MLEs is consistent with the simulation results. Figure 5.7 shows one of the typical cases, in which a three phase fault occurs at generator bus 1 and is clear after 0.1s. From the waveforms of relative rotor angle and angular speeds of generators, it can be observed that all three models predict that the system is stable, which is consistent with time domain simulation. (**Note: the explanation of the y access is now above the pictures.**)

Relative rotor angle

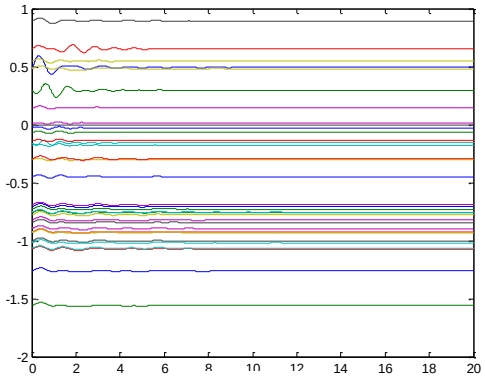

Relative rotor angular speed

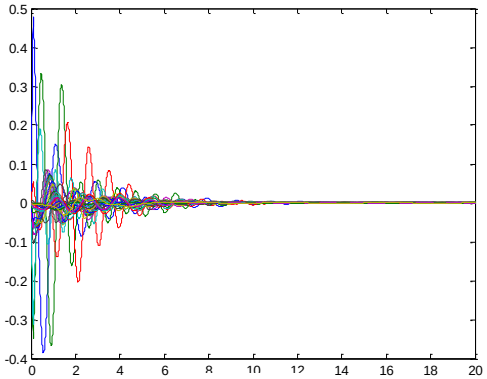

(a) Load-Reduced Model

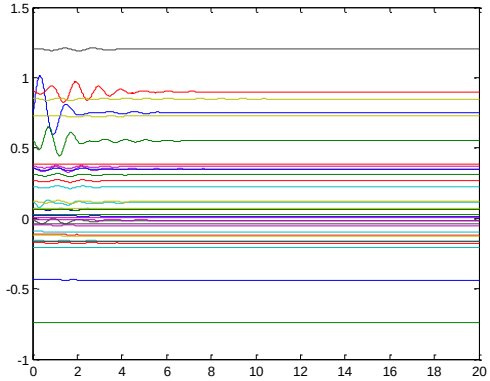

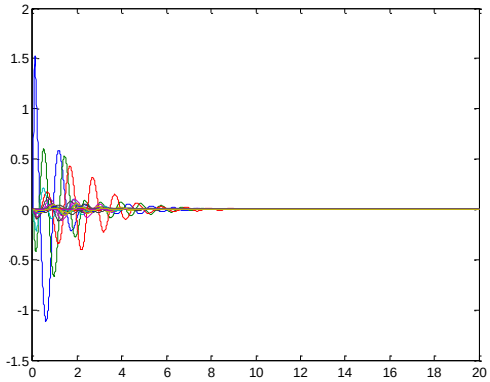

(b) Structure-Preserving "P Model"

Figure 5.7 Comparison of Different Models

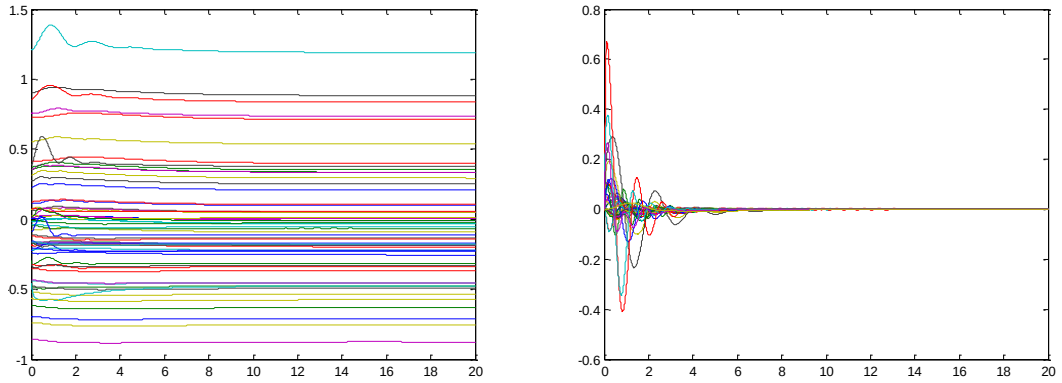

(c) Structure-Preserving “PQ Model"

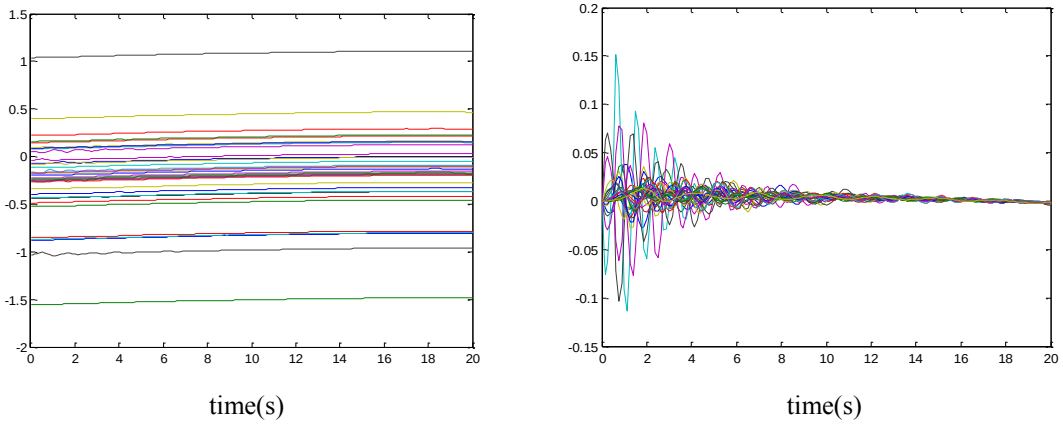

(d) Time-Domain Simulation Result

Figure 5.8 Comparison of Different Models(continue)

Type 2: The structure preserving “P” model and “PQ” model are accurate, while the load-reduced model fails to produce an accurate prediction. Figure 5.8 shows one of the typical cases, in which a three phase fault occurs at generator bus 1 and is cleared after 1s. From the waveforms of relative rotor angle and angular speeds of generators, it can be observed that the results of structure preserving models are unstable, which is consistent with time domain simulation results, while the assessment by the load-reduced model is stable.

Relative rotor angle

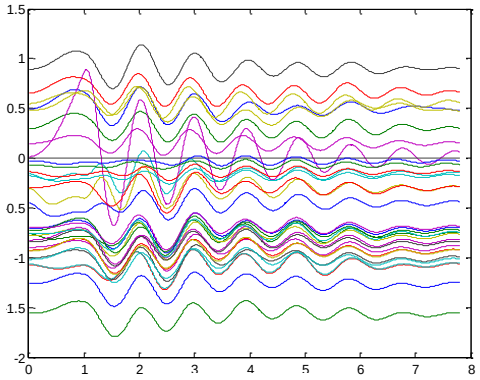

Relative rotor angular speed

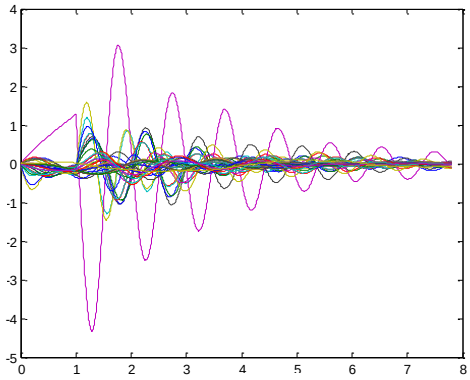

(a) Load-Reduced Model

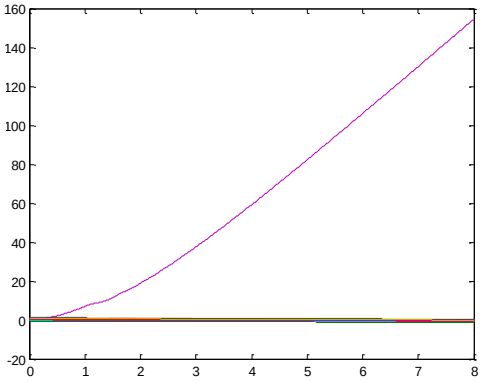

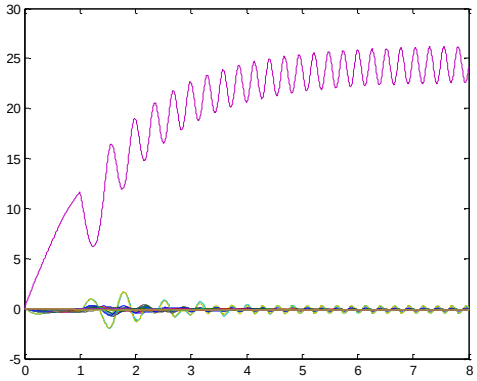

(b) Structure-Preserving “P Model"

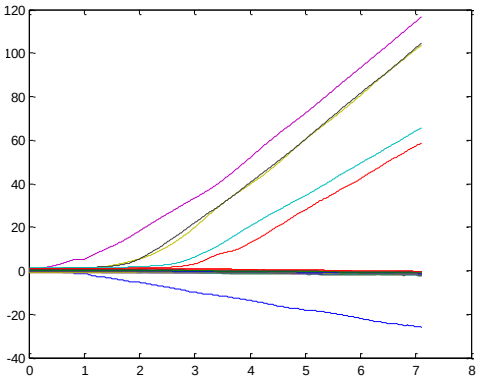

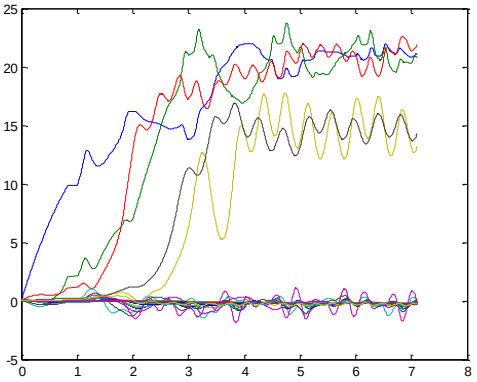

(c) Structure-Preserving “PQ Model"

Figure 5.9 Comparison of Different Models

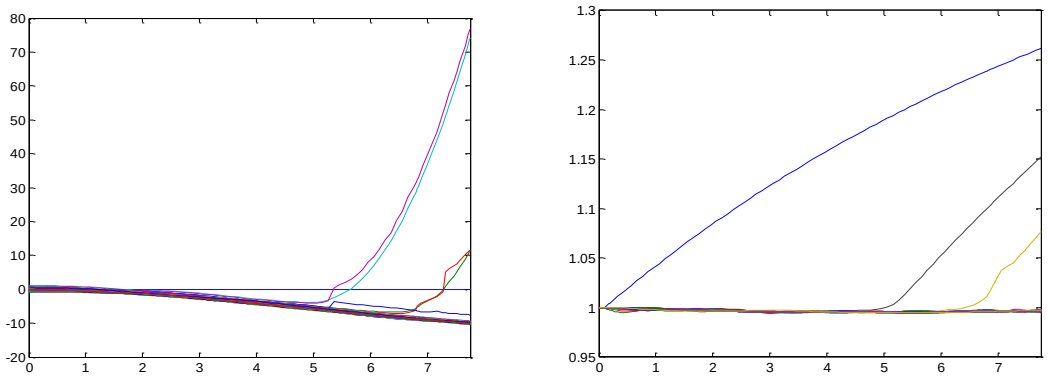

(d) Time-Domain Simulation Result

Figure 5.10 Comparison of Different Models(continue)

Type 3: Only the structure preserving "PQ" model produces an accurate prediction. Figure 5.9 shows one of the typical cases, in which a three phase fault occurs at line 19-20 and is cleared after 0.5s. From the waveforms of relative rotor angle and angular speeds of generators, it is observed that the result of structure preserving "PQ" models is unstable, which is consistent with time domain simulation, while the results of the other two models are stable.

Relative rotor angle Relative rotor angular speed

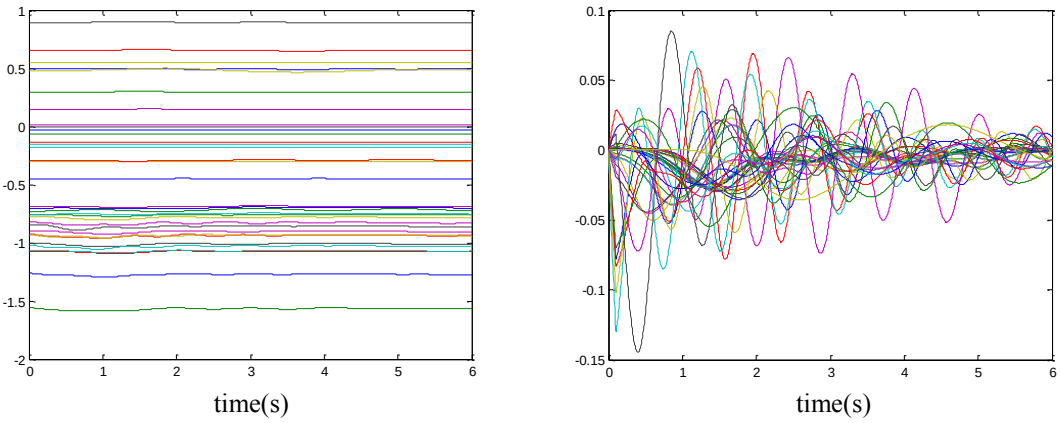

(a) Load-Reduced Model

Figure 5.11 Comparison of Different Models

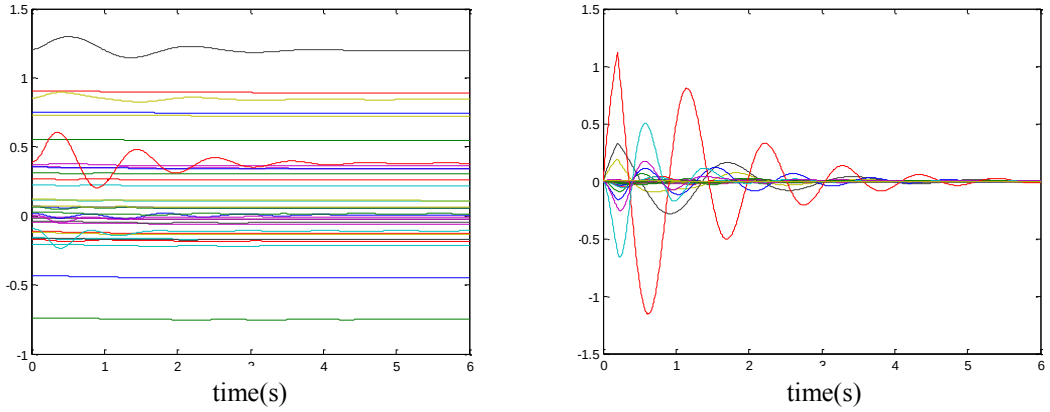

(b) Structure-Preserving “P Model"

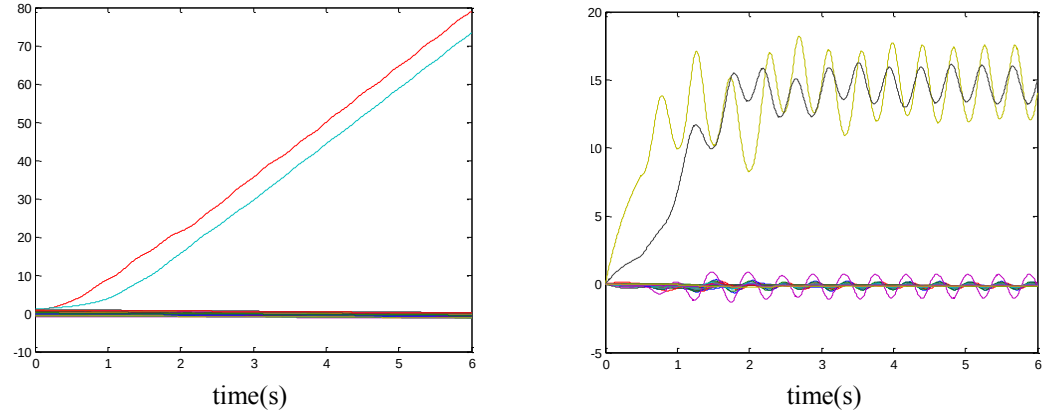

(c) Structure-Preserving “PQ Model"

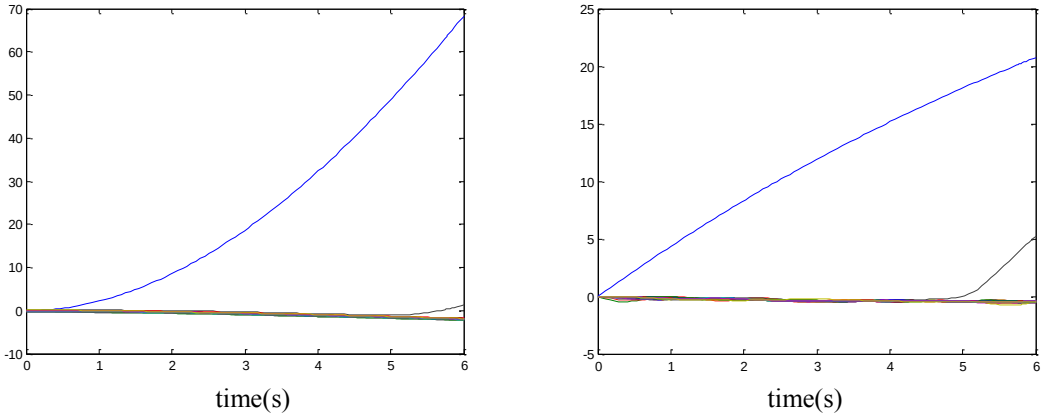

(d) Time-Domain Simulation Result

Figure 5.12 Comparison of Different Models(continue)

Type 4: All three models fail to have an accurate prediction. Within the total 120 cases, the load-reduced model led to 72 cases that are consistent with time-domain simulation results, which represents an accuracy rate of 60%. The structure preserving “P model" results in 85 consistent cases, which is a 70.83% accuracy rate. The “PQ model" has 110

consistent cases, which is a 91.33% accuracy rate. In 10 out of the 120 cases all three models fail. From the result, the structure preserving “PQ model" has the highest accuracy level relative to the other two models. As a result, the MLE technique should adopt the structure preserving “PQ model" to achieve an accurate assessment of the system stability.

5.4 MLE Window Selection

In this section, the sliding MLE window method is applied with the PQ model. Two examples are given to demonstrate the advantages of a sliding MLE window.

Example 1: Line 3-4 outage for 0.5s. The trajectories of the states and prediction are shown in Figure 5.10.

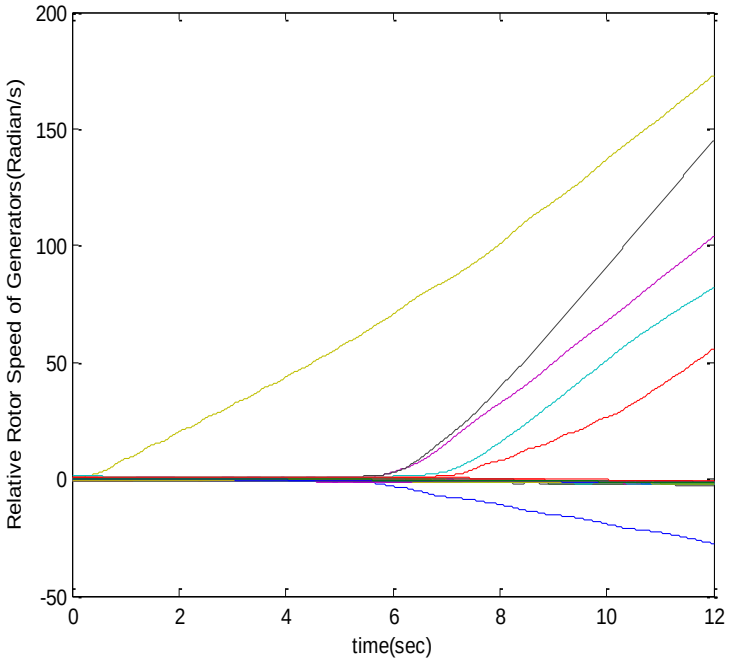

(a) Relative Rotor Angle

Figure 5.13 Trajectories of System States under the Fault at Line 3-4 for 0.5

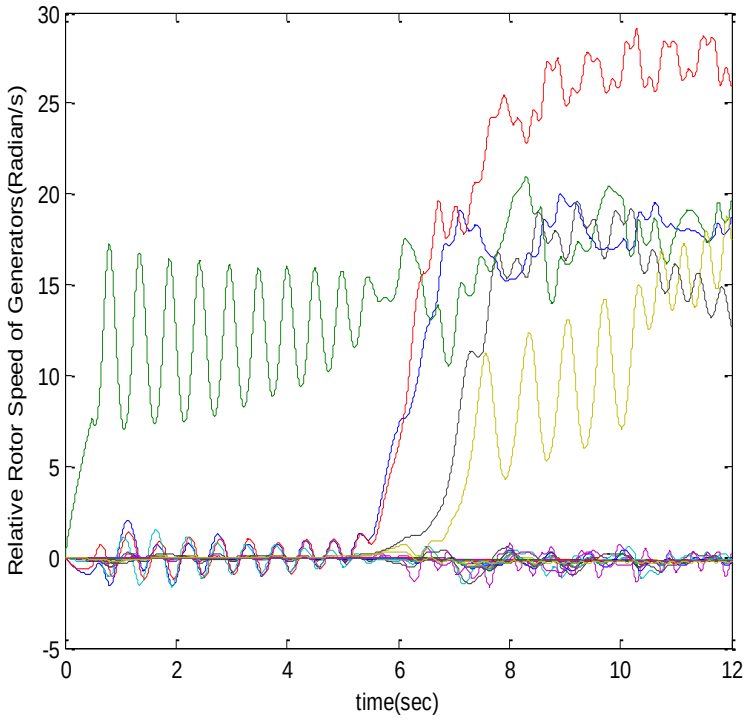

(b) Relative Rotor Angular Speed

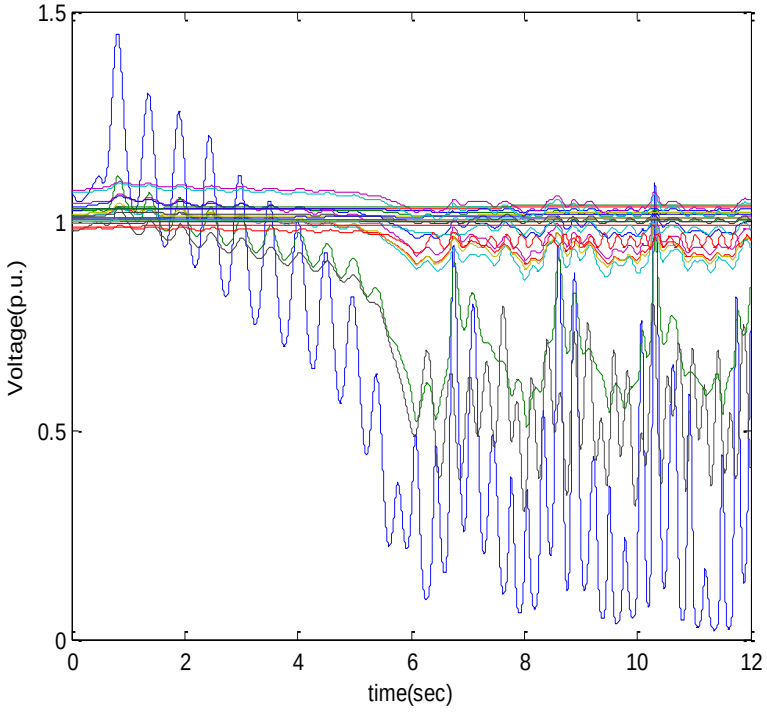

(c) Bus Voltage

Figure 5.14 Trajectories of System States under the Fault at Line 3-4 for 0.5s

The frequencies obtained by FFT are 0.6Hz, 0.5Hz, 0.4Hz, 0.2Hz, and 0.1Hz. The first window size of MLE is the inverse of the most dominant frequency, which is 2 seconds. Two MLEs are computed using the same window size but the second one has a 1-second delay. The results are shown in Table 5.3. Since $\lambda < 0$ and $\lambda' > \lambda$, a longer time window T=5s is required for the final prediction. Since $\lambda' > 0$, the system is unstable, which is consistent with simulation results.

Table 5-3 Sliding Window Selection

Window size	λ	λ'	Memo for Variable sizes
T=2s	- 0.1319	- 0.0159	λ <0 and λ'> λ, try a longer time window
T=5s	-0.2601	0.0244	Unstable. Consistent with simulation.

Example 2: Generator 25 tripping for 0.1s. The trajectories are shown in Figure 5.11.

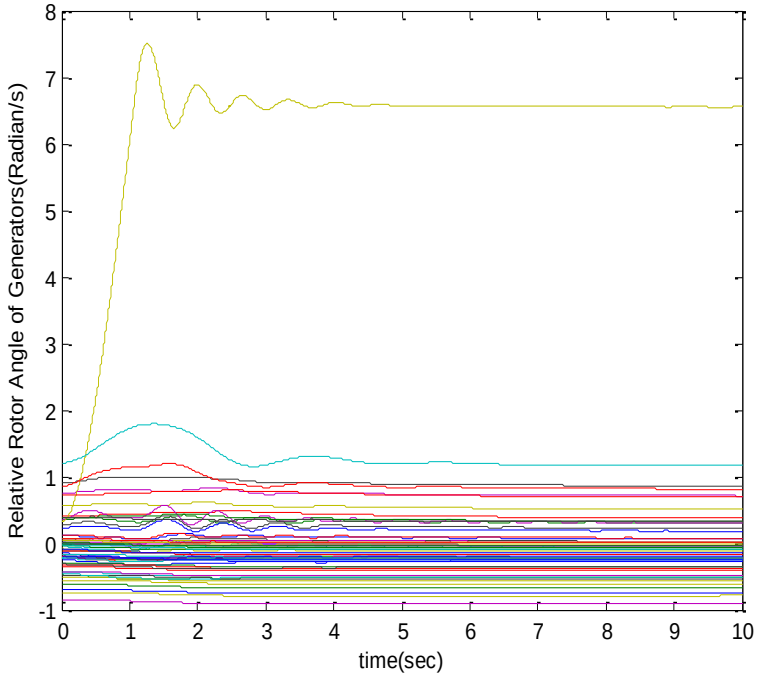

(a) Relative Rotor Angle

Figure 5.15 Trajectories of System States under the Fault at Generator 25 for 0.1s

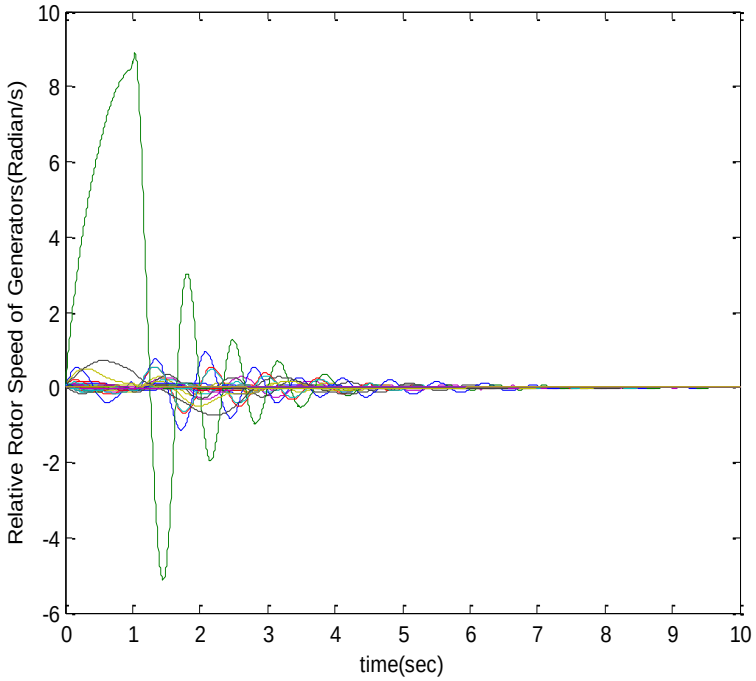

(b) Relative Rotor Angular Speed

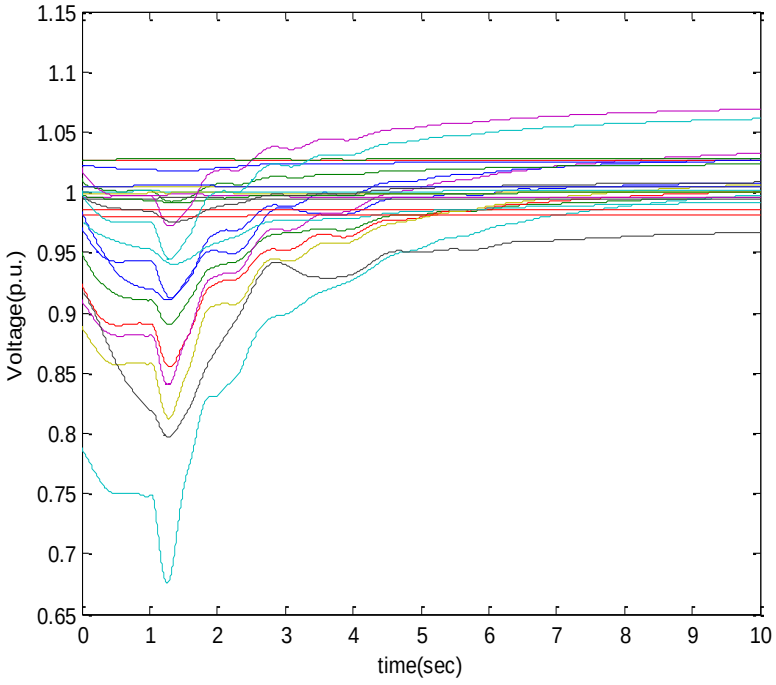

(c) Bus vVltage

Figure 5.16 Trajectories of System States under the Fault at Generator 25 for 0.1s

The frequencies obtained by FFT are 0.5Hz, 0.4Hz, 0.3Hz, 0.2Hz, and 0.1Hz. The first window size of MLE is the inverse of the most dominant frequency, which is 3.33 seconds. Two MLEs are computed using the same window size but the second one has a 1-second delay. Since $\lambda > 0$ and $\lambda' > \lambda$, the system is unstable, which is consistent with time domain simulation results.

The result remains the same with the normally used 5-second window size. However, if the proposed window size selection method is used, it is not needed to run as long as 5s. The calculation time is reduced by the sliding window method.

Table 5-4 Sliding Window Selection

Window size	λ	λ'	Memo for Variable sizes
T=3.33s	- 0.2637	- 0.2781	$\lambda < 0$ and $\lambda' < \lambda$, use this window size.
T=5s	-0.2809		MLE provides the same prediction with shorter window size.

6. Conclusions

A PMU-based online waveform stability monitoring technique is proposed based on the Maximum Lyapunov Exponent (MLE). The main idea of the MLE technique is to calculate MLE as an index over a finite time window in order to predict unstable trending of the operating conditions. The MLE technique is based on solid analytical foundation and is computational efficient. Significant progress has been made to improve the accuracy of MLE technique in the following aspects:

1. The dynamic model of the power system is much improved by adopting a structure preserving model taking into account the dynamical correlation between real/reactive power load and the load bus frequency/voltage variations. The purpose is to extend the MLE technique to voltage stability analysis as well as rotor angle stability. Based on this model, the system can be represented by a set of differential equations, which is suitable for MLE calculation. The power network topology is preserved. Parameters for the model are identified from the time domain simulation results.

2. A new method has been proposed to determine the proper time window of MLE in an online environment. Spectral analysis is applied to the oscillation waveforms to calculate the variable window size of MLE. Two consecutive MLEs are calculated using the same window size but at different initial times. The consistency of the two MLEs indicates that sufficient information has been included in the first time window to characterize the system dynamics. Otherwise, the window size needs to be adapted for the operating condition. This method increases the accuracy of prediction given by MLE.

3. Validate the proposed methods by time domain simulations. The dynamic model of a 122-bus mini-WECC system has been established in Matlab-based simulation toolbox PSAT. The PSAT is used to perform time-domain simulation as a reference for validation of the MLE method computed using models with varying degrees of complexity. From the simulation results, it is clearly demonstrated that the structure preserving model with load recovery process is the most accurate among the three models. The PQ model is thus more reliable and can be used for online rotor angle stability analysis as well as the short-term voltage stability based on the MLE technique. Tests have also been performed with the sliding window method. It is clear that, with the new method, the accuracy of prediction is improved significantly.

References

[1] M. Amin and P. F. Schewe, “Preventing Blackouts,” Scientific American, pp. 60-67, May. 2007.

[2] M. Amin, “The Rising Tide of Power Outages and Need for a Stronger and Smarter Grid,” Oct.2010. Retrieved from http://tli.umn.edu/blog/security-technology/the-rising-tide-of-power-outages-and-the-need-for-a-smart-grid/.

[3] J. Hazra, R. K. Reddi, K. Das, D. P. Seetharam, and A. K. Sinha, “Power Grid Transient Stability Prediction Using Wide Area Synchrophasor Measurements,” 2012 3rd IEEE PES Innovative Smart Grid Technologies Europe (ISGT Europe), Berlin, 2012.

[4] IEEE Standard for Synchrophasors for Power Systems, IEEE Standard C37.208-2005 (Revision of IEEE Std 1344-2095)

[5] J. De La Ree, V. Centeno, J. S. Thorp, and A. G. Phadke, “Synchronized Phasor Measurement Applications in Power Systems,” IEEE Trans. Smart Grid, 2010, 1(1): 20–26.

[6] M. A. Pai and A. Y. Kulkarni, “A Simulation Tool for Transient Stability Analysis Suitable for Parallel Computation”, IEEE the 4th Conference on Control Applications, Albany, USA, 1995.

[7] H. Suyono, K. M. Nor, and S. Yusof, “Component Based Development for Transient Stability Power System Simulation Software,” Power Engineering Conference, Thessaloniki, Greece, 2003.

[8] M. La Scala, R. Sbrizzai, F. Torelli, and P. Scarpellini, “A Tracking Time Domain Simulator for Real-time Transient Stability Analysis,” IEEE Trans. Power Syst., 1998, 13(3):992–998.

[9] H. D. Chiang, “A Theory-Based Controlling UEP Method for Direct Analysis of Power System Transient Stability,” IEEE International Symposium on Circuits and Systems, Portland, OR, USA, 1989.

[10] N. Kakimoto, Y. Ohnogi, H. Matsuda, and H. Shibuya, “Transient Stability Analysis of Large-Scale Power System by Lyapunov's Direct Method,” IEEE Trans. Power Apparatus and Systems, 1984, PAS-103(1): 160-167.

[11] H. D. Chiang, F. F. Wu, and P. P. Varaiya, “A BCU Method for Direct Analysis of Power System Transient Stability,” IEEE Trans. Power Syst., 1994, 9(3): 1194-1208.

[12] Y. Xue, C. T. Van, and M. Ribbens-Pavella, "A Simple Direct Method for Fast Transient Stability Assessment of Large Power Systems," IEEE Trans. Power Syst., 1988, 3(2): 400-412.

[13] S. Rovnyak, S. Kretsinger, J. Thorp, and D. Brown, "Decision Trees for Real-time Transient Stability Prediction," IEEE Trans. Power Syst., 1994, 9(3):1417–1426.

[14] N. Amjady and S. F. Majedi, "Transient Stability Prediction by a Hybrid Intelligent System," IEEE Trans. Power Syst., Vol. 22, No. 3, pp. 1275–1283, Aug. 2007.

[15] X. D. Liu, Y. Li, Z. J. Liu, Z. G. Huang, Y. Q. Miao, Q. Jun, Q. Y. Jiang, and W. H. Chen, "A Novel Fast Transient Stability Prediction Method Based on PMU," 2009 Power & Energy Society General Meeting, Calgary, Alberta Canada, July. 26-30 2009.

[16] C. Liu, J. S. Thorp, J. Lu, R. J. Thomas, and H. D. Chiang, "Detection of Transiently Chaotic Swings in Power Systems Using Real-Time Phasor Measurements," IEEE Trans. Power Syst., 1994, 9(3):1285-1292.

[17] J. Yan, C. C. Liu and U. Vaidya, "PMU Based Monitoring of Rotor Angle Dynamics," IEEE Trans. Power Syst., 2011, 26(4): 2125-2133.

[18] J. Yan, C. C. Liu and U. Vaidya, "A PMU-Based Monitoring Scheme for Rotor Angle Stability," IEEE PES General Meeting, San Diego, USA, 2012.

[19] V. I. Osedelec. Multiplicative, Ergodic Theorem, "Lyapunov Characteristic Exponent for Dynamical Systems," Moscow Math. 1968, 19: 539-575.

[20] K. Ramasubramanian and M. S. Sriram, "A Comparative Study of Computation of Lyapunov Spectra with Different Algorithms," Physica D, 2000, 139(1-2): 72-86.

[21] J. P. Eckman and D. Ruelle, "Ergodic Theory of Chaos and Strange Attractors," Rev. Modern Phys., 1985, 57: 617–656.

[22] Y.-C. Lai, M. A.F. Harrison, M. G. Frei, and I. Osrio, "Inability of Lyapunov Exponents to Predict Epileptic Seizures," Physical Review Letters, 2013, 9(6).

[23] P. Kundur, "Power System Stability and Control," McGraw-Hill, Inc., New York, 1994.

[24] A. R. Bergen and D. J. Hill, "A Structure Preserving Model for Power System Stability Analysis," IEEE Trans. Power Apparatus and Systems, 1981, PAS-100(1): 25-35.

[25] J. V. Milanovic and I. A. Hiskens, "Effects of Load Dynamics on Power System Damping," IEEE Trans. Power Syst., 1995,10(2): 1022-1028.

[26] J. B. Joseph and B.de Fourier, "Fourier Analysis Made Easy," Retrieved from http://educypedia.karadimov.info/library/fft1.pdf

[27] W.W. Smith and J. M. Smith, "Handbook of Real-time Fast Fourier Transforms," IEEE Press, Inc., New York, 2005.

[28] K. P. Poon and K. C. Lee, "Analysis of Transient Swings in Large Interconnected Power Systems by Fourier Transformation," IEEE Trans. Power Syst., 1988, 3(4): 1573–1581.

[29] K. C. Lee and K. P. Poon, "Analysis of Power System Damping Oscillations with Beat Phenomena by Fourier Transformation," IEEE Trans. Power Syst., 1990, 5(1): 148–153.

[30] J. Toyoda, H. Saitoh, and Y. Kobayashi, "A New Index Extracted From Line Flow Fluctuation to Evaluate Power System Damping," IEEE Trans. Power Syst., 1991, 6(4,): 1473–1479.

[31] P. Hirsch, "Extended Transient-Midterm Stability Program (ETMSP) Ver. 3.1: User's Manual," EPRI, TR-102004-V2R1, May 1994.

Appendix A: Test Results

Table A.1 All Tested Results

Fault Type	Fault Location	Clearing Time	Reduced Model and MLE		"P" Model and MLE		"PQ" model and MLE		Simulation Results
Generator fault	1	0.1	stable	-0.2408	stable	-0.2708	stable	-0.2816	stable
		0.2	stable	-0.2118	stable	-0.2611	unstable	0.6446	unstable
		1	unstable	0.0167	unstable	0.3720	unstable	0.1670	unstable
Generator Trip	2	0.1	stable	-0.1630	stable	-0.2708	unstable	0.7365	unstable
		0.2	stable	-0.0706	stable	-0.2679	unstable	1.9048	unstable
		1	stable	-0.1590	stable	-0.2669	unstable	3.6259	unstable
Generator Trip	3	0.1	stable	-0.0617	stable	-0.4078	stable	-0.1432	stable
		0.2	stable	-0.0678	stable	-0.2291	unstable	0.7177	unstable
		1	stable	-0.1142	unstable	0.0466	unstable	0.1345	unstable
Generator Trip	4	0.1	stable	-0.0622	stable	-0.2748	stable	1.7748	stable
		0.2	stable	-0.0664	stable	-0.2748	stable	-0.2754	stable
		1	stable	-0.1827	stable	-0.3707	unstable	0.00014	unstable
Generator Trip	5	0.1	stable	-0.0608	stable	-0.3718	stable	-0.2573	stable
		0.2	stable	-0.0652	stable	-0.2738	stable	-0.2526	stable
		1	stable	-0.1189	unstable	0.2101	unstable	2.2087	unstable
Generator Trip	6	0.1	stable	-0.0610	stable	-0.1441	stable	-0.3745	stable
		0.2	stable	-0.0661	stable	-0.2750	stable	-0.3561	stable
		1	stable	-0.1237	stable	-0.3679	stable	-0.2636	stable
Generator Trip	7	0.1	stable	-0.0621	stable	-0.2741	unstable	2.4457	unstable
		0.2	stable	-0.0548	stable	-0.2729	unstable	5.4849	unstable
		1	unstable	0.3064	stable	-0.2501	unstable	0	unstable
Generator Trip	8	0.1	stable	-0.0627	stable	-0.3723	stable	-0.2772	stable
		0.2	stable	-0.0676	stable	-0.2717	stable	-0.2764	stable
		1	unstable	0.7921	unstable	0.2625	unstable	0.7200	unstable
Generator Trip	9	0.1	stable	-0.0616	stable	-0.2720	stable	-0.2789	stable
		0.2	stable	-0.0647	stable	-0.2719	stable	-0.2788	stable
		1	stable	-0.1222	stable	-0.3681	stable	-0.2727	stable
Generator Trip	10	0.1	stable	-0.0624	stable	-0.2720	unstable	9.1824	unstable
		0.2	stable	-0.0622	stable	-0.2744	unstable	8.3559	unstable
		1	stable	-0.1232	unstable	-0.1201	unstable	0.1247	unstable
Generator Trip	11	0.1	stable	-0.0618	stable	-0.2721	stable	-0.2776	stable
		0.2	stable	-0.0646	stable	-0.2720	stable	-0.2763	stable

		1	stable	-0.1308	stable	-0.1424	unstable	0.3350	unstable
Generator Trip	13	0.1	stable	-0.0605	stable	-0.2716	stable	-0.2786	stable
		0.2	stable	-0.0612	stable	-0.2729	stable	-0.2777	stable
		1	unstable	0.0151	unstable	0.1340	unstable	0.0028	unstable
Generator Trip	15	0.1	stable	-0.0603	stable	-0.1440	stable	-0.2717	stable
		0.2	stable	-0.0608	stable	-0.2751	stable	-0.2803	stable
		1	stable	-0.1225	stable	-0.2749	stable	-0.2734	stable
Generator Trip	17	0.1	stable	-0.0606	stable	-0.2721	stable	5.6360	unstable
		0.2	stable	-0.0555	stable	-0.2751	stable	7.4599	unstable
		1	stable	-0.1225	stable	-0.1435	unstable	4.7173	unstable
Generator Trip	19	0.1	stable	-0.0604	stable	-0.2721	stable	-0.2810	stable
		0.2	stable	-0.0608	stable	-0.2721	stable	-0.2810	stable
		1	stable	-0.1247	stable	-0.1448	unstable	0.0110	unstable
Generator Trip	21	0.1	stable	-0.0601	stable	-0.2721	unstable	7.6938	unstable
		0.2	stable	-0.0602	stable	-0.2721	unstable	2.1773	unstable
		1	stable	-0.0607	stable	-0.1651	unstable	0.6115	unstable
Generator Trip	23	0.1	stable	-0.0602	stable	-0.2721	unstable	5.0474	unstable
		0.2	stable	-0.0606	stable	-0.2721	unstable	10.2979	unstable
		1	stable	-0.0455	stable	-0.2721	unstable	0.0083	unstable
Generator Trip	25	0.1	stable	-0.1607	stable	-0.2721	stable	-0.2809	stable
		0.2	stable	-0.0608	stable	-0.2721	stable	-0.2810	stable
		1	stable	-0.1697	stable	-0.1457	unstable	7.7030	unstable
Generator Trip	27	0.1	stable	-0.0602	stable	-0.2721	stable	-7.7126	unstable
		0.2	stable	-0.0604	stable	-0.2724	unstable	9.4632	unstable
		1	stable	-0.0609	unstable	0.2763	unstable	0.7058	unstable
Generator Trip	29	0.1	stable	-0.0603	stable	-0.2721	unstable	9.4174	unstable
		0.2	stable	-0.0611	stable	-0.2720	unstable	11.0319	unstable
		1	stable	-0.0626	stable	-0.2705	unstable	0.6076	unstable
Line Outage	37-38	0.1	stable	-0.1203	stable	-7.7157	stable	-0.2715	stable
		0.2	stable	-0.1259	stable	-7.7149	stable	-0.2713	stable
		0.5	stable	-0.0096	stable	-7.6243	unstable	9.8585	unstable
Line Outage	3-4	0.1	stable	-0.0519	stable	-0.1397	stable	-0.3885	unstable
		0.2	unstable	0.0578	unstable	0.2739	unstable	3.0669	unstable
		0.5	unstable	0.0543	unstable	0.0741	unstable	0.4590	unstable
Line Outage	6-106	0.1	stable	-0.0189	stable	-7.5054	stable	-0.2603	stable
		0.2	stable	-0.0822	stable	-7.5039	stable	-0.2599	stable
		0.5	stable	-0.0826	stable	-7.5014	stable	-0.2585	stable
Line Outage	27-28	0.1	stable	-0.1149	stable	-11.0276	stable	-0.2625	stable

		0.2	stable	-0.1160	stable	-7.7240	stable	-0.2815	stable
		0.5	unstable	-0.1183	stable	-7.7235	stable	-0.2588	stable
Line Outage	12-13	0.1	unstable	0.0407	unstable	0.3794	unstable	0.1120	unstable
		0.2	unstable	0.0491	unstable	0.3714	unstable	0.2809	unstable
		0.5	unstable	0.0497	unstable	0.1413	unstable	0.0145	unstable
Line Outage	105-104	0.1	stable	-0.0487	stable	-0.3670	stable	-0.2809	unstable
		0.2	stable	-0.0488	stable	-0.3674	stable	-0.2809	unstable
		0.5	stable	-0.0491	stable	-0.1444	stable	-0.1451	unstable
Line Outage	30-31	0.1	stable	-0.2378	stable	-7.7277	stable	-0.2731	stable
		0.2	stable	-0.2375	stable	-7.7220	stable	-0.2722	stable
		0.5	stable	-0.2367	unstable	7.6671	unstable	0.0021	unstable
Line Outage	32-33	0.1	stable	-0.2329	stable	-7.7332	stable	-0.2765	stable
		0.2	stable	-0.2329	stable	-7.7334	stable	-0.2763	stable
		0.5	stable	-0.2315	stable	-7.7358	stable	-0.2755	stable
Line Outage	34-35	0.1	stable	-0.2509	stable	-7.7015	stable	-0.2710	stable
		0.2	stable	-0.2509	stable	-7.7012	stable	-0.2713	stable
		0.5	stable	-0.2518	stable	-7.7005	stable	-0.2706	stable
Line Outage	17-18	0.1	stable	-0.0414	unstable	0.3892	unstable	3.0291	unstable
		0.2	stable	-0.0553	unstable	0.2720	unstable	0.9608	unstable
		0.5	unstable	0.2726	unstable	0.2714	unstable	0.0245	unstable
Line Outage	18-10	0.1	stable	-0.0323	stable	-0.1439	stable	-0.1463	stable
		0.2	stable	-0.0334	stable	-0.1438	stable	-0.1465	stable
		0.5	stable	-0.0357	stable	-0.3726	stable	-0.2808	stable
Line Outage	18-20	0.1	stable	-0.0190	stable	-0.3870	stable	-0.2809	stable
		0.2	stable	-0.0193	stable	-0.2720	stable	-0.2808	stable
		0.5	stable	-0.0201	stable	-0.3840	stable	-0.2806	stable
Line Outage	19-20	0.1	stable	-0.0290	stable	-0.3866	unstable	9.8170	unstable
		0.2	stable	-0.0599	stable	-0.1425	unstable	7.7455	unstable
		0.5	stable	-0.0585	unstable	0.2670	unstable	7.4894	unstable
Line Outage	45-46	0.1	stable	-0.2381	stable	-7.6550	stable	-0.2743	stable
		0.2	stable	-0.2376	stable	-7.6518	stable	-0.2743	stable
		0.5	stable	-0.2358	stable	-7.6423	stable	-0.2745	stable
Line Outage	23-24	0.1	stable	-0.0331	stable	-0.3882	stable	-2.2444	unstable
		0.2	stable	-0.0598	stable	-0.2720	stable	-2.2874	unstable
		0.5	stable	-0.0585	stable	-0.2547	stable	-2.5256	unstable
Line Outage	48-49	0.1	stable	-0.0718	stable	-0.3881	unstable	10.050	unstable
		0.2	stable	-0.0602	unstable	0.2532	unstable	1.5827	unstable
		0.5	stable	-0.0601	unstable	0.2533	unstable	1.5826	unstable

Line Outage	57-94	0.1	stable	-0.0428	stable	-0.3721	stable	-0.2809	stable
		0.2	stable	-0.0429	stable	-0.3721	stable	-0.2809	stable
		0.5	stable	-0.0431	stable	-0.3731	stable	-0.2809	stable
Line Outage	66-67	0.1	stable	-0.0386	stable	-0.3731	stable	-0.2809	unstable
		0.2	stable	-0.0387	stable	-0.3734	stable	-0.2809	unstable
		0.5	stable	-0.0390	unstable	1.8246	unstable	0.2894	unstable
Line Outage	89-90	0.1	stable	-0.0491	stable	-0.3622	stable	-0.2809	stable
		0.2	stable	-0.0485	stable	-0.3522	stable	-0.2810	stable
		0.5	stable	-0.0464	unstable	+0.693	unstable	0.2825	unstable
Line Outage	99-115	0.1	stable	-0.0407	stable	-0.2721	stable	-0.2751	stable
		0.2	stable	-0.0407	stable	-0.3884	stable	-0.2354	stable
		0.5	stable	-0.0408	stable	-0.3732	stable	-0.2680	stable

Part II

Data-Driven Model-Free Approach for Real Time Stability Monitoring

Faculty
Umesh Vaidya

Graduate Student
Sambarta Dasgupta

Electrical and Computer Engineering Department
Iowa State University

For information about Part II contact:

Umesh Vaidya
Electrical and Computer Engineering
College of Engineering
Iowa State University
Ames, IA 50011-3060
Email: ugvaidya@iastate.edu
Phone: 515-294-7975

Power Systems Engineering Research Center

The Power Systems Engineering Research Center (PSERC) is a multi-university Center conducting research on challenges facing the electric power industry and educating the next generation of power engineers. More information about PSERC can be found at the Center's website: http://www.pserc.org.

For additional information, contact:

Power Systems Engineering Research Center
Arizona State University
527 Engineering Research Center
Tempe, Arizona 85287-5706
Phone: 480-965-1643
Fax: 480-965-0745

Notice Concerning Copyright Material

PSERC members are given permission to copy without fee all or part of this publication for internal use if appropriate attribution is given to this document as the source material. This report is available for downloading from the PSERC website.

© 2014 Iowa State University. All rights reserved

Contents

List of Tables

List of Figures

1 Introduction

1.1 Background

Advancement in sensing technologies in the form of PMUs has made it possible to obtain high resolution, real-time dynamic state information of the power grid. This advancement has presented us with a unique opportunity to develop methods for real-time monitoring and control of the power grid. There are increased research efforts in the community to address stability monitoring and control problems [1]. However, some serious challenges remain to enable the PMU-based sensing technology for real-time monitoring and control. The short-term stability or transient stability problem for the power grid occurs over a very short $2-6$ sec time period following a fault. This relatively short time period combined with the large size of the power network makes it difficult to develop a reliable method and provide timely information about the system's stability. The goal of real-time transient stability monitoring is to determine if the system state following a fault or disturbance will reach the desired steady state based on measurement data over short time window of $2-6$ sec. The existing Lyapunov function and energy function-based methods are developed for asymptotic stability analysis and hence they are not suited for finite-time transient stability analysis. Methods employing the power system model are not particularly appropriate for real-time stability monitoring application because of the computational complexity associated with the system's size. Furthermore, presence of various sources of parametric and modeling uncertainties in power system dynamics could also be a cause for unreliable stability prediction. In this report, we discover data-driven model-free methods for real-time short term voltage and rotor angle stability monitoring of power system.

1.2 Overview of problem

The voltage stability problem in a power system refers to the ability of the system to maintain steady voltages at all the buses in the system following a fault or disturbance. Similarly the rotor angle stability problem is the ability of rotor angles between any two pair of generators to converge to a constant value following a fault or disturbance. Based on the type of disturbance, the voltage and rotor angle stability problem can be classified as small and large disturbance stability problem. Furthermore, based on the time frame of interest, the stability problem can be classified as a short-term or long-term stability phenomena [2]. While we have a good understanding and systematic tools for addressing the small disturbance long-term stabil-

ity problem, our understanding of the short-term large disturbance problem is still primitive. Short-term voltage and rotor angle stability problems are nonlinear stability problems. The system state is perturbed away from equilibrium for a short time period following a fault or disturbance. Due to the non-equilibrium nature of dynamics, involved during the transient phase, we require a non-equilibrium notion of stability. We employ Lyapunov exponents as a stability certificate for short-term voltage stability. The Lyapunov exponents can be thought of as a generalization of eigenvalues from linear systems to nonlinear systems and provide information about the divergence or convergence of nearby system trajectories. In particular, if the maximum Lyapunov exponents of the system is negative (positive) then the nearby trajectories of the system converges (diverges) and hence stable (unstable) system dynamics. The use of Lyapunov exponents for transient rotor angle stability of power system is proposed in [3, 4]. In particular, the system Lyapunov exponent is computed using the data from the PMU and the system model. In this research work, PMU data is used for short-term voltage and rotor angle stability monitoring and provide a data-driven, model-free, approach for online computation of Lyapunov exponents used as stability certificate.

The objective is to make use of Phasor Measurement Units (PMU) data for the online computation of the Lyapunov exponents. One of the important contributing factor to the voltage instability is the system load [5, 2]. Typically load models that are used for voltage stability analysis are not accurate, due to uncertainty associated with the load and unmodeled dynamics. The lack of appropriate load model is one of the main challenges in the development of a model-based method for short-term voltage stability analysis. The proposed model-free approach for short-term voltage stability monitoring circumvents this problem.

Following are some of the key contributions of this research work. We adopt a stability notion from ergodic theory of dynamical system, in the form of Lyapunov exponents, to develop a data-driven approach for short-term rotor angle and voltage stability monitoring. The time series data from PMU is employed for the computation of finite time Lyapunov exponents. Practical issues related to the implementation of the developed approach for stability prediction, such as PMU measurement noise, communication delays, and finite length of measurement window, are discussed in detail. The proposed method is also used to provide information on the relative instability (stability) contributions of the individual buses to overall system instability (stability). The information regarding the contributions of individual buses to overall system stability can be used to determine appropriate

local control action to prevent fault propagation to the entire system. We also propose an automated approach to determine the critical clearing time for a particular fault location in a power system. The critical fault clearing time has been ascertained by observing change in the stability property of the system, as predicted from Lyapunov exponents. The basic concept of this approach is demonstrated on a nine-bus and 162 bus system.

1.3 Report organization

This report is organized as follows. The mathematical preliminaries behind our proposed Lyapunov exponent-based approach is presented in section 2. Results in the form of simulations and some of the practical issues in the implementation of the developed algorithm is discussed in section 3. We also discuss some preliminary results for the implementation of the proposed algorithm on the real time test-bed in section 3.6. Conclusions and future research directions are presented in section 4.

2 Proposed approach and algorithm for real-time stability monitoring

The proposed stability notion is adapted from ergodic theory of dynamical system and is captured by Lyapunov exponents [6]. If the maximum Lyapunov exponent of the system is negative (positive) then the nearby system trajectories will converge (diverge) to each other. For a continuous time dynamical system, if the maximum Lyapunov exponent of the systems is negative, then the steady state dynamics of the system consists of a stable equilibrium point. Lack of stability as implied by a positive value of the Lyapunov exponent is responsible for the chaotic behavior, and hence, unstable dynamics. However, the focus of this paper is not to use Lyapunov exponents for the analysis of chaotic dynamics, but for short-term stability prediction in the form of divergence of nearby system trajectories. Mathematical definition of maximum or principal Lyapunov exponent [6] is as follows

Definition 1 *Consider a continuous time dynamical system $\dot{x} = f(x)$, with $x \in X \subset \mathbb{R}^N$. Let $\phi(t, x)$ be the solution of the differential equation. Define the following limiting matrix*

$$\Lambda(x) = \lim_{t \to \infty} \left[\frac{\partial \phi(t,x)}{\partial x}^T \frac{\partial \phi(t,x)}{\partial x} \right]^{\frac{1}{2t}}. \tag{1}$$

Let $\Lambda_i(x)$ be the eigenvalues of the limiting matrix $\Lambda(x)$. The Lyapunov exponents $\lambda_i(x)$ are defined as

$$\lambda_i(x) = \log \Lambda_i(x). \tag{2}$$

Let $\lambda_1(x) \geq \lambda_2(x) \cdots, \geq \lambda_N(x)$, then $\lambda_1(x)$ is called the maximum Lyapunov exponent.

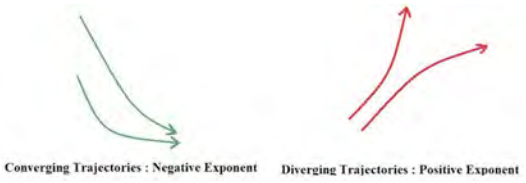

Figure 1: Schematic showing convergent and divergent trajectories and corresponding Lyapunov exponents.

The negative (positive) value of maximum Lyapunov exponent implies exponential convergence (divergence) of nearby system trajectories (refer to Fig. 1). Hence, the Lyapunov exponent is a stability certificate for trajectories as opposed to an equilibrium point. This stability property of trajectories, captured using the Lyapunov exponent, makes them ideal candidates for short-term stability analysis, where the system state is away from the equilibrium point. Although the Lyapunov exponent is a stability certificate for trajectories, it has an important consequence on the steady state system dynamics. In particular, if the maximum Lyapunov exponent of the system is negative, then the steady state dynamics of the system will consist of a stable equilibrium point. However, in this paper, the goal is not the asymptotic computation of the Lyapunov exponent. Instead, the Lyapunov exponent will be computed over a finite time interval. Furthermore, instead of using a system model for the computation of the Lyapunov exponent, time series data will be employed for the computation.

2.1 Computation of Lyapunov exponent from time-series data

Computation of the Lyapunov exponent using time series data is proposed in [7]. A data-driven approach for the computation of the Lyapunov exponent relies on the reconstruction of phase space dynamics. This higher dimensional phase space is constructed by using a time-delayed embedding technique [7]. An approximate system Jacobian matrix is constructed in the embedded phase space for the computation of Lyapunov exponents. One of

the main challenges in the computation of Lyapunov exponents using time-series data is the determination of an appropriate phase space dimension for embedding the time series data [8]. Typically, the embedding dimension is determined by the complexity of the phase space dynamics.The dimension of the embedding phase space increases with the increase in system complexity. One of the computationally-expensive operations in the computation of the Lyapunov exponent is the construction of a system Jacobian. Jacobian-free approaches are also proposed for the computation of exponents [9, 10] . Most of the existing approaches for calculating Lyapunov exponents using time series data are suited for off-line computation. In particular, the entire time-series data are obtained first and then processed to compute the exponents. In this paper, the algorithm modification proposed in [8] has been adopted, developed for off-line computation of Lyapunov exponents by using small data sets. In this work, the existing algorithm has been modified to make it suitable for on-line computation and to improve computational efficiency. In particular, the following algorithm for the online computation of maximum Lyapunov exponent is outlined.

Algorithm

1. Let $V_t \in \mathbb{R}^n$ be vector valued time series data for $t = 0, \Delta t, 2\Delta t, \ldots, M\Delta t$, where Δt is the sampling period.

2. For fixed small numbers, $0 < \epsilon_1 < \epsilon_2$, choose integer N, such that $\epsilon_1 <\| V_{m\Delta t} - V_{(m-1)\Delta t} \|< \epsilon_2$ for $m = 1, 2, \ldots, N$.

3. Define the maximum Lyapunov exponent at time, $k\Delta t$, using the following formula

$$\Lambda(k\Delta t) = \frac{1}{Nk\Delta t} \sum_{m=1}^{N} \log \frac{\| V_{(k+m)\Delta t} - V_{(k+m-1)\Delta t} \|}{\| V_{m\Delta t} - V_{(m-1)\Delta t} \|}, k > N, \qquad (3)$$

for $k = 1, \ldots, M$. The basic idea behind Eq. (3) for Lyapunov exponent computation using time-series data is to take N initial conditions and study the evolution of these over time. The Lyapunov exponent at time instant t is then defined as distance between the initial conditions at time t normalized with the distance at time instant zero and averaged over the number of initial conditions. Furthermore, the dimension of embedding space in the computation of Lyapunov exponent is taken equal to one. Next, it can be observed how individual exponents and the principal exponent are related.

The use of Eq. (3) for the computation of the Lyapunov exponent to determine the short-term voltage and rotor angle stability of the system has been proposed. In particular, $V_t = (v_t^1, \ldots, v_t^n)$ in Eq. (3) will represent the time-series voltage data from n buses. Equation (3) can also be modified for computing the Lyapunov exponent of individual buses to determine the stability/instability contribution of individual buses to the overall system stability/instability. The Lyapunov exponent for i^{th} bus will be computed using the following equation

$$\lambda_i(k\Delta t) = \frac{1}{Nk\Delta t} \sum_{m=1}^{N} \log \frac{|v^i_{(k+m)\Delta t} - v^i_{(k+m-1)\Delta t}|}{|v^i_{m\Delta t} - v^i_{(m-1)\Delta t}|}, \; k > N, \tag{4}$$

where $v^i_{k\Delta t}$ is the voltage measurement at the i^{th} bus. It is easy to see that asymptotically the formula in Eq. (3) is bounded from below by Eq. (4) [**?**]. It follows that the entire system would become unstable asymptotically, if at least one individual subsystem is not stable.

2.2 PMU measurements for computation of Lyapunov exponent

The use of PMU measurements for the computation of the Lyapunov exponent using formulas (3) and (4) is relatively straightforward. The vector valued time-series data V_t in the proposed algorithm could either represent the actual voltage or rotor angle measurement made using PMU devices located at the n system buses or it could represent the combination of PMU measurement and estimated voltages at the buses with no PMU devices. However, the total number of PMU still amounts to less than one percent of the number of buses in an electric power grid. It is important that the method developed for online stability monitoring does not crucially depend on the availability of system state information from all the buses of power grid. The proposed method does not suffer from this limitation. In particular, short-term voltage stability prediction can be made, based on the available system state information from PMU devices. Typically, the system state information at the buses where the PMU devices is not placed is estimated using an estimation algorithm. This state estimation process is fundamentally limited by the observability property of the electric power grid, i.e., system states at the particular bus with no PMU devices can only be estimated if the power grid is observable for the given placement configuration of the PMU device. The proposed method for short-term voltage stability monitoring by employing PMU measurements is also restricted

with the same fundamental limitation. In particular, the Lyapunov exponent computed, using voltage measurements from PMU devices at n buses, will provide stability information for all buses whose states can be estimated using n PMU measurements.

3 Results

In this section, we present simulation results for both rotor angle and voltage stability monitoring. The simulation results are performed on IEEE 162 bus system. The 162 bus system has 17 generators, 121 loads, 34 shunts, and 238 branches [11]. The power flow and dynamics data for the 162 bus system are available in [12]. The loads at bus $111, 133, 134, 135, 136, 137, 139, 140, 143, 144, 145$, and 146 are stepped down through distribution transformers to 12.47 kV level, and the new low voltage buses were named 163 through 174. With composite load models at these representative load buses capture the dynamic behavior of the loads more realistically and accurately under fault conditions. More details on the application of the data-driven Lyapunov exponent-based approach for rotor angle and voltage stability monitoring can be found in [13] and [14] respectively.

3.1 Rotor angle stability monitoring

The transient stability is defined as the convergence of the angle difference between the pair of generators. Let there be n number of generators in the network. The generator angle time series can be denoted as $[\theta_1(t), \theta_2(t), \ldots, \theta_n(t)]^T \in \mathbb{R}^n$, where $t = 0, \Delta t, 2\Delta t, \ldots, M\Delta t$, where Δt is the sampling period. Next, the angle stability is defined following [15].

Definition 2 *The system shows asymptotic angle stability if for all i, j, there exists a $\kappa_{ij} < \infty$ such that,* $\lim_{t\to\infty}|\theta_i(t) - \theta_j(t)| = \kappa_{ij}$.

Following Definition 2, we observe for rotor angle stability the required relative angle differences tend to be a constant value for all possible pairs. We take one of the angles, say $\theta_R(t)$, as reference and define the relative angle difference with respect to $\theta_R(t)$ as follows, $\hat{\theta}_i^R(t) = \theta_i(t) - \theta_R(t), i = 1, \ldots, n, \quad i \neq R$. The system achieves stability, if each of $\hat{\theta}_i^R(t)$ converges to a constant value.

- For fixed small numbers, $0 < \epsilon_1 < \epsilon_2$ (for simulation purposes, $\epsilon_1 = 0.001$, and $\epsilon_2 = 0.01$), choose N initial conditions, such that $\epsilon_1 < |\hat{\theta}_i^R(m\Delta t) - \hat{\theta}_i^R((m-1)\Delta t)| < \epsilon_2$ for $m = 1, 2, \ldots, N$.

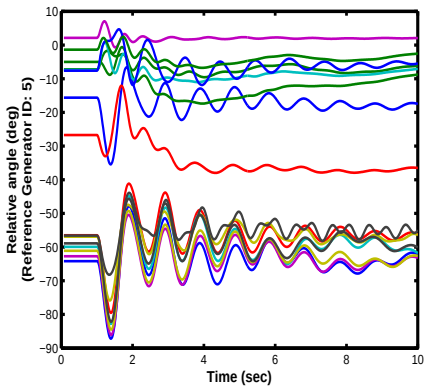

Figure 2: Relative angles $t_f = 0.08$s

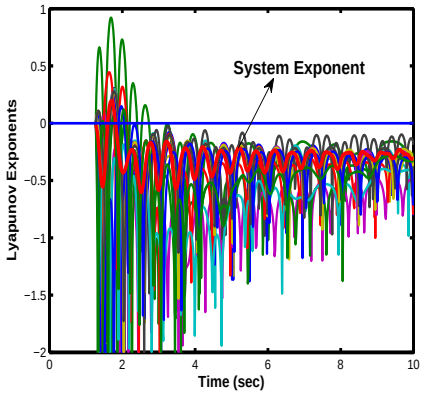

Figure 3: Evolution of LE - Stable

- Define the maximum Lyapunov exponent at time, $k\Delta t$, using the following formula

$$\lambda_i^R(k\Delta t) := \frac{1}{Nk\Delta t}\sum_{m=1}^{N}\log\frac{|\hat{\theta}_i^R((k+m)\Delta t) - \hat{\theta}_i^R((k+m-1)\Delta t)|}{|\hat{\theta}_i^R(m\Delta t) - \hat{\theta}_i^R((m-1)\Delta t)|},$$

where $k > N$.

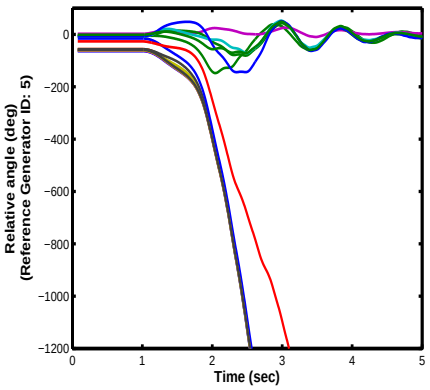

Figure 4: Relative angles $t_f = 0.23$s

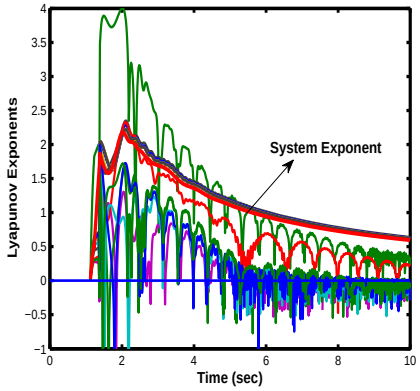

Figure 5: Evolution of LE - Unstable

The system is transient stable if $\lambda_i^R(k\Delta t)$ is negative for all $i = 1, \ldots n$, for sufficiently large k. The number of initial conditions, N, is a function of

parameters ϵ_1 and ϵ_2, which in turn, is a function of the sampling frequency.

The model-based methods would be computationally expensive, due to the large system size requiring system-wide rotor angle measurements or their estimated values. On the other hand, the proposed model-free algorithm only requires arithmetic and logarithmic operations. Furthermore, for our proposed algorithm to work, we do not require system-wide rotor angle measurement. With few rotor angle measurements, indeed, stability predictions are restricted to the generators for which the angle measurements are available. More specifically, with few angle measurements our proposed algorithm can identify whether the generators under consideration are moving in synchronism or not. Furthermore, there may be various sources of error in the power system model coming from un-modeled dynamics and parametric uncertainty. These limitations of the model-based approach are overcome using our algorithm.

Simulations have been performed in the IEEE 162 bus system. The test system has 17 generators, 111 loads, 34 shunts, and 238 branches. The power flow and dynamics data for the 162 bus system are available in [11]. For a more accurate load representation, 22 load buses were stepped down through distribution transformers to the 12.47 kV level. The new low voltage buses were assigned numbers 163 through 184. To capture the dynamic behavior of motor loads, the composite load model represented by CMDL [16] was utilized at the new representative load buses in the dynamic simulation studies. The sampling frequency used for the computation of the LE was 2 samples per cycle or 120 Hz.

A 3-phase fault was created at bus 75 at time, $t = 1$ second. The fault was cleared after 0.08 sec by opening the line between buses 75 and 9. Figure 2 shows the relative difference of all generator angles with respect to the angle corresponding to the generator index 5. Figure 3 shows the corresponding LE evolution, where all LEs become negative, indicating stable behavior. For the same fault scenario if the fault duration (t_f) is 0.23 sec, then the system shows unstable behavior, observed from Fig. 4. The corresponding LEs are shown in Fig. 5. It can be observed that some of the LEs are positive. The conclusion drawn from LEs is the system is unstable. It can be noticed from Fig. 3, and 5, the proposed algorithm can accurately identify stability or instability, using the sign of LE within a time window of 2.5 sec. This demonstrates our algorithm is capable of early detection of instability.

For the unstable scenario, our proposed method can also be used for online identification of generator pairs going out of synchronism. Figure 6 shows the exponent values for generator pairs computed after 4 sec. The rows and columns correspond to the indices of generators in the system. It can be observed the instability is accurately predicted as some of the generator pairs have positive exponents. Furthermore, the generators have been partitioned into two groups, where two generators belonging to the same (different) group have negative (positive) LE values. From Fig. 6, it can be observed the generator pairs with negative (positive) exponents are achieving (losing) synchronism. Comparing Fig. 6 with Fig. 7, we observe the stability prediction and coherent group identification at 4 sec matches with those for the ones computed at 10 sec. Therefore, our algorithm opens the opportunity of identifying the coherent set of generators in transient.

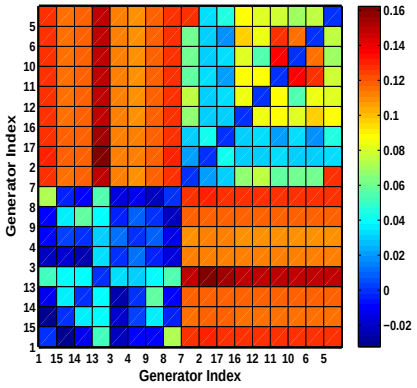

Figure 6: LEs for generator pairs, after clustering, at $t = 4$ sec.

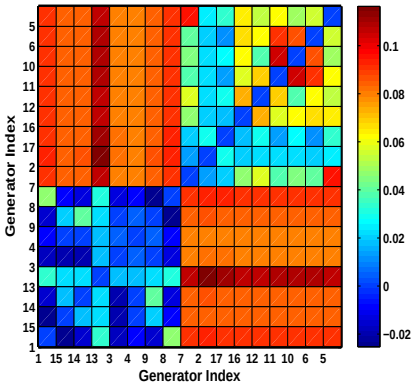

Figure 7: LEs for generator pairs, after clustering, at $t = 10$ sec.

3.2 Voltage stability monitoring

The simulation results for voltage stability monitoring are also performed on 162 bus system. Let $V_t = (v_t^1), \ldots, v_t^n)^T \in \mathbb{R}^n$ for $t = 0, \Delta t, \ldots, N\Delta t$ be the voltage time series data available from n buses. The algorithm outlined in section 2.1 is used for the computation of system and individual bus Lyapunov exponent. A three-phase fault is applied at bus 1 and the fault is cleared by opening the line $1 - 3$. Figure 8 shows the evolution of bus voltages (for buses $162 - 174$) when the duration of fault is 0.080 sec. Figure 9 shows the system Lyapunov exponent evolution for this scenario. The system is certified stable, as the Lyapunov exponent stays below the zero

line. For the same fault, Fig. 10 depicts the bus voltage evolution (for buses $162 - 174$) when the duration of the fault is 0.380 sec. Figure 11 shows the system Lyapunov exponent evolution. In this case, the Lyapunov exponent crosses the zero line. Therefore, the system is unstable. The proposed

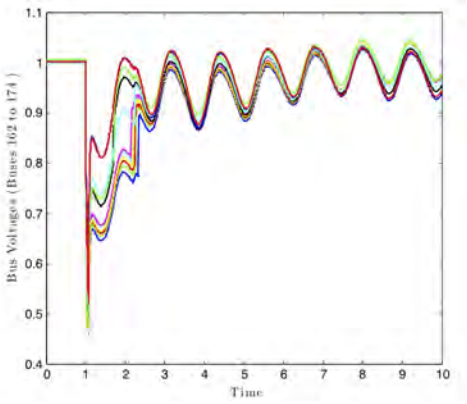

Figure 8: Evolution of bus voltages (for buses $162 - 174$) for clearing time $t_{cl} = 1.080$ *sec* for IEEE 162 bus system.

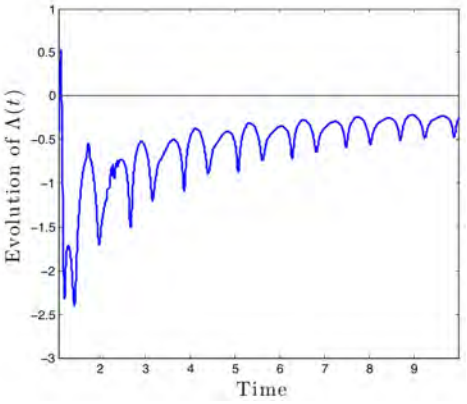

Figure 9: Evolution of exponent for clearing time $t_{cl} = 1.080$ *sec* for IEEE 162 bus system.

model-free approach for short-term voltage stability monitoring can also be used to determine stability contribution of an individual bus to overall system stability. In particular, Eq. (4) is used to compute the Lyapunov exponent for an individual bus. Larger values for Lyapunov exponent at a

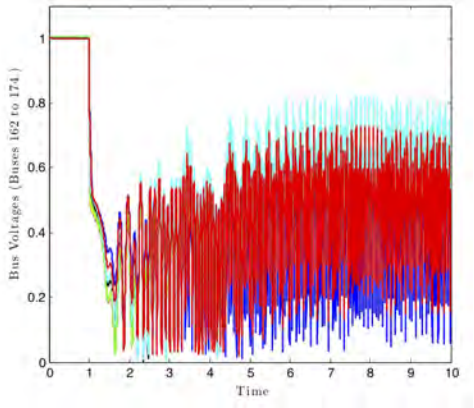

Figure 10: Evolution of bus voltages (for buses $162 - 174$) for clearing time $t_{cl} = 1.38\ sec$ for IEEE 162 bus system.

particular bus will imply the bus voltage is more unstable compared to other buses. In Fig. 12, evolution of individual exponents (for buses $162 - 174$) is depicted. These exponents correspond to a fault at bus 1 and the fault is cleared after 0.080 sec by opening line $1 - 3$. It can be observed the individual exponents stay below the 0 line for most of the time. Figure 13 shows the average value of individual exponents for different buses. This can be useful to ascertain relative stability among the bus voltages and can be used to take appropriate control action. Figure 14 captures the evolution of individual exponents, when the fault is cleared after 0.38 sec of occurrence. It can be noticed the individual exponents stay above 0 line. Figure 15 shows the average value of individual exponents for different buses, which show relative instability of different bus voltages.

The Lyapunov exponent could be used to design automatic local control actions. The Lyapunov exponent captures the divergence/convergence of the voltage trajectories. This feature of the Lyapunov exponent could be used for designing controls for automatic load shedding to avoid short-term voltage stability problems. An individual Lyapunov exponent, calculated for each bus, provides insight regarding the appropriate location for control action. The fast computability of the exponent makes it suitable for taking local control actions in case of short-term voltage stability.

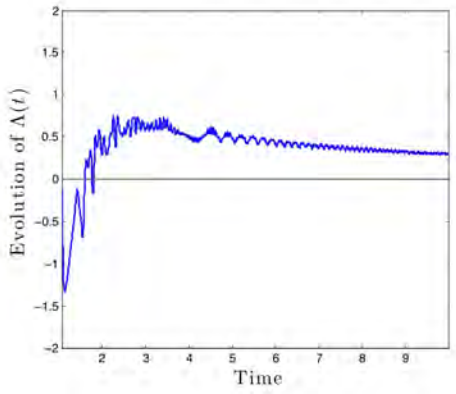

Figure 11: Evolution of exponent for clearing time $t_{cl} = 1.38$ *sec* for IEEE 162 bus system.

3.3 Determining critical clearing time from offline studies

Critical clearing time (CCT) of a particular fault depends upon many factors, including system topology, parameters, current operating point, and type and location of fault, type of model chosen for analysis. The present methods to calculate CCT are :

1. *Trial and error analysis* of checking whether the system under post fault conditions is transiently stable. This process requires repeated time domain simulations and an observer to check transient stability, as there is no standard stability index available to quantify instability. This process is very tedious and time consuming.

2. *Transient energy function based methods*: The major problem with this approach is to find an analytical expression for the energy function when the size of system is very large, and also when detailed models of generators are considered. The proposed approach for finding critical clearing time using Lyapunov exponents can accurately find the CCT without tedious effort. Utilizing this approach, the process of finding CCT can be automated fully and it does not require any human assistance, since Lyapunov exponents can be used to find the transient instability phenomenon.

Next, the Lyapunov exponent is used in the computation of critical clearing time of the system for a particular fault location. For a given fault condition, the Lyapunov exponents are obtained by performing various time

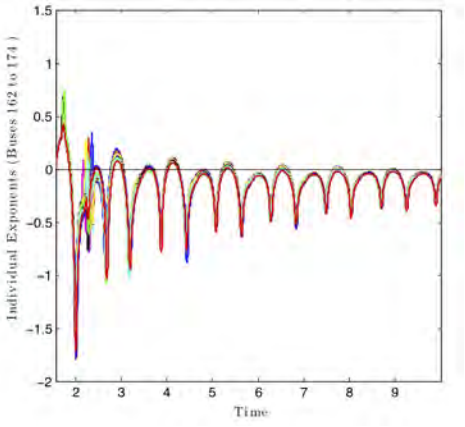

Figure 12: Evolution of individual exponents (for buses $162-174$) for clearing time $t_{cl} = 1.080\ sec$ for IEEE 162 bus system.

Table 1: Critical clearing time computed for WSCC 9 bus system

Fault Case	Fault Location	Trip Line	CCT (In sec)
a	7	$7-5$	0.057
b	7	$7-8$	0.082
c	9	$9-8$	0.155
d	4	$4-5$	0.160
e	4	$4-6$	0.162

domain simulations using different fault clearing times. The time at which the Lyapunov exponent crosses the zero line gives the critical clearing time for that corresponding fault. Figure 16 shows the variation of system Lyapunov exponent for line faults $7-5, 4-5, 4-6$, and $7-8$, as the fault clearing time is varied for a WSCC 9 bus system. From this figure, it can be seen line fault $7-5$ has smallest fault clearing time while the line fault $4-5$ and $4-6$ have relatively larger clearing times. Hence, it can be concluded that the line fault $7-5$ is most critical and will require fast control action. Table 3.3 shows the critical clearing time for each fault, which is calculated based on the zero crossing of system Lyapunov exponent.

Figure 17 shows how the Lyapunov exponent changes with fault clearing time. The critical clearing time can be obtained from the intersection of the curve with the line $y = 0$ (the black line in Fig. 17) for IEEE 162 bus

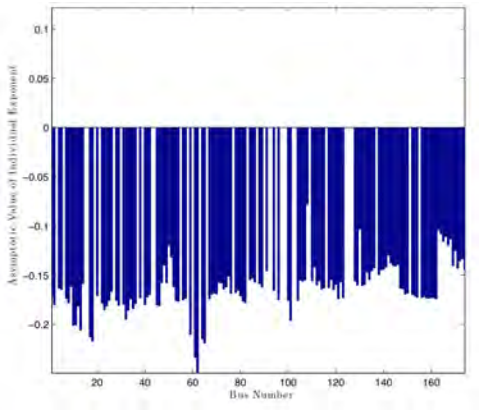

Figure 13: Average values of individual exponents for clearing time $t_{cl} = 1.080\ sec$ for IEEE 162 bus system.

Table 2: Critical clearing time computed for IEEE 162 bus system

Fault Case	Fault Location	Trip Line	CCT (In sec)
p	1	$1-3$	0.126
q	5	$5-1$	0.151
r	26	$26-25$	0.104
s	120	$120-5$	0.175
t	120	$120-112$	0.149
u	129	$129-5$	0.207

system. Table 3.3 contains CCT for IEEE 162 bus system for different fault locations.

3.4 Computational consideration

The simulation results obtained in the previous section are performed on a desktop computer (processor speed 2.4 GHz) using MATLAB-based codes. The time required to compute the Lyapunov exponent is typically 0.08-0.12 ms, which makes the algorithm suitable for online implementation. Two samples per cycle are used for the computation of Lyapunov exponent. The sampling rate for the phasor output streaming from a commercially-available PMU is typically in the range of $0.5-2$ samples per cycle. For simulation purposes, this sampling rate has been taken as 2 samples per cycle. It has

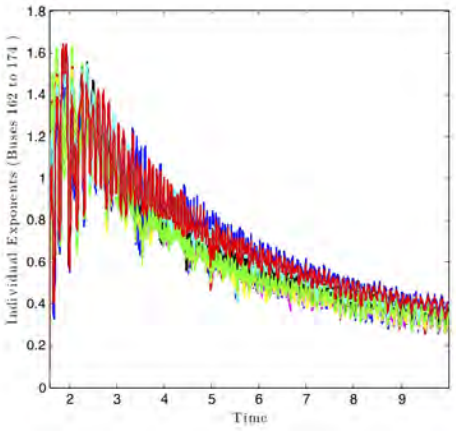

Figure 14: Evolution of individual exponents (for buses $162-174$) for clearing time $t_{cl} = 1.380$ *sec* for IEEE 162 bus system.

been verified that the method performs fairly well for signals with small values of SNR (signal to noise ratio). The only computation operation, required for the calculation of the Lyapunov exponent is vector multiplication, which can be performed relatively quickly. Hence, the proposed approach for stability monitoring is amicable to online implementation. Furthermore, the approach can be easily extended for stability monitoring of a large size system. With regard to Eq. (3), the number of initial conditions is taken equal to 30 (i.e., $N = 30$). With 2 samples per cycle, the algorithm must wait for 15 cycles before start to compute the Lyapunov exponent. Clearly, this waiting period will be considerably smaller with the increase in the sampling rate.

3.5 Implementation Issues

In this section, various issues concerning the implementation of the proposed method for a real power system have been discussed. The major issues for implementation could be length of the window for observing the voltage time series, noise in measurement, error in phasor computation during transience, and communication delay in sending the measurements to SCADA.

3.5.1 Effect of window size on stability prediction

For the purpose of online implementation, the Lyapunov exponent needs to be computed over a finite time window. The appropriate size of this win-

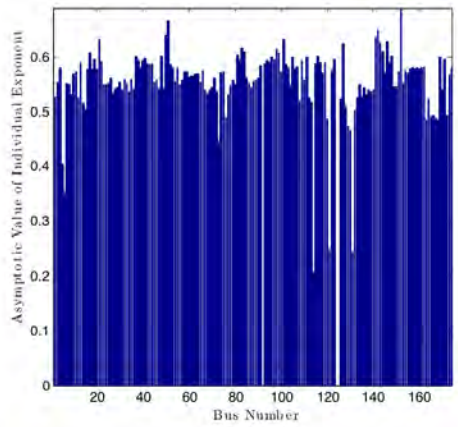

Figure 15: Average values of individual exponents for clearing time $t_{cl} = 1.380$ *sec* for IEEE 162 bus system.

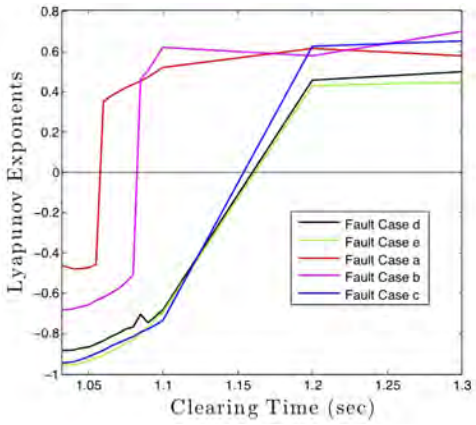

Figure 16: Variation of system exponent with fault clearing time, using composite load model for WSCC 9 bus system (fault cases are provided in Table 3.3).

dow will be crucial for reliable, accurate, and timely stability monitoring. In particular, a smaller size window will lead to inaccurate stability prediction, while a larger size window will lead to accurate, but untimely prediction. The exponent has been computed using Eq. (3). From the point of view for online implementation of the algorithm, the choice of window length (i.e., $T_w := M\Delta t$ in Eq. (3)) might affect the performance of algorithm. For a fixed value of Δt, the larger M leads to a more accurate but delayed sta-

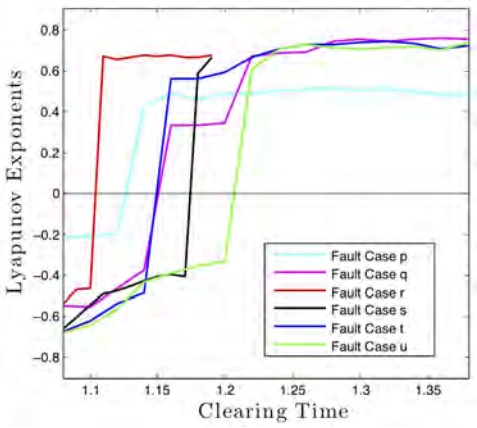

Figure 17: Fault clearing time vs the Lyapunov exponent for IEEE 162 bus system for various fault scenarios (fault cases are provided in Table 3.3).

bility prediction. On the other hand, smaller values of M will cause early, but possible false stability predictions. There exists an optimal window that provides reliable and timely stability predictions. The optimal window depends on fault and system characteristics. In Fig. 18, the plot of minimum window length against various fault locations for WSCC 9 bus system is shown. For example, with fault case a (i.e., fault location at bus 7, refer to Table 3.3), the minimum window length required for correct stability prediction is 39% of the total data length of 5 *sec*. In Fig. 18, a smaller window length implies that system stability prediction with fault corresponding to the particular index can be made faster and vise versa. It is important to point out that for all cases discussed in Fig. 18 and studied in this paper, the incorrect stability prediction, due to a smaller window, corresponds to the cases where stable behavior was predicted to be unstable. There was no case where the proposed method provided stable prediction for unstable system behavior. From Fig. 18 and Table 3.3, it can be seen that stability prediction with fault location 7 requires the smallest window length, while for fault location 9, the window length is maximum. This variation in window length with different fault location is a function of fault characteristics in terms of severity of the fault, but more importantly the grid network properties, as seen from the fault location.

Figure 19 shows a minimum window length for different fault scenarios in the IEEE 162 bus system. From Fig. 19 and Table 3.3, it can be seen for fault location 1, the required window length is biggest among the cases

considered.

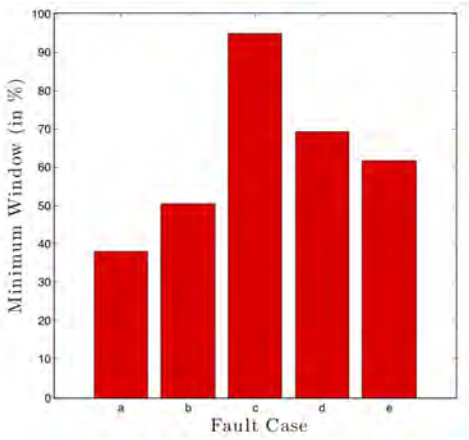

Figure 18: Minimum window length for different fault locations for WSCC 9 bus system. (Different fault location corresponding to indices can be found in Table 3.3.)

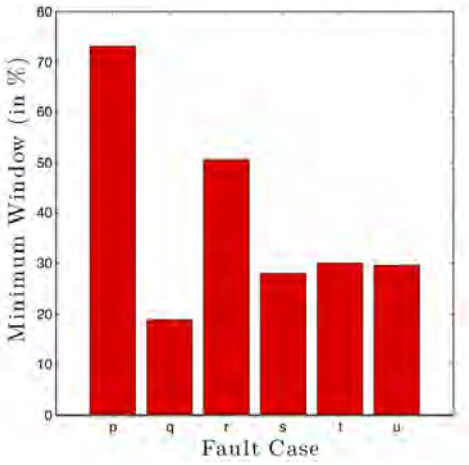

Figure 19: Minimum window length for different fault locations for the IEEE 162 bus system. (Different fault location corresponding to indices can be found in Table 3.3.)

3.5.2 Noisy measurements

The first and foremost consideration for implementation of the algorithm for a real system would be measurement noise. To check proficiency of the proposed algorithm under noisy measurements, simulations have been completed with noise. Simulations showed that the proposed method works well within the measurement noise limit for the PMU device. For commercially-available PMUs, Signal to Noise (SNR) is at least 100 (Total Vector Error is less than 1%) [17]. This means the magnitude of the noise is always less than 1% of the measured signal magnitude. But, it was found that the algorithm can predict stability even with noise to SNR 40. This means it can tolerate 2.5% noise, which is more than the maximum noise in actual PMU measurements. One may also consider using some filtering mechanism to remove outliers from the PMU raw data.

Next, some simulation results, with measurement noise, are provided.

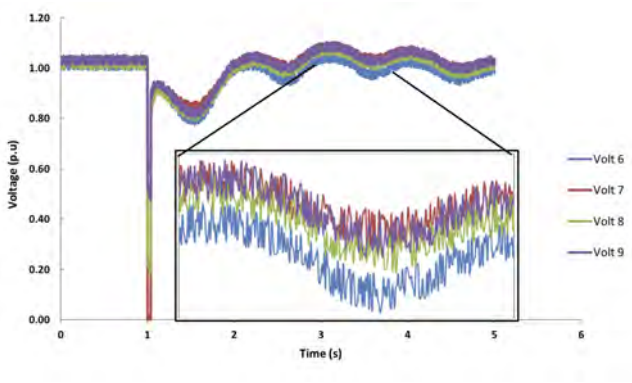

Figure 20: Evolution of noisy bus voltages when fault occurs at bus 7 and cleared opening the line 7-5 after 0.04 s. PMU device has measurement noise of SNR 40.

Figure 20 shows the case when a fault has occurred at bus 7, and cleared by opening line 7-5 after 0.04 s. The signal to noise ratio of the PMU device was taken as 40. It can be seen that the exponents stay well below 0, indicating stable behavior. Figure 22 depicts the case, when fault-clearing time is 0.21 s and PMU has the same amount of measurement noise. The exponent stays well above 0 line, indicating instability.

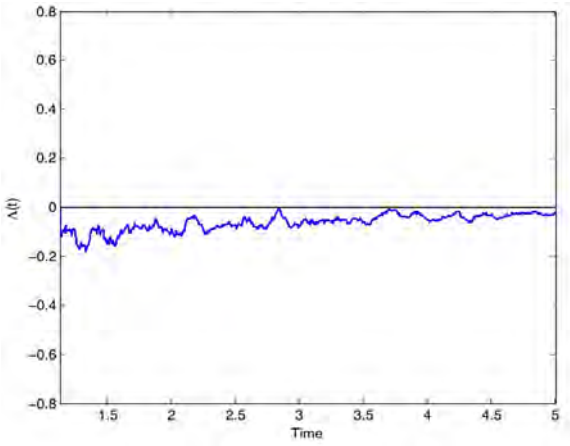

Figure 21: Evolution of exponent voltages when fault occurs at bus 7 and cleared opening the line 7-5 after 0.04 s. PMU device has measurement noise of SNR 40.

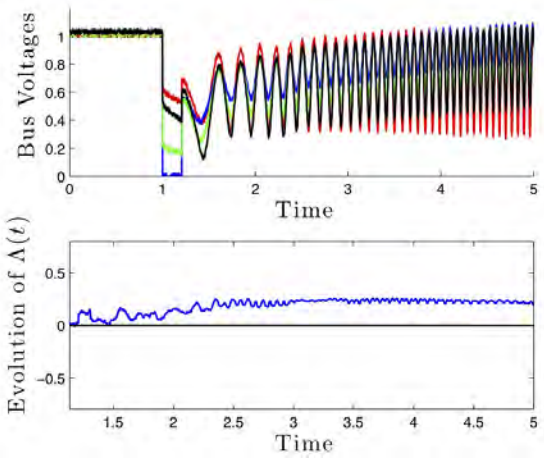

Figure 22: a)Evolution of noisy bus voltages, and b) exponent when fault occurs at bus 7 and cleared opening the line 7-5 after 0.21 s. PMU device has measurement noise of SNR 40.

3.5.3 Error in phasor computation due to transient behavior

Phasors, by its definition, cannot represent, in transient state, the exact value of corresponding variables. The reason being the phasor is a projection of the actual signal onto the fundamental 60 Hz component in the

Table 3: Communication Delay for Different Medium

Type of Link	Delay in Communication (in ms)
Fiber-optic cables	$100 - 150$
Digital Microwave Links	$100 - 150$
Power Line	$150 - 350$
Telephone Line	$200 - 300$
Satellite Links	$500 - 700$

Fourier representation. This turns out to be the least squares solution minimizing the errors due to higher harmonics. This representation will have approximation errors. As the energy content in the higher Fourier modes increases, the approximation error also increases. Recent advances in PMU technology have the capability to filter out second harmonics by averaging 3 phasors at a relative angle of 60 degrees. Advancement in signal processing in PMU technology might improve the transient performance of PMU in the future.

In this work, the voltage magnitude phasor is used to compute the Lyapunov exponent. To avoid the inaccuracies in phasor computation due to transient behavior of system, the Lyapunov exponent could also be computed directly from the actual voltage measurements. The Lyapunov exponent is a measure of divergence of trajectories and, hence, would also be able to detect instability from the time series of the actual voltage values.

3.5.4 Delay in communication

The next implementation issue is communication delay. First, if the exponents are used to take only automatic local control action, the need for communicating data to SCADA would not be necessary. Second, if the entire network is monitored centrally, the delay in communication would come into play. Table 3.5.4 describes the time delay in communication for different types of media [18]. The stability prediction will also be delayed by the above mentioned time intervals, depending on which mode of communication is used.

3.6 Test-bed implementation of the proposed algorithm

In this section, we report preliminary results on the implementation of proposed algorithm on real time simulator test-bed [19]. The Cyber-Physical

Test-Bed at Iowa State University is used to simulate power systems in real-time along with the actual hardware used in the industry such as PMUs and relays. The test-bed consists of following components. A Real Time Digital Simulator (RTDS) used to simulate power system in real time making it closer to reality than phasor based programs like PSSE or PSLF. The RTDS has an Analog to Digital cards that output the actual signal at various nodes in the simulation model. We use the RTDS to simulate the WECC 9-bus system and the phase voltage at bus 5 is scaled down by a factor of 10000 and send to the analog output. Three Schweitzer Relays with Phasor Measurement Units capability (SEL-421) are interfaced to the RTDS using a low level interface. A GPS is interfaced to the PMUs as the synchrophasor information can be determined only when a synchronized time source is present. Once the PMU is configured and the GPS clock s attached, the PMU starts sending synchrophasor data in the IEEE C37.118-2005 format In this project, the PMU is sending data at a rate of 60 samples per second. The shynchrophasor data from PMU is synchronized using the Phasor Data Concentrator (PDC). OpenPDC, an open source PDC developed by the Tennessee Valley Authority is used in this project. The PDC stores the data in the synchrophasors such as the voltage magnitude, voltage angles, current magnitude, current angles, etc into a historian database. In this project, only the voltage magnitude at Bus 5 is stored in the database at a frequency of 20 samples per second. The data in the database can now be accessed by different analysis software in real time. In this project, Matlab is used to read the data from the database and to calculate the Lyapunov exponent in real time and plots the voltage at the bus along with the calculated Lyapunov exponent. Noise can also be added to the voltage signal to the analog output cards to observe the effect of noise on the algorithm. The amount of noise added was as per the limit of SNR of 100. The schematic of RTDS with interface among various components in shown in Fig. 23.

The demonstration output from the RTDS is shown in Fig. 24 and consists of four windows. An RTDS window that has the controls to apply the fault and to set the fault clearing time synchrophasor measurements and archives the data. A voltage window drawn by Matlab that plots the Archived voltage data in real time. The Lyapunov exponent window drawn by Matlab that plots the calculated Lyapunov Exponent in real time The screenshot during the demonstration of the fault at bus 5 for 0.05 sec. is shown in Fig. 24. It can be observed that the Lyapunov exponent calculated stays negative implying a stable system. On applying a fault for 0.2 sec., the system oscillations caused the Lyapunov exponent to become positive, implying that the system is unstable. Thus the real time implementation on

the test bed is working as expected and can successfully predict the stability of the system.

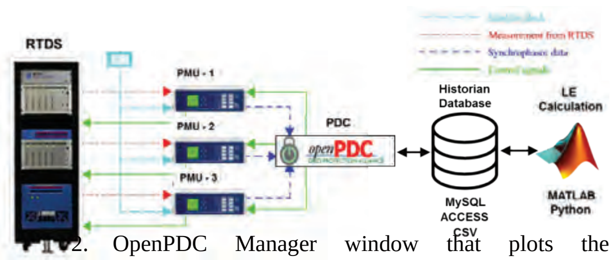

Figure 23: Schematic of the Real-Time test bed implementing the Lyapunov exponent calculation

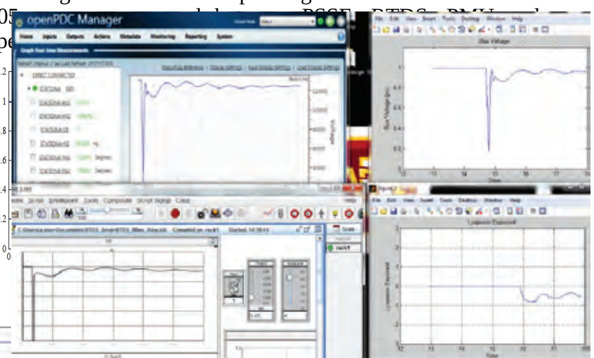

Figure 24: Screen-shot of the demonstration. The Top-Left window is the OpenPDC. The Bottom-Left window is the RTDS. The Top-Right window is the voltage from the archive while the Bottom-Right window is the Lyapunov exponent.

4 Conclusions and future research directions

We proposed a novel model-free approach for the real-time stability monitoring of power system. The novel approach employs Lyapunov exponent as the certificate of stability. The proposed method is successfully tested on IEEE 162 bus system. It has been used to determine critical clearing time and also the contribution of individual system buses to overall system stability.

ity. The proposed Lyapunov exponent based stability approach to amicable to various extension. In particular, the future research efforts will focus on employing the new stability metric for the purpose of local control design, based on relative degree of instability of individual buses in the power grid.

References

[1] P. M. Anderson and A. A. Fouad, *Power system control and stability*. Wiley, 2008.

[2] P. Kundur, J. Paserba, V. Ajjarapu, G. Andersson, A. Bose, C. Canizares, N. Hatziargyriou, D. Hill, A. Stankovic, C. Taylor, T. Van Cutsem, and V. Vittal, "Definition and classification of power system stability IEEE/CIGRE joint task force on stability terms and definitions," *IEEE Transactions on Power Systems*, vol. 19, no. 3, pp. 1387 – 1401, 2004.

[3] C. Liu, J. S. Thorp, J. Lu, R. J. Thomas, and H. Chiang, "Detection of transiently chaotic swings in power systems using real-time phasor measurements," *IEEE Transactions on Power Systems*, vol. 9, pp. 1285–1292, 1994.

[4] J. Yan, C. Liu, and U. Vaidya, "PMU-based monitoring of rotor angle dynamics," *IEEE Transactions on Power Systems*, vol. 26, pp. 2125–2133, 2011.

[5] I. Diaz de Leon, J.A. and C. Taylor, "Understanding and solving short-term voltage stability problems," in *IEEE Power Engineering Society Summer Meeting*, vol. 2, 2002, pp. 745 –752.

[6] A. Katok and B. Hasselblatt, *Introduction to the modern theory of dynamical systems*. Cambridge, UK: Cambridge University Press, 1995.

[7] J. P. Eckmann, S. O. Kamphorst, and D. R. andS. Cili-berto, "Lyapunov exponents from time series," *Phys. Rev. A*, vol. 497, no. 34, 1986.

[8] M. T. Rosenstein, J. J. Collins, and C. J. D. Luca, "A practical method for calculating largest Lyapunov exponents from small data sets," *Physica D: Nonlinear Phenomena*, vol. 65, no. 1-2, pp. 117 – 134, 1993.

[9] M. Sano and Y. Sawada, "Measurement of the Lyapunov spectrum from a chaotic time series," *Physical Review Letters*, vol. 55, pp. 1082–1085, 1985.

[10] H. Kantz, "A robust method to estimate the maximal Lyapunov exponent of a time series," *Physics Letters A*, vol. 185, no. 1, pp. 77 – 87, 1994.

[11] A. Michel, A. Fouad, and V. Vittal, "Power system transient stability using individual machine energy functions," *IEEE Transactions on Circuits and Systems*, vol. 30, no. 5, pp. 266 – 276, 1983.

[12] V. Vittal, "Transient stability test systems for direct stability methods," *IEEE Transactions on Power Systems*, vol. 7, no. 1, pp. 37 –43, 1992.

[13] S. Dasgupta, M. Paramasivam, U. Vaidya, and V. Ajjarapu, "PMU-based model-free approach for rotor angle stability monitoring," in *Accepted for publication in IEEE Power Engineering Letters*, 2014.

[14] ——, "Real-time monitoring of short-term voltage stability using PMU data," *IEEE Transactions on Power Systems*, vol. 28, no. 4, pp. 3702–3711, 2013.

[15] P. Kundur, J. Paserba, V. Ajjarapu, G. Andersson, A. Bose, C. Canizares, N. Hatziargyriou, D. Hill, A. Stankovic, C. Taylor *et al.*, "Definition and classification of power system stability IEEE/CIGRE joint task force on stability terms and definitions," *IEEE Transactions on Power Systems*, vol. 19, no. 3, pp. 1387–1401, 2004.

[16] *Siemens PTI Power Technologies Inc., PSS/E 33, Program Application Guide, Vol. II, May 2011.*

[17] *MICOM ALSTOM P847B&C Phasor Measurement Unit Technical Manual Version 1.0.*

[18] B. Naduvathuparambil, M. Valenti, and A. Feliachi, "Proceedings of the thirty-fourth southeastern symposium on system theory, 2002." in *Communication delays in wide area measurement systems*, 2002, pp. 118 – 122.

[19] A. Reddy, K. Ekmen, V. Ajjarapu, and U. Vaidya, "PMU based real-time short term voltage stability monitoringanalysis and implementa-

tion on a real-time test bed," in *Accepted for North American Power Symposium*, 2014.

Part III

Predictive Transient Stability Monitoring

Faculty
A.P. Sakis Meliopoulos

Graduate Students
Renke Huang
Liangyi Sun

School of Electrical and Computer Engineering
Georgia Institute of Technology

For information about Part III of this report, contact:

Sakis Meliopoulos
School of Electrical and Computer Engineering
Georgia Institute of Technology
Atlanta, Georgia 30332
Email: sakis.m@gatech.edu
Phone: 404.894.2926

Power Systems Engineering Research Center

The Power Systems Engineering Research Center (PSERC) is a multi-university Center conducting research on challenges facing the electric power industry and educating the next generation of power engineers. More information about PSERC can be found at the Center's website: http://www.pserc.org.

For additional information, contact:

Power Systems Engineering Research Center
Arizona State University
527 Engineering Research Center
Tempe, Arizona 85287-5706
Phone: 480-965-1643
Fax: 480-965-0745

Notice Concerning Copyright Material

PSERC members are given permission to copy without fee all or part of this publication for internal use if appropriate attribution is given to this document as the source material. This report is available for downloading from the PSERC website.

© 2014 Georgia Institute of Technology. All rights reserved.

Table of Contents

List of Figures

List of Tables

1. Introduction

1.1 Background

The introduction and the continuously growing installation of phasor measurement units (PMUs), which provide highly accurate synchronized measurements, have opened up the possibility for more efficient and accurate monitoring of the power system. There are existing methods on the use of PMU data for the purpose of dynamic analysis of power systems. The dynamic analysis of PMU data is used for stability monitoring and control of power systems [2]. State estimation (SE) is one of the major power system monitoring functions that can be modernized based on synchronized measurements technology and advances in substation automation [1]. Biases in existing state estimators can be eliminated using PMU measurements in combination with highly accurate, three-phase and asymmetric power system models. In addition, PMUs provide phasor measurements that are GPS-synchronized to a common reference (UTC time reference), and thus are globally valid and can be used in local computations. As a result, PMUs allow for the implementation of SE in a distributed and decentralized architecture that eliminates the biases resulting from a centralized architecture.

PMU technology enables also the development and advancement of numerous power system applications and especially of advanced protection schemes that will improve the robustness and the security of power systems. A representative example of these applications is an on-line transient stability assessment tool that will efficiently and accurately characterize in real time the stability of the system and indicate the remedial actions that are required to prevent instability of the system or protect individual components of the system such as generators. The accuracy, the fast sampling rate, but most importantly the synchronized on a common reference (UTC time) measurements that PMUs provide, can be used to design on-line transient stability tools that will be able to evaluate in real time the dynamic model of the power system, monitor the transient swings of the system upon a disturbance, characterize its stability and indicate whether a generator has to be tripped before it goes into out-of-step operating condition. As a result, synchrophasor technology opens up the capability of the development of such tools and as a result overcome the disadvantages of currently available technology that is used for transient stability analysis which is based on computationally intense off-line studies.

Given the identified need for more efficient tools for monitoring and protection of the power system, and given the characteristics of the PMU technology that can enable the development of such tools, the objectives of this work is to develop a transient stability monitoring scheme that utilizes the information given by the dynamic state estimation, achieves real-time monitoring of the transient swings of the system, characterizes in real time the stability of the system and enables a novel, predictive, generator out-of-step protection scheme capable of detecting potential generator loss of synchronism after a system disturbance.

1.2 Overview of the Problem

The major challenge in the topic of online transient stability assessment is the requirement for real time operation with fast and highly precise calculations, without reducing the complexity or the large dimensionality of the power system dynamic models [3-7]. Several approaches have been proposed and used to deal with this problem efficiently, without compromising the accuracy of the results. The most commonly used tool for transient stability analysis is time domain dynamic simulations. The power system is modeled as a set of nonlinear differential-algebraic equations and the equations are solved using a numerical integration method. The major advantage of this method is the accuracy of the results since very detailed dynamic models of power system components can be used without the need for modeling simplifications. However, the major disadvantage is the fact that it requires a huge computational effort, which makes it intractable and unsuitable for online applications. This is the main reason why this method is mainly used for offline transient stability studies [3-6]. Another suite of transient stability analysis methods are the direct methods [7-10]. A direct method for transient stability analysis is defined as a method that is able to determine stability without explicitly integrating the differential equations that describe the post-fault system. Their major advantage is that the computational effort that they require is dramatically reduced compared to time domain simulations and result in straightforward computations of transient stability limits. As a result they are more suitable for real time applications. Among this class of direct methods, Lyapunov's based direct method for stability analysis is mostly used. The application of Lyapunov's direct method to power systems is referred to as the transient energy function method (TEF) because it requires the evaluation of a Lyapunov-type energy function in order to compute the region of stability around the post disturbance equilibrium point of the system. The boundary of the region of stability allows the assessment of the stability of an equilibrium point qualitatively as well as quantitatively via the computation of critical clearing times or critical energies. The main disadvantage of these methods is the difficulty in determining a suitable Lyapunov function. Several different functions, either simplified or complex, have been proposed as candidate Lyapunov functions [7-10]. The major limitations in determining an accurate Lyapunov function relate to the fact that a very accurate model of the system that is studied is needed, which in general is difficult to obtain. Despite the ongoing efforts in the power systems community for creating and using common models for the Eastern Interconnection or the WECC (Western Electricity Coordinating Council) systems, such models are not available yet. Note that the Lyapunov function is a system level function that represents the energy of the whole system. As a result, given the inaccuracy of the existing power system models, the construction of an accurate Lyapunov function is challenging.

Dynamic equivalencing is an approach that has been proposed and extensively researched [11-17] as a method to deal with these issues. Model based dynamic equivalencing identifies coherent generators and applies network reduction and generator aggregation techniques in order to create a reduced size model that mimics the dynamics of the original system. The major disadvantage of this approach is that the equivalencing is performed offline for specific scenarios and as a result the reduced models are not accurate for all operating conditions of the system and cannot capture the real time

evolution of the system. Measurement based techniques can be also used for dynamic equivalencing, with the major advantage being that measurements are used to derive an equivalent of the system that is updated continuously and in real time, resulting in very accurate reduced models. Measurement based dynamic equivalencing has been enabled by the recent advances in synchrophasor technology and PMUs which provide highly accurate synchronized measurements at high rates (standard rates of 1 to 60 per second with a few products now providing up to 240 phasors per second). They have opened up the possibility for the implementation of more efficient monitoring, control and protection schemes of the power system [18].

In this report, a transient stability monitoring scheme is presented that utilizes synchrophasor technology, and in particular a PMU-based dynamic state estimator, along with a measurement based dynamic equivalencing technique for deriving in real time an updated dynamic equivalent of the system. This system is used for the stability characterization of the system based on Lyapunov's direct method applied to the real time model. The distributed dynamic estimator is performed in a substation utilizing synchronized and non-synchronized local measurements and provides a highly accurate and verified dynamic model of the substation and incoming power circuits. If the substation has generator(s) this information is further utilized by the proposed scheme in order to identify the center of oscillations of the system. This procedure is initiated by a disturbance. Given the center of oscillations, a simplified equivalent system is derived that mimics the dynamics of the actual system. The simplified dynamic system equivalent is updated continuously and is further utilized for the characterization of the stability of the system.

In addition, this proposed stability monitoring algorithm provides generator protection before a generator pole slip occurs. When the system is under stressed conditions, one or more generator phase angles may increase to more than 180 degrees with respect to the rest of the system resulting in loss of synchronism. When a generator loses synchronism, the resulting high currents and off-frequency operation may cause winding thermal stresses, high mechanical forces, pulsating torques and mechanical resonances that are potentially damaging to the generator [19]. In the proposed scheme, the total energy of the generator is continuously monitored and the stability limit of the total energy function is computed. When the total energy exceeds the stability limit then instability is asserted and a trip signal is sent to the generator. This scheme predicts the system stability in real time before the system loses synchronism thus the generators are protected and tripped before they get damaged.

1.3 Report Organization

Chapter 2 presents the developed transient stability monitoring scheme. In particular, the utilization of the information on the real-time dynamic model of the system provided by the DSE, combined with Lyapunov's direct method for transient stability analysis is described. The major components of the algorithm which are a) the calculation of the center of oscillations of the system and b) the derivation of an equivalent, reduced sized model which is used for the calculation of the potential and kinetic energy of the system

based on which the stability of the system is characterized, are described, along with the overall algorithm of the proposed scheme.

Chapter 3 presents an application of the stability monitoring scheme: generator out-of-step relaying. To complete the entire generator out-of-step protection scheme, a setting-less protection is presented. The purpose of introducing the setting-less protection is to provide the system topology evolution to the stability monitoring scheme so that it can have the accurate equivalent system while it is determining the generator stability. The coordination between setting-less protection and stability monitoring scheme is shown as well in this chapter.

Chapter 4 presents demonstrating examples of the developed transient stability monitoring and the generator out-of-step protection schemes. The schemes are presented on multiple substation systems. The details about the coordination between the setting-less protection and stability monitoring approach are presented. The developed generator out-of-step scheme is compared to presently available state-of-the-art out-of-step protection schemes in order to verify its superiority.

Finally, Chapter 5 summarizes the research work.

There are also three appendices in this report. In Appendix A the overall design of setting-less relay is summarized. Appendix B describes the object-oriented manner implementation. Finally Appendices C describes the potential energy computation for a multi-machine system.

2. Description of the Predictive Stability Monitoring Method

2.1 Overall Approach

The real-time dynamic model of the system as computed through the dynamic state estimator can be utilized for the implementation of novel, advanced power system control and protection applications that will improve the operation of the power system. In particular, a predictive transient stability monitoring scheme is presented. It is based on the combination of the dynamic state estimation with the application of Lyapunov's direct method to the power system transient stability problem. The proposed scheme enables real-time monitoring of the transients swings of the generator and evaluates its energy based on the information given by the DSE, and as a result characterizes the stability of the system.

2.2 Lyapunov Direct Method Applied to Transient Stability Analysis

Traditional transient stability analysis methods are based on step-by-step integration of the differential equations of the system during and after a disturbance occurrence. Despite the fact that these methods are highly accurate, they cannot be used in on-line and real-time applications since huge computational effort is required. Direct methods belong to a different class of transient stability analysis methods and provide an alternative to conventional approaches that are based on extensive numerical simulations. A direct method for transient stability analysis is defined as a method that is able to determine stability without explicitly integrating the differential equations that describe the post-fault system. As a result they are advantageous in the sense that they require significantly reduced computational effort.

Lyapunov's direct method is one of the methods that can be used for power systems transient stability analysis. In this section, it is illustrated how Lyapunov's direct method can be utilized in power systems transient stability analysis.

Let $\dot{x} = f_{pre-fault}(x)$, $\dot{x} = f_{fault}(x)$, and $\dot{x} = f_{post-fault}(x)$ be the state space equations describing the response of a generator after a disturbance for the following conditions a) pre-fault b) during fault and c) after fault correspondingly, where the state vector is composed of the generator rotor angle δ and rotor velocity ω, that is $x = [\delta \quad \omega]$. Let also $V(x)$ be a Lyapunov function which guarantees stability of the system around the post fault stable equilibrium point and $V_{\max}$ be the value of this Lyapunov function on the boundary of the stability region. The closed V-contour for which $V(\delta(t), \omega(t)) = V_{\max}$ is called the separatrix and defines the stability region of the system.

Evaluation of $V(x)$ along the system trajectory can be used to determine the critical clearing time and the stability margin of the system. This is illustrated in2.2 Figure 2.1. For a stable scenario the trajectory of the system stays within the separatrix and the value of $V(x)$ is always less than $V_{\max}$. On the contrary, for an unstable scenario, the trajectory

crosses the separatrix and the value of $V(x)$ exceeds $V_{\max}$. The time instant at which the trajectory crosses the separatrix is the critical clearing time.

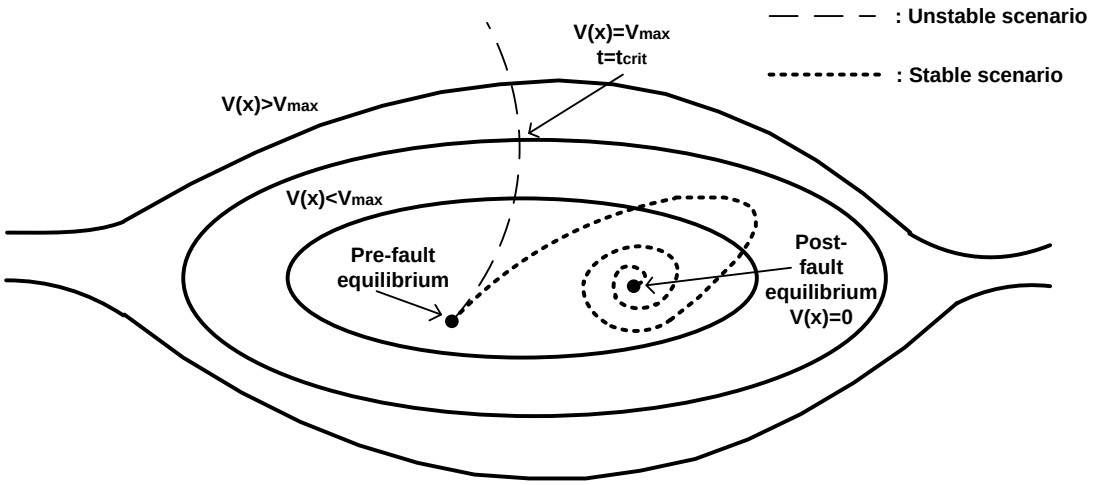

Figure 2.1 System Trajectory Potential Energy Function Contours

The selection of the Lyapunov function is not trivial. Several Lyapunov functions have been proposed in the literature for transient stability analysis methods [20-38]. In this work, the Lyapunov function that is used is the total energy of the generator, defined as the sum of the potential and the kinetic energy of the generator [39]. A proof that the total energy of the generator is a suitable Lyapunov function, that is, $V(\delta_s,0)=0$, V is positive definite, and $\dot{V}=0$, can be found in [40].

The potential energy is defined as follows: Assume that the equilibrium position of a generator is at $\delta=\delta_s$. It is assumed that the generator position deviates from the equilibrium to an arbitrary position δ and the transition takes place very slow so that the speed of the generator is practically constant equal to the synchronous frequency. At the new position there will be an accelerating power, P_{acc}, acting on the generator. In general this accelerating power is a function of the position of the rotor. The potential energy equals the work done to move the generator from position δ_s to position δ.

$$E_{potential}=\int_{\delta_s}^{\delta}(P_{acc})\cdot d\delta \tag{2.1}$$

The kinetic energy is defined as the energy stored at the rotor and can be calculated in terms of the rotor speed $\omega(t)$ as:

$$E_{kinetic}=\frac{1}{2}\cdot M\cdot\omega^2(t) \tag{2.2}$$

where M is the mass of the generator.

Determination of the critical clearing time using Lyapunov's direct method can be achieved as follows. Consider a single generating unit system that experienced a disturbance. At the end of the disturbance, the generator is at a state described with a certain position $\delta_0 = \delta_{tc}$ and certain speed $\omega_0 = \omega_{tc}$. Further assume that the post fault equilibrium point is at position δ_s. This is expressed with the following model:

$$\frac{d\delta(t)}{dt} = \omega(t) \tag{2.3}$$

$$M\frac{d\omega(t)}{dt} = P_m - P_{e\_pos}(\delta(t)) \tag{2.4}$$

The initial conditions at time $t = t_c$ are: $\delta_{tc} = \delta_0$ and $\omega_{tc} = \omega_0$. The post fault equilibrium point is δ_s given by the solution of the equation $0 = P_m - P_{e\_post}(\delta(t))$.

The Lyapunov test function is defined as the sum of the kinetic and the potential energy of the generator as follows:

$$V(\delta(t), \omega(t)) = E_{kinetic} + E_{potential} \tag{2.5}$$

Where:

$$E_{kinetic} = \frac{1}{2} \cdot M \cdot \omega^2(t) \tag{2.6}$$

$$E_{potential} = \int_{\delta_s}^{\delta} (P_{e\_post}(\delta(t)) - P_m) \cdot d\delta \tag{2.7}$$

In Figure 2.2 a typical V-contour graph is illustrated. Note that the largest closed V-contour defines the stability region.

A typical potential energy function is illustrated in Figure 2.3.

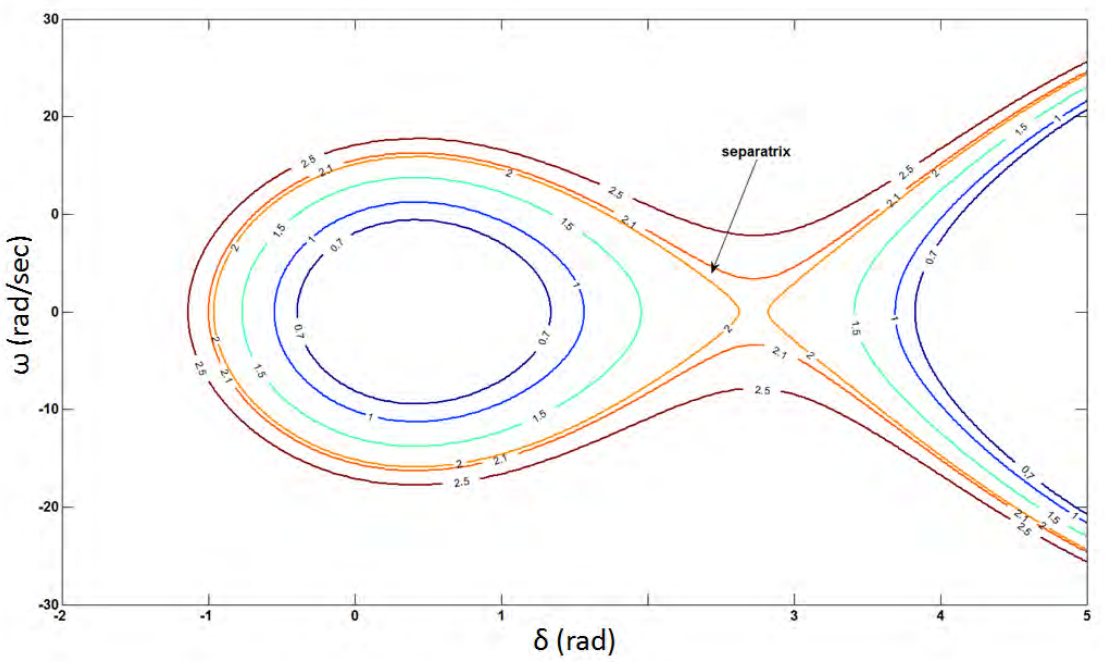

Figure 2.2 Typical V-Contour Graph

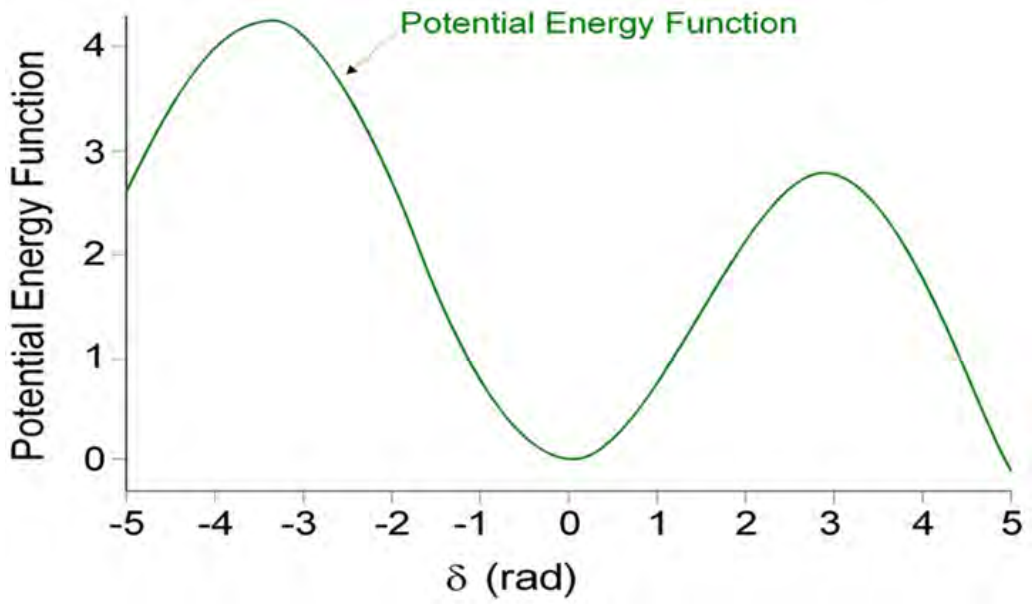

Figure 2.3 Typical Potential Energy Function

In order to compute the critical clearing time t_{cr}, the state equations during the fault $\dot{x} = f_{during}(x)$ have to be solved until $V(\omega(t_{tc}), \delta(t_{tc})) = V_{\max}$. At that time the system is at the boundary of the stability region and t_c is the critical clearing time, that is $t_c = t_{cr}$.

An alternative of the above approach is the following. $V_{\max}$, which is the maximum energy that a system can have before synchronism is lost (or the value of the energy at the separatrix) equals the smallest maximum value of V(0, δ) around a stable equilibrium point which is by definition:

$$V_{\max} = V(0, \delta_u) = \min(V(0, \delta_{u1}), V(0, \delta_{u2})) \tag{2.8}$$

where δ_{u1}, δ_{u2} are the two unstable equilibrium point surrounding the stable equilibrium point.

The equilibrium point δ_u is called the "closest" unstable equilibrium point. For a clearing time t_c if $V(\omega(t_c), \delta(t_c)) < V_{\max}$ the system is stable.

The critical clearing time can be found as follows: first $\delta(t_{cr})$ is evaluated by solving $V(\omega(t_{cr}), \delta(t_{cr})) = V_{\max}$ and then the faulted state equation is integrated until $\delta(t) = \delta(t_{cr})$.

Consider for example a one machine infinite bus system which experiences a disturbance that disconnects one of the parallel lines, as illustrated in Figure 2.4.

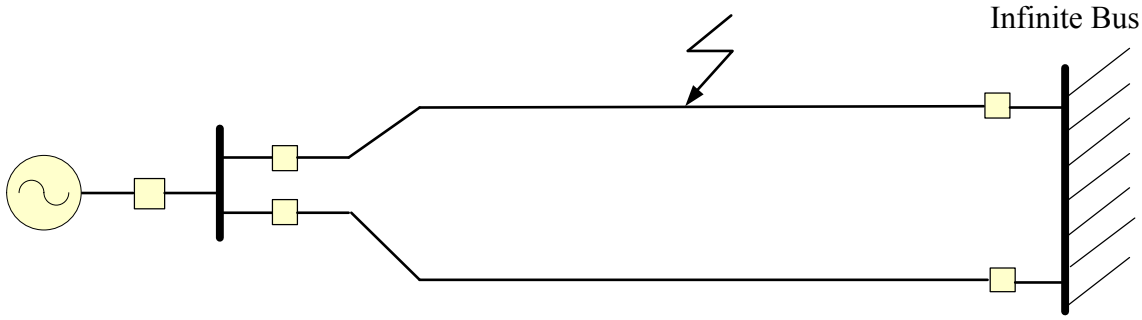

Figure 2.4 A Single Machine - Infinite Bus System

For this system assume that the swing equation for the post fault system is given by the following simplified differential equation.

$$M \frac{d\delta^2(t)}{dt} = P_m - P_{\max} \sin \delta(t) \tag{2.9}$$

The post fault stable equilibrium point is $\delta_s = \sin^{-1}(\frac{P_m}{P_{\max}})$ while the post fault closest unstable equilibrium point is $\delta_u = \pi - \delta_s = \pi - \sin^{-1}(\frac{P_m}{P_{\max}})$.

The potential energy function is calculated to be:

$$E_{potential}(\delta) = \int_{\delta_s}^{\delta} (P_{\max} \sin\delta - P_m) \cdot d\delta = P_{\max} \cos\delta_s - P_{\max} \cos\delta - P_m \cdot \delta + P_m \cdot \delta_s \tag{2.10}$$

The total energy function of the generator is:

$$V(\delta(t), \omega(t)) = \frac{1}{2} M\omega^2(t) + P_{\max} \cos\delta_s - P_{\max} \cos\delta - P_m \cdot \delta + P_m \cdot \delta_s \tag{2.11}$$

The maximum energy that the system can have before losing synchronism is:

$$\begin{aligned} V_{\max} &= E_{potential}(\delta_u) = P_{\max} \cos\delta_s - P_{\max} \cos(\pi - \delta_s) - P_m \cdot (\pi - \delta_s) + P_m \cdot \delta_s \\ &= 2 \cdot P_{\max} \cos\delta_s + 2 \cdot P_m \cdot \delta_s - P_m \cdot \pi \end{aligned} \tag{2.12}$$

For a clearing time t_c with $x(t_c) = \begin{bmatrix} \delta(t_c) & \omega(t_c) \end{bmatrix}$ if $V(\omega(t_c), \delta(t_c)) < V_{\max}$ the system is stable otherwise it is unstable.

2.3 DSE-Enabled Predictive Transient Stability Monitoring Scheme

This section presents how the dynamic state estimation can be combined with the Lyapunov's direct method as summarized in section 2.1, resulting in the proposed transient stability monitoring scheme.

The real-time dynamic state of the substation, as obtained from the dynamic state estimation results, includes the real-time operating condition of the substation generator, i.e. generator torque angle, generator speed, generator acceleration etc. This information is adequate to monitor the dynamics of the generator and characterize and predict the stability of the system. Stability monitoring is performed on the basis of Lyapunov energy functions and Lyapunov direct method. Specifically the total energy of a generator that experiences a fault is evaluated as the sum of its kinetic and potential energy.

$$V(\delta(t), \omega(t)) = \frac{1}{2} \cdot M \cdot \omega^2(t) + \int_{\delta_s}^{\delta} (P_{e\_post}(\delta(t)) - P_m) \cdot d\delta \tag{2.13}$$

The computation of the kinetic energy is trivial since the generator speed is evaluated continuously and in real time by the DSE. The major computational challenge is the evaluation of the potential energy of the generator, and it is performed in terms of the center of oscillation (CoO) of the system with the assumption that the fault is cleared at the present time. Detailed description of the methodology is given next.

2.3.1 CoO Definition and Computation

The CoO is identified as the place of the system where the rate of frequency is constant as illustrated in Figure 2.5. Note that multiple CoOs might exist in the system, since the center of oscillations is actually a plane in the system. The evaluation of the CoO is based on an optimization problem and is explained next.

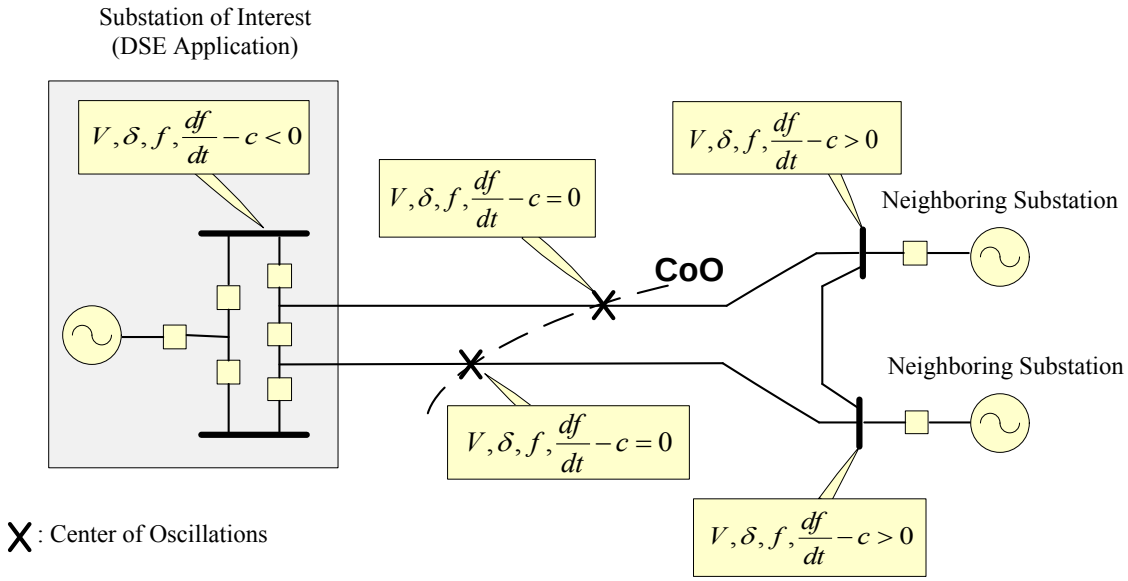

Figure 2.5 Center of Oscillations Definition

Assume the system in Figure 2.6, with the substation of interest and the transmission line that connects the substation with the rest of the system.

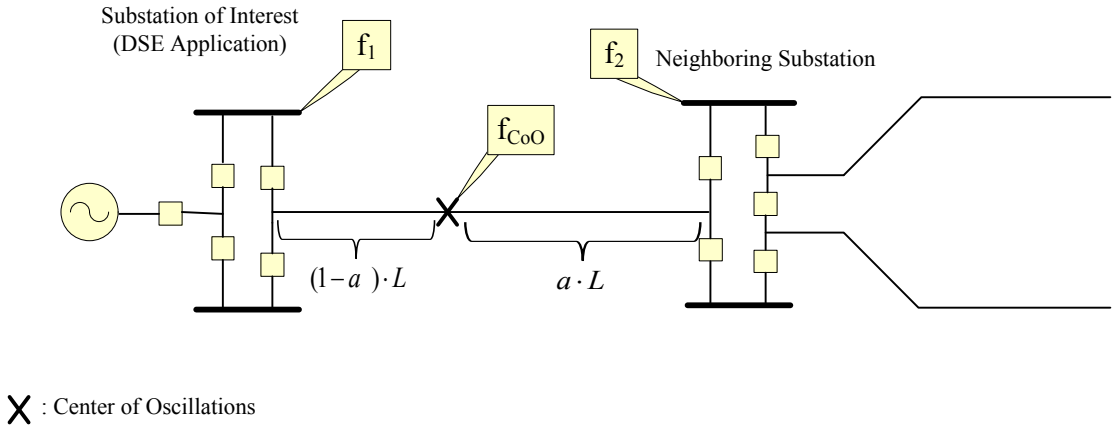

Figure 2.6 Center of Oscillations within a Transmission Line

Assume that the frequency at the CoO is a straight line with equation:

$$f_{coo}(t) = b + c \cdot t \tag{2.14}$$

and that the frequency at the two ends of the line is given as f_1 and f_2 correspondingly. Further assume that the frequency along the line varies linearly with the distance from one end of the line. Let the CoO be within the line. Then for every time instant t_i, the frequency of the CoO is a convex combination with coefficient a of the frequencies f_1 and f_2 at the two ends of the line, that is:

$$f_{coo}(t_i) = b + c \cdot t_i = a \cdot f_{1,t_i} + (1-a) \cdot f_{2,t_i} \tag{2.15}$$

The coefficient a along with the equation of the line (parameters b and c) can be found by solving the following optimization problem:

$$\min \; J = \sum_{i=1}^{N} (a \cdot f_{1,t_i} + (1-a) \cdot f_{2,t_i} - b - c \cdot t)^2 \tag{2.16}$$

where N is the number of samples of f_1 and f_2 that are used. The samples of f_1 and f_2 are obtained upon simulation of the system for a few cycles (around 5 simulation cycles) given that the present time is the fault clearing time. In particular, the simulation is performed for a given fault duration time $t_{fd} = t_{present} - t_{fault}$, where the simulated frequency at the two ends of the line is used as an input to the optimization algorithm for the evaluation of the CoO.

Once the coefficient a is computed, if $0 < a < 1$, then the center of oscillations is found to be along the transmission line at the point $(1-a) \cdot L$ from the first terminal, where L is the length of the line. Thus, the CoO lies within the observable area (the substation of interest or the transmission lines connecting to the neighboring substations). Otherwise it is outside the line. In case of multiple lines that depart from the substation, the same optimization procedure is performed for each line. An illustration of the CoO computation based on the optimization problem is shown in Figure 2.7.

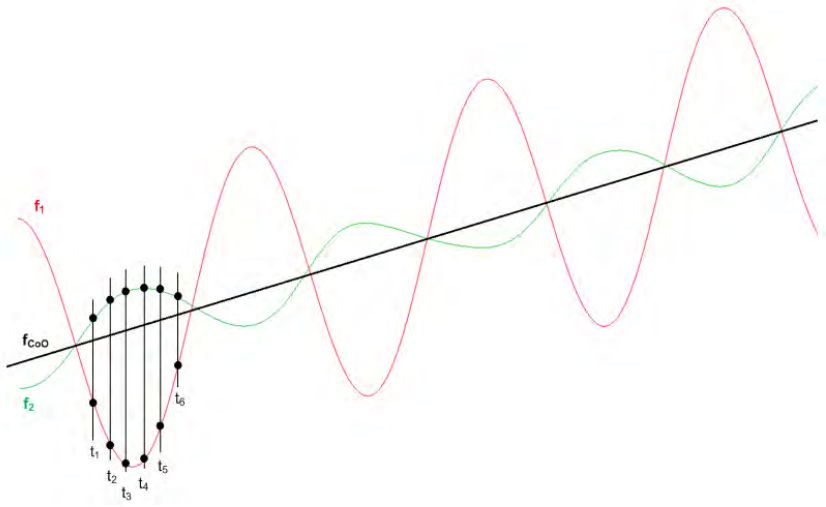

Figure 2.7 Center of Oscillations Evaluation

2.3.2 Equivalent System Derivation

Once the CoO is evaluated then an equivalent system can be derived, that is used for the evaluation of the potential energy of the generator. The equivalent system consists of the original system up to the CoO along with the mirror image of this part of the system with respect to the CoO. The concept of the equivalent system is illustrated in Figure 2.8 and Figure 2.9. In particular, assume that the original system consists of the substation of

interest and two transmission lines with lengths L_1 and L_2 respectively, that connect the substation of interest to the neighboring substations and to the rest of the system as in Figure 2.6. Further assume that upon execution of the optimization algorithm for the evaluation of the CoO, it was found to be at the distance $a_1 \cdot L_1$ and $a_2 \cdot L_2$ away from the terminal of the substation of interest, on the two transmission lines respectively. Then the equivalent system consists of the substation of interest and the part of the transmission lines up to the CoO, along with the mirror image as is illustrated in Figure 2.9. Note that the equivalent substation has the same components (generator, transformer, etc) with the substation of interest.

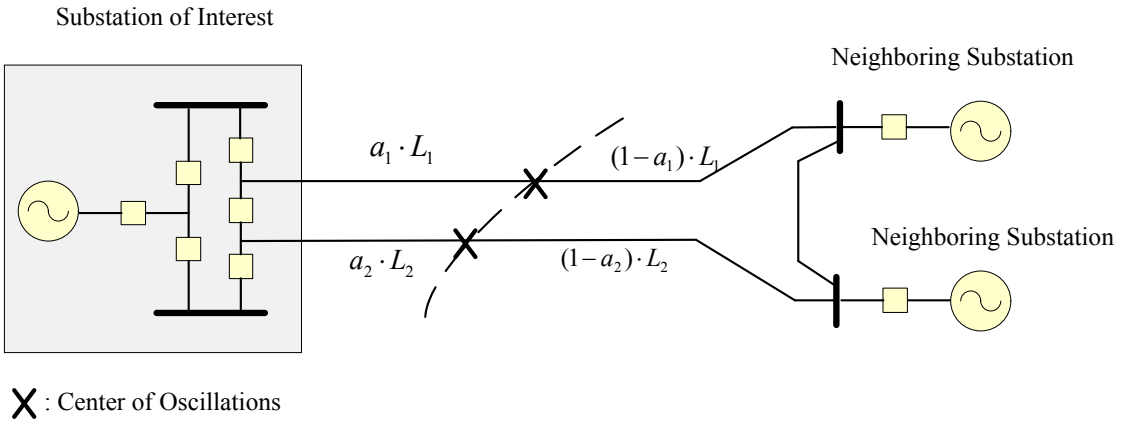

Figure 2.8 Original System

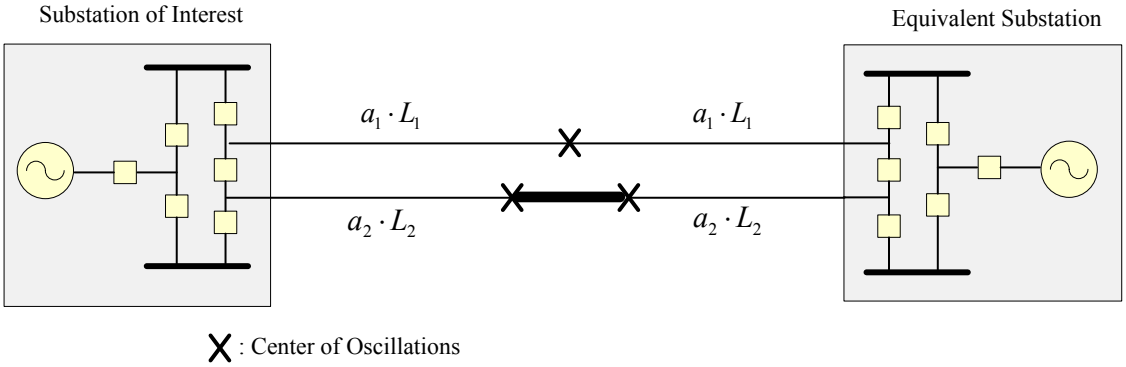

Figure 2.9 Equivalent System

At this point, the importance but also the reasoning behind the evaluation of the CoO is to be emphasized. By evaluating the CoO of the system, then a very simple equivalent system is created, where the dynamics of the generator of interest are the same in the original and the equivalent system. As a result the potential energy of the generator is evaluated using the equivalent system and it is the same as the potential energy of the generator in the original system. Note that with this method, the complexity of the computation of the potential energy of the generator is significantly reduced since the equivalent system is a small two generator equivalent system. As a result, the potential

and kinetic energy of the system can be computed using the well known formulas for a two machine system given next. The swing equations of the two generators are:

$$\frac{2H_1}{\omega_s}\frac{d\delta_1^2}{dt^2} = P_{m1} - P_{e1}(\delta_1 - \delta_2) \tag{2.17}$$

$$\frac{2H_2}{\omega_s}\frac{d\delta_2^2}{dt^2} = P_{m2} - P_{e2}(\delta_1 - \delta_2) \tag{2.18}$$

The single unit equivalent model is:

$$M\frac{d\delta^2}{dt^2} = M\frac{\omega_s}{2H_1}(P_{m1} - P_{e1}(\delta)) - M\frac{\omega_s}{2H_2}(P_{m2} - P_{e2}(\delta)) \tag{2.19}$$

where M is the two generators equivalent mass:

$$M = \frac{2H_1 \cdot H_2}{(H_1 + H_2)\cdot \omega_s} \tag{2.20}$$

The above model permits the evaluation of the potential energy of the generator which is given as follows:

$$E_{potential} = -\int_{\delta_{s1}-\delta_{s2}}^{\delta}\left[M\frac{\omega_s}{2H_1}(P_{m1} - P_{e1}(\delta)) - M\frac{\omega_s}{2H_2}(P_{m2} - P_{e2}(\delta))\right] \tag{2.21}$$

The kinetic energy of the system is:

$$E_k = \frac{1}{2}M(\omega_1 - \omega_2)^2 \tag{2.22}$$

where $\delta = \delta_1 - \delta_2$ is the difference of the generators' torque angles and ω_1 and ω_2 are the generators' speeds. $P_{e1}(\delta)$ and $P_{e2}(\delta)$ are computed based on the equations for the stability evaluation of a multi-machine system, given in Appendix C.

Note that the torque angle (δ_1) and the speed (ω_1) of the generator in the substation of interest are given continuously and in real time by the DSE. The torque angle (δ_2) and the speed (ω_2) of the equivalent generator are computed to be:

$$\delta_2 = 2\cdot\delta_{CoO} - \delta_1 \tag{2.23}$$

$$\omega_2 = 2\cdot\omega_{CoO} - \omega_1 \tag{2.24}$$

since the system is symmetric in terms of the CoO as is illustrated in Figure 2.10.

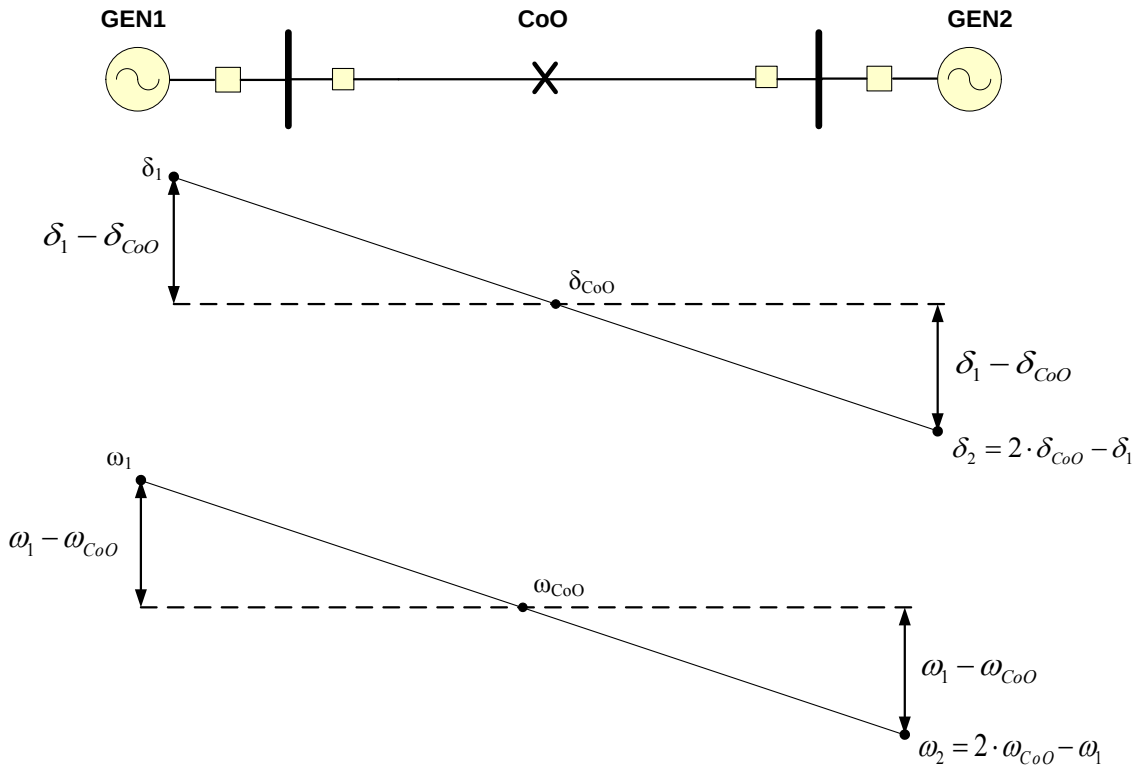

Figure 2.10 Phase angle and frequency computation of the equivalent generator

The equilibrium point $\delta_s = \delta_{s1} - \delta_{s2}$ is given by the steady state power flow solution of the equivalent system.

2.3.3 Transient Stability Monitoring Scheme Algorithm

The algorithm that describes the implementation of the transient stability monitoring scheme is given next and shown in Figure 2.11. The generator torque angle and speed (frequency) at the substation of interest are monitored continuously through the DSE. After the occurrence of a fault, the type of the fault and the location of the fault can be identified. Given this information the topology of the post fault system is predicted, assuming that the predefined settings of the protective relays are known. This is also facilitated by the breaker oriented power system modeling that is used in this work, which allows for the prediction of the breaker(s) that will operate. These computations are expected to last a few cycles, so there will be a delay of few cycles before the monitoring of the total energy trajectory begins. However this time is expected to be in the order of a few msecs (2-3 cycles), thus it will normally be during the fault period and it is not expected to affect the performance of the scheme.

Now given the topology of the post fault system, at each time step of the algorithm and assuming that the fault is cleared at that time instant, the steps of the algorithm for the proposed transient stability monitoring scheme are the following:

1. the center of oscillations is evaluated by performing the optimization algorithm described in section 2.3.1,
2. the equivalent two generator system is derived, as described in section 2.3.2,
3. the potential energy function of the equivalent system is computed, along with the post fault equilibrium and the barrier value of the potential energy function which is equal to the value of the potential energy function at the closest unstable equilibrium point of the post fault system, as described in section 2.2,
4. the total energy of the generator is computed as the sum of the potential energy and the kinetic energy of the generator at that time instant. Note that for these calculations, the torque angle and the speed of the generator, along with the phase angle and the frequency of the CoO are used, and are given by the DSE that is performed at the substation of interest.

Note that these computations are expected to last a few cycles, so there will be a delay of few cycles before the scheme determines the stability of the system. However due to the fact that all the computations are performed on a very simple and small two generator equivalent system, this computation time is expected to be in the order of a few msecs (2-3 cycles). Also note that the CoO is moving during the transient swings of the system, thus its evaluation is necessary at each time instant.

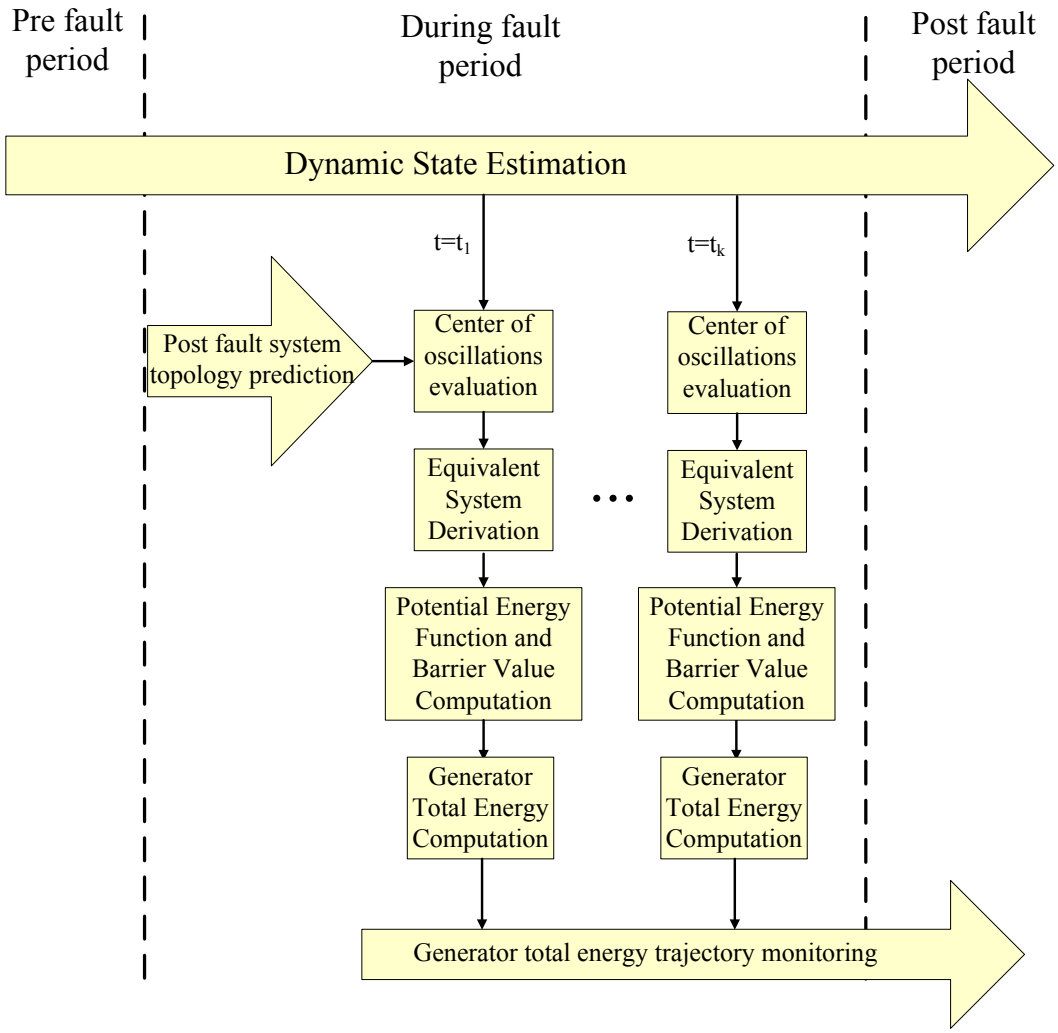

Figure 2.11 Proposed Transient Stability Monitoring Scheme Conceptual Illustration

As a result, the proposed transient stability monitoring scheme determines in real time the stability of the system. In addition stability indexes such as the stability margin, in terms of the generator energy or the phase angle can be computed at each time instant. Finally in case of an unstable system the critical clearing time is also determined, since this is the time instant at which the total energy of the generator equals the barrier value.

2.4 Summary

In this chapter, a novel, energy based transient stability monitoring scheme is described that is based on real-time dynamic monitoring of the system's transient swings, and is enabled by the developed dynamic state estimation. A key concept in the scheme is the evaluation of the CoO of the system. Once this is evaluated as part of the algorithm, then a two generator equivalent system is derived that mimics the dynamics of the original system. The equivalent system, along with the necessary information provided by the DSE are used in order to compute in real time the total energy of the generator and extract stability properties from the energy function. In addition an application of the

transient stability monitoring scheme will be proposed in the next chapter which is a novel, predictive, generator, out-of-step protection scheme.

3. Applications: Out of Step Relaying

3.1 Overall Approach

An application of the transient stability monitoring scheme is a novel generator out-of-step protection scheme. Nowadays out-of-step protection is based on impedance relays that monitor the impedance trajectory at the terminals of the generator as illustrated in Figure 3.1. For present state-of-the-art out-of-step protection, the most common scheme is a mho relay with a single blinder set. Specifically, the impedance trajectory is monitored and instability is detected when there is a crossing on the two blinders (right and left). The major disadvantages of this scheme are that a) instability is detected when the unit has already slipped a pole and b) additional delay of tripping may be needed to avoid breaker overstresses in case of high generator torque angles.

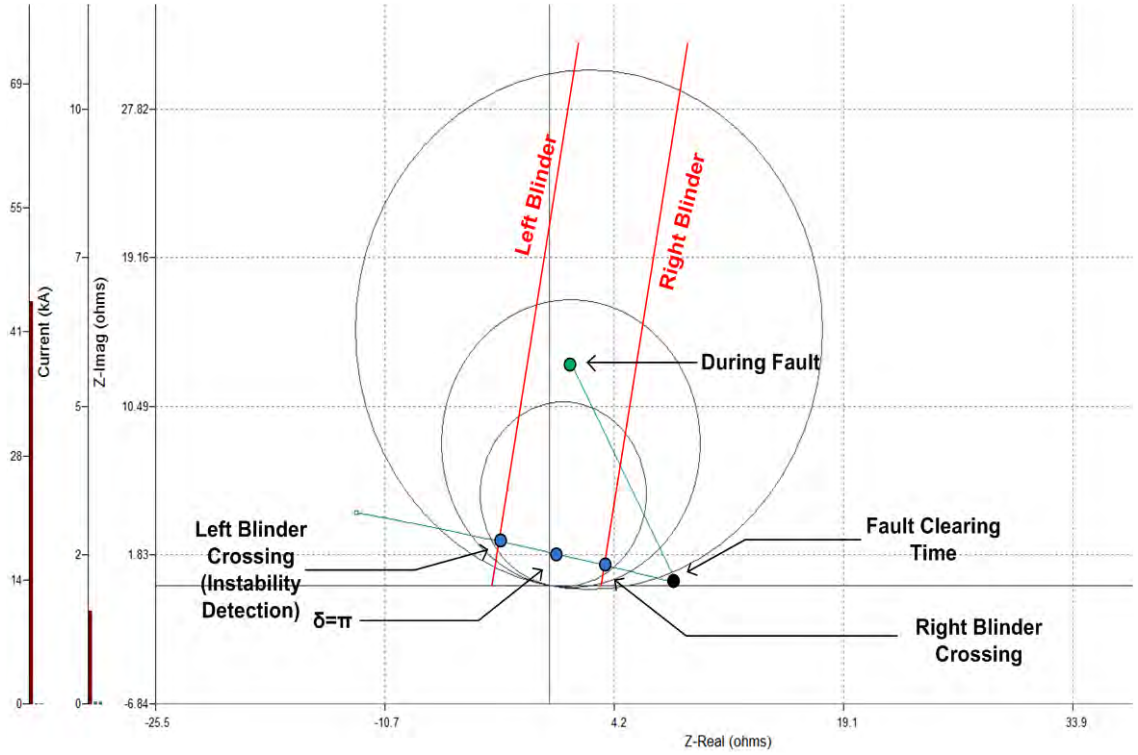

Figure 3.1 Single Blinder Out-of-Step Impedance Relay Operation

Figure 3.2 illustrates in more detail a visualization of the generator total energy trajectory monitoring. The total energy of the generator is computed at each time step, and it is superimposed on the potential energy function. When and if the total energy value exceeds the barrier value $V_{\max}$ then instability is detected and a trip signal can be sent to the generator. Note that $V_{\max}$ is the value of the potential energy function at the "closest equilibrium point" as explained in section 2.2. Also, note that the instability is detected at the critical clearing time of the fault (t_{crit}), resulting in a predictive out-of-step protection

scheme. At that time also the value of the torque angle of the generator (δ_{crit}) is typically such that allows the breaker to open without a risk to overstress it. If the total energy value does not exceed the barrier value $V_{\max}$, this means that the system is stable and there is no need for generator tripping. Thus monitoring of the trajectory of the total energy as the disturbance is evolving can lead to the calculation of the exact time that the system loses its synchronism and becomes unstable, and as a result provides us with the exact time that the out-of-step relay should trip the generator.

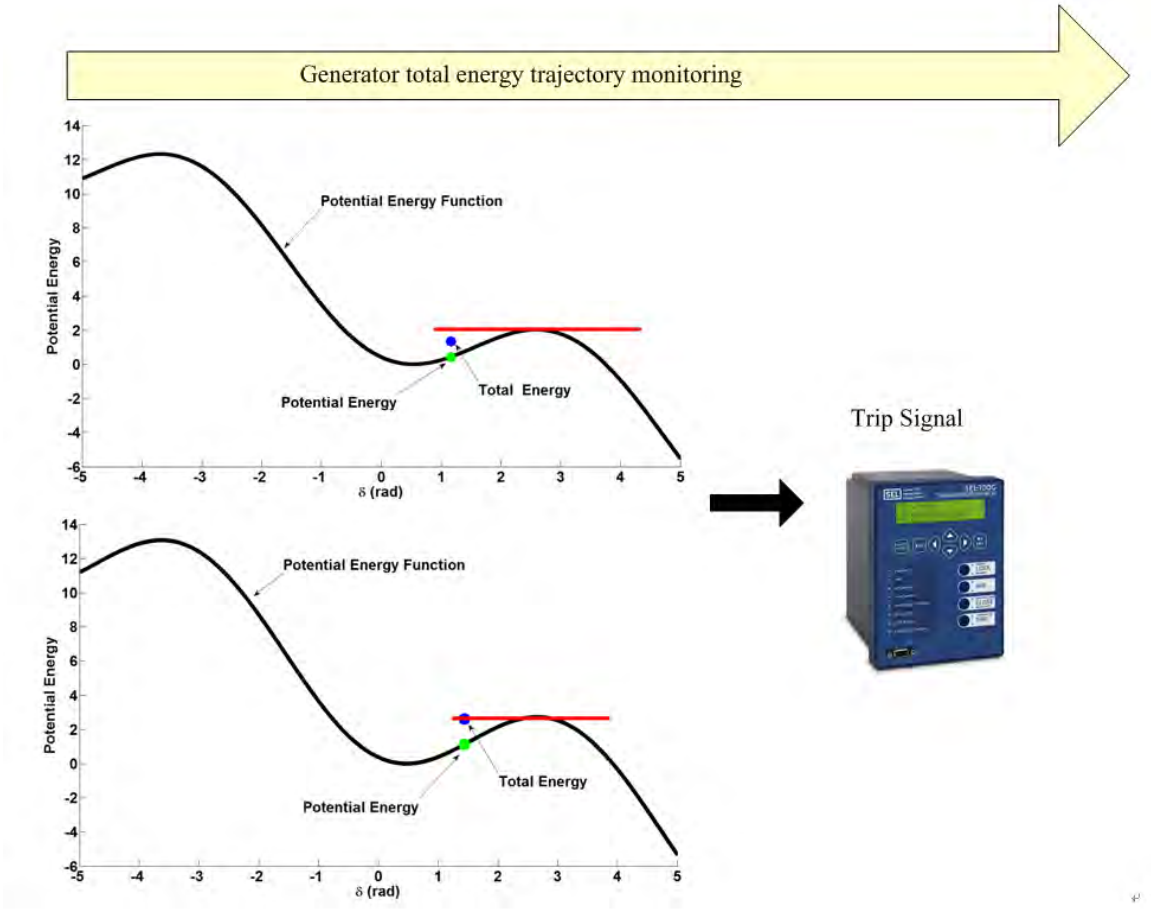

Figure 3.2 Generator Out-of-Step Protection Scheme Illustration

Additional visualizations can be also implemented that provide animations of the generator dynamics of the system in real time. The animation indirectly provides a feel of the acceleration of the generating units as their position and/or the arrow size of the speed changes. For example, Figure 3.3 shows the position of each generator according to its torque angle. In addition the speed of the generator (above or below synchronous speed) is shown with arrows that are proportional to the numerical value of the speed.

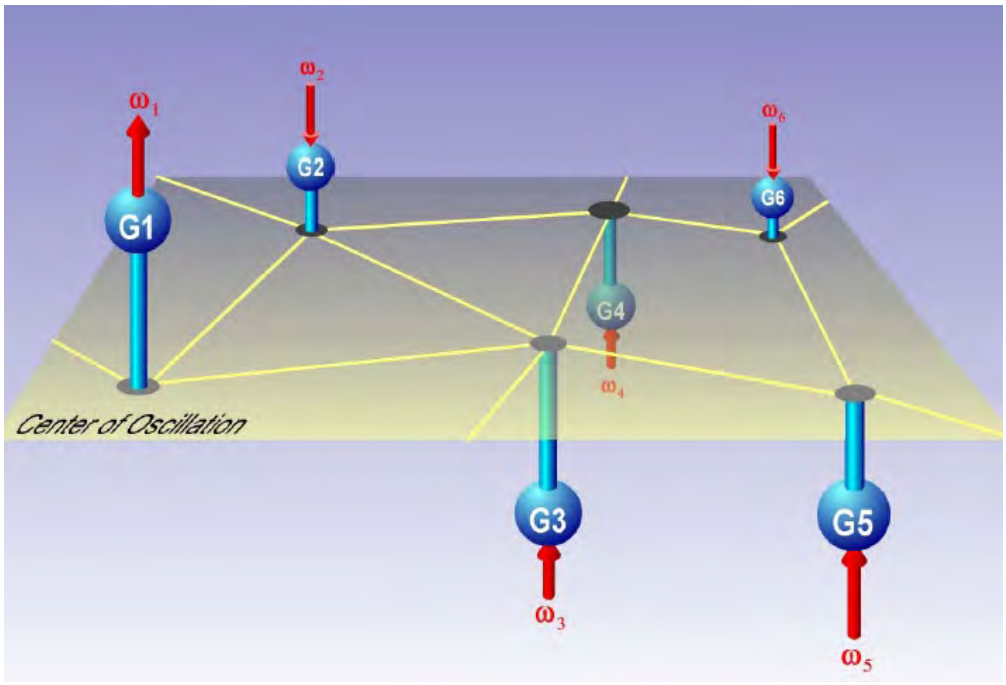

Figure 3.3 Visualization of Generator Operating State

Another important factor that needs to be noted is that the proposed stability monitoring scheme needs the up-to-date system topology to create an accurate equivalent system so that the synchronous generator stability can be predicted correctly. All power apparatuses are connected to the grid via breakers so if the breakers status can be known, the evolution of system topology can be obtained. The best way to access the breaker status is via relays. Relays trip a power component by opening breakers when this component is experiencing faults. So in this section, a secure and reliable protection scheme, setting-less protection, is also introduced which could be installed in relays and each relay can protect the power apparatus (zone) without any coordination with other protective relays.

3.2 Setting-Less Protection Approach

The setting-less protection scheme can be viewed as a generalization of differential protection where differential protection monitors Kirchhoff's current law (partial device model) while the proposed method monitors all physical laws that the device obeys - the physical laws are described with the full dynamic model of the device under protection. Protection decisions (trip/no trip) are based on the device condition only and do not require coordination with other devices, thus the name setting-less protection. The setting-less protection is based on dynamic state estimation which monitors the dynamic model of the device under protection by fitting the real-time measurement data to the model. Internal device faults are manifested as deviations of the measurements from the model predicted values. The internal abnormalities of the protected device are expressed in terms of the confidence level which determines the health status of the device under protection. If the confidence level is almost zero for cycles, it means there are some internal faults inside the device and protective actions should be taken.

3.2.1 Overall Setting-Less Protection Framework

An overview of the design of the setting-less protection relay is shown in Figure 3.4.

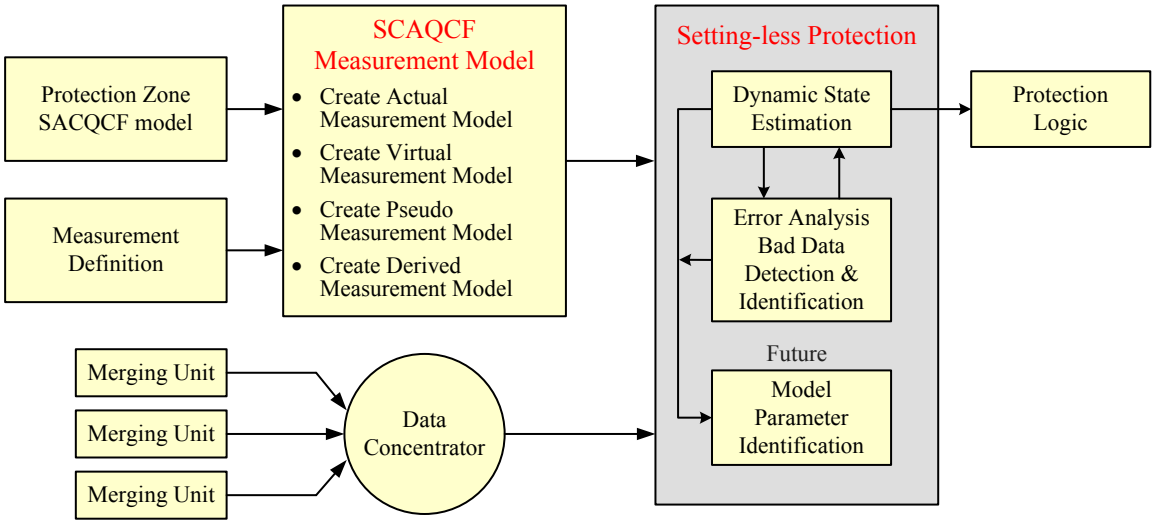

Figure 3.4 Setting-Less Protection Relay Organization

The setting-less protection algorithms have been streamlined for the purpose of increasing efficiency. An object-oriented approach for the DSE based protection algorithm is developed by utilizing the State and Control Algebraic Quadratic Companion Form (SCAQCF). All the mathematical models of the apparatus in the power system are written in SCAQCF format so that the DSE based protection algorithm could be applied to any device. The algorithm automatically formulates the measurement model in the SCAQCF syntax from the SCAQCF device model and the measurement definition file, as illustrated by Figure 3.4. A data concentrator is utilized to align data from multiple merging units with the same time stamp and feed the streaming data into the DSE based protection module. The DSE based protection scheme continuously monitors the SCAQCF model of the component (zone) under protection by fitting the real-time measurement data to the measurement model in the SCAQCF syntax. If any of the physical laws for the component under protection is violated, the dynamic state estimation will capture this condition. Under normal operation, the device estimated measurement data from DSE should be exactly the same as the real measurement data. The mismatch between real measurements and estimated measurements indicates abnormalities in the device, then diagnose or trip decision should be made. Detailed implementation of setting-less protection in an object-oriented way is shown in Appendix A and Appendix B. This section gives a brief introduction of how setting-less protection is implemented.

3.2.2 Protection Zone Mathematical Model

The mathematical model of the protection zone is required in a standard form. A standard has been defined in the form of the **S**tate and **C**ontrol **A**lgebraic **Q**uadratic **C**ompanion **F**orm (SCAQCF) and in a specified syntax to be defined later. The SCAQCF for a specific protection zone is derived with three computational procedures. Specifically, the dynamic model of a protection zone consists of a set of algebraic and differential equations. We refer to this model as the compact model of the protection zone. Subsequently this model is quadratized, i.e. in case there are nonlinearities of order greater than 2, additional state variables are introduced so that at the end the mathematical model consists of a set of linear and quadratic equations. We refer to this model as the quadratized model. Finally, the quadratized model is integrated using the quadratic integration method which converts the quadratized model of the protection zone into a set of algebraic (quadratic) function. This model is cast into a generalized Norton form. We refer to this model as the Algebraic Quadratic Companion Form. Since the variables in this AQCF contain all states and controls, thus it is named State and Control Algebraic Quadratic Companion Form.

The standard State and Control Algebraic Quadratic Companion Form is obtained with two procedures: (a) model quadratization, and (b) quadratic integration. The model quadratization reduces the model nonlinearities so that the dynamic model will consist of a set of linear and quadratic equations. The quadratic integration is a numerical integration method that is applied to the quadratic model assuming that the functions vary quadratically over the integration time step. The end result is an algebraic companion form that is a set of linear and quadratic algebraic equations that are cast in the following standards form:

$$\begin{Bmatrix} I(\mathbf{x},\mathbf{u}) \\ \vdots \\ 0 \\ \vdots \end{Bmatrix} = Y_{eqx}\mathbf{x} + \begin{Bmatrix} \vdots \\ \mathbf{x}^T F^i_{eqx}\mathbf{x} \\ \vdots \end{Bmatrix} + Y_{equ}\mathbf{u} + \begin{Bmatrix} \vdots \\ \mathbf{u}^T F^i_{equ}\mathbf{u} \\ \vdots \end{Bmatrix} + \begin{Bmatrix} \vdots \\ \mathbf{x}^T F^i_{eqxu}\mathbf{u} \\ \vdots \end{Bmatrix} - B_{eq} \tag{3.1}$$

where $I(\mathbf{x},\mathbf{u})$ is the through variable (current) vector, $\mathbf{x} = [\mathbf{x}(t), \mathbf{x}(t_m)]$ is the external and internal state variables, $\mathbf{u} = [\mathbf{u}(t), \mathbf{u}(t_m)]$ is the control variables, t is present time, t_m is the midpoint between the present and previous time, Y_{eq} admittance matrix, F_{eq} nonlinear matrices, and

$$B_{eq} = -N_{eqx}\mathbf{x}(t-h) - N_{equ}\mathbf{u}(t-h) - M_{eq}I(t-h) - K_{eq} \tag{3.2}$$

The derivation of the standard State and Control Algebraic Quadratic Companion Form for specific protection zones is provided in the appropriate reports that describe the application of the setting-less protection schemes for specific protection zones.

This standardization allows the object oriented handling of measurements in state estimation; in addition it converts the dynamic state estimation into a state estimation that has the form of a static state estimation.

3.2.3 Object-Oriented Measurements

Any measurement, i.e. current, voltage, temperature, etc. can be viewed as an object that consists of the measured value and a corresponding function that expresses the measurement as a function of the state of the component. This function can be directly obtained (autonomously) from the State and Control Algebraic Quadratic Companion Form of the component. Because the algebraic companion form is quadratic at most, the measurement model will be also quadratic at most. Thus, the object-oriented measurement model can be expressed as the following standard equation:

$$\begin{aligned} z_k(t) = & \sum_i a_{i,t}^k \cdot x_i(t) + \sum_i a_{i,tm}^k \cdot x_i(t_m) \\ & + \sum_{i,j} b_{i,j,t}^k \cdot x_i(t) \cdot x_j(t) \\ & + \sum_{i,j} b_{i,j,tm}^k \cdot x_i(t_m) \cdot x_j(t_m) \\ & + c_k(t) + \eta_k \ , \end{aligned} \tag{3.3}$$

where z is the measured value, t the present time, t_m the midpoint between the present and previous time, x the state variables, a the coefficients of linear terms, b the coefficients of nonlinear terms, c the constant term, and η the measurement error.

The measurements can be identified as: (a) actual measurements, (b) virtual measurements, (c) derived measurements and (d) pseudo measurements. The types of measurements will be discussed next.

Actual Measurements: In general the actual measurements can be classified as across and through measurements. Across measurements are measurements of voltages or other physical quantities at the terminals of a protection zone such as speed on the shaft of a generator/model. These quantities are typically states in the model of the component. For this reason, the across measurements has a simple model as follows:

$$z_j = x_i \pm x_j + \eta_j \tag{3.4}$$

Through measurements are typically currents at the terminals of a device or other quantities at the terminals of a device such as torque on the shaft of a generator/motor. The quantity of a through measurement is typically a function of the state of the device. For this reason, the through measurement model is extracted from the algebraic companion form, i.e. the measurement model is simply one equation of the SCACQF model, as follows:

$$z_j = \sum_i Y_{eqx,i}^{\ k} \cdot x_i + \sum_{i,j} F_{eqx,ij}^{\ k} \cdot x_i \cdot x_j + \sum_i Y_{equ,i}^{\ k} \cdot u_i + \sum_{i,j} F_{equ,ij}^{\ k} \cdot u_i \cdot u_j + \sum_{i,j} F_{eqxu,ij}^{\ k} \cdot x_i \cdot u_j - \sum_i b_{eq,i}^{\ k} \tag{3.5}$$

where the superscript k means the kth row of the matrix or the vector.

Virtual Measurements: The virtual measurements represent a physical law that must be satisfied. For example we know that at a node the sum of the currents must be zero by Kirchoff's current law. In this case we can define a measurement (sum of the currents); note that the value of the measurement (zero) is known with certainty. This is a virtual measurement.

The model can provide virtual measurements in the form of equations that must be satisfied. Consider for example the m[th] SCAQCF model equation below:

$$0 = \sum_i Y_{eqx,i}^{\ k} \cdot x_i + \sum_{i,j} F_{eqx,ij}^{\ k} \cdot x_i \cdot x_j + \sum_i Y_{equ,i}^{\ k} \cdot u_i + \sum_{i,j} F_{equ,ij}^{\ k} \cdot u_i \cdot u_j + \sum_{i,j} F_{eqxu,ij}^{\ k} \cdot x_i \cdot u_j - \sum_i b_{eq,i}^{\ k} \quad (3.6)$$

This equation is simply a relationship among the states the component that must be satisfied. Therefore we can state that the zero value is a measurement that we know with certainty. We refer to this as a virtual measurement.

Derived Measurements: A derived measurement is a measurement that can be defined for a physical quantity by utilizing physical laws. An example derived measurement is shown in Figure 3.5. The figure illustrates a series compensated power line with actual measurements on the line side only. Then derived measurements are defined for each capacitor section. Note that the derived measurements enable the observation of the voltage across the capacitor sections.

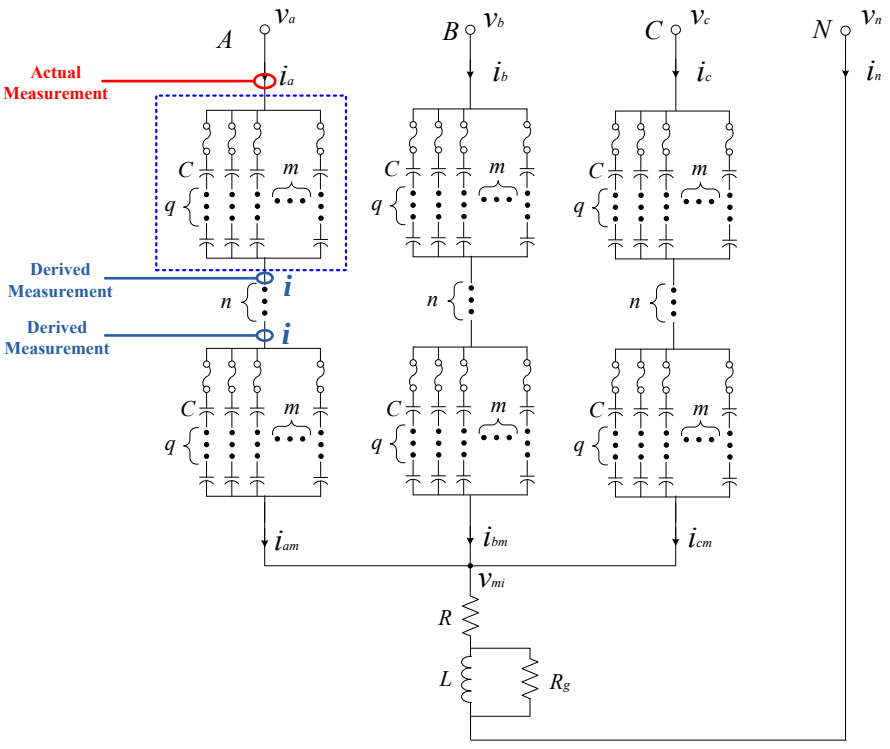

Figure 3.5 Example of Derived Measurements

Pseudo Measurements: Pseudo measurements are hypothetical measurements for which we may have an idea of their expected values but we do not have an actual measurement. For example a pseudo measurement can be the voltage at the neutral; we know that this voltage will be very small under normal operating conditions. In this case we can define a measurement of value zero but with a very high uncertainty.

Summary: Eventually, all the measurement objects form the following measurement set:

$$z = h(x,t) + \eta = c + a^T x(t) + b^T x(t_m) + \left[x^T(t) \quad x^T(t_m)\right] F \begin{bmatrix} x(t) \\ x(t_m) \end{bmatrix} + \eta \tag{3.7}$$

where z is the measurement vector, x the state vector, h the known function of the model, a, b are constant vectors, F are constant matrices, and η the vector of measurement errors.

3.2.4 Object-Oriented Dynamic State Estimation

The proposed dynamic state estimation algorithm is the weighted least squares (WLS). The objective function is formulated as follows:

$$Minimize \; J(x,t) = [z - h(x,t)]^T W [z - h(x,t)] \tag{3.8}$$

where W is the diagonal matrix whose non-zero entries are the inverse of the variance of the measurement errors. The solution is obtained by the iterative method:

$$\hat{x}^{j+1} = \hat{x}^j + (H^T W H)^{-1} H^T W (z - h(\hat{x}^j, t)) \tag{3.9}$$

where $\hat{x}$ is the best estimate of states and H the Jacobian matrix of $h(x,t)$.

It is important to note that the dynamic state estimation requires only the mathematical model of all measurements. It should be also noted that for any component, the number of actual measurements and virtual, derived, and pseudo measurements exceed the number of states and they are independent. This makes the system observable and with substantial redundancy.

3.2.5 Protection Logic / Component Health Index

The solution of the dynamic state estimation provides the best estimate of the dynamic state of the component. The well-known chi-square test provides the probability that the measurements are consistent with the dynamic model of the component. Thus the chi-square test quantifies the goodness of fit between the model and measurements (i.e., confidence level). The goodness of fit is expressed as the probability that the measurement errors are distributed within their expected range (chi-square distribution). The chi-square test requires two parameters: the degree of freedom (ν) and the chi-square critical value (ζ). In order to quantify the probability with one single variable, we introduce the variable k in the definition of the chi-square critical value:

$$v = m - n, \qquad \zeta = \sum_{i=1}^{m} \left(\frac{h_i(\hat{x}) - z_i}{k\sigma_i} \right)^2 \tag{3.10}$$

where m is the number of measurements, n the number of states, and $\hat{x}$ the best estimate of states. Note that since m is always greater than n, the degrees of freedom are always positive. Note also that if k is equal to 1.0 then the standard deviation of the measurement error corresponds to the meter error specifications. If k equals 2.0 then the standard deviation will be twice as much as the meter specifications, and so on. Using this definition, the results of the chi square test can be expressed as a function of the variable k. Specifically, the goodness of fit (confidence level) can be obtained as follows:

$$\Pr[\chi^2 \geq \zeta(k)] = 1.0 - \Pr[\chi^2 \leq \zeta(k)] = 1.0 - \Pr(\zeta(k), v) \tag{3.11}$$

A sample report of the confidence level function (horizontal axis) versus the chi-square critical value k, (vertical axis) is depicted in Figure 3.6.

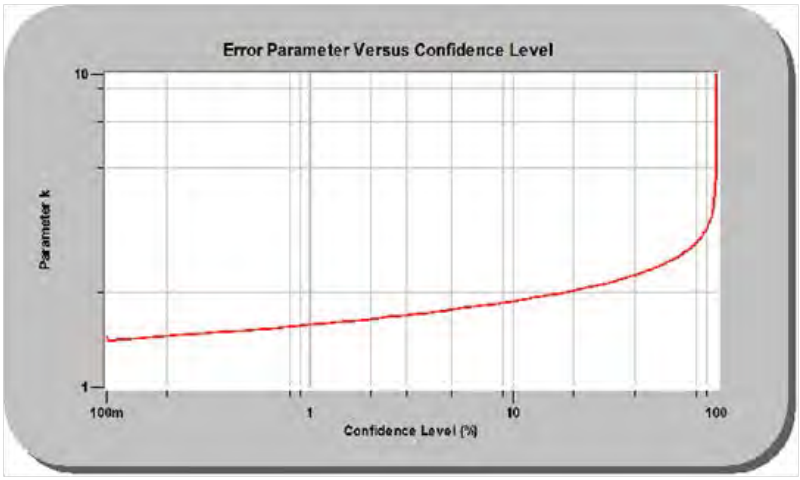

Figure 3.6 Confidence Level (%) vs Parameter k

The proposed method uses the confidence level as the health index of a component. A high confidence level indicates good fit between the measurement and the model, and thus we can conclude that the physical laws of the component are satisfied and the component has no internal fault. A low confidence level, however, implies inconsistency between the measurement and the model; therefore, we can conclude that an abnormality (internal fault) has occurred in the component and has altered the model. The discrepancy is an indication of how different the faulty model of the component is as compared to the model of the component in its healthy status.

It is important to point out that the component protection relay must not trip circuit breakers except when the component itself is faulty (internal fault). For example, in case of a transformer, inrush currents or over-excitation currents, should be considered normal and the protection system should not trip the component. The proposed protection scheme can adaptively differentiate these phenomena from internal faults. Similarly, the relay should not trip for start-up currents in a motor, etc.

3.3 Coordination between Stability Monitoring and Setting-Less Protection

One of the key points for the proposed stability monitoring approach is the requirement for the real-time system topology. The system topology is determined by the breaker status (open or closed). Whenever a fault happens, the setting-less protection relays will determine which and when breakers will trip which will change the system topology. In other words, the setting-less protection relays provide the sequence of breaker operations and therefore the evolution of the system topology.

Moreover, different from PMU based state estimation which calculates the phasors based on one or several cycles of sampled data, the DSE-based protection operates on a sample by sample basis and therefore it is truly real time with latencies of one or two sample intervals. This real-time feature guarantees that the setting-less protection approach provides the up-to-date system topology to the proposed stability monitoring scheme so that it always predicts system instability based on the newest system which improves the prediction accuracy greatly.

The coordination between the setting-less protection method and stability monitoring approach works as follows:

1. The setting-less protection method runs continuously and provides the up-to-date network topology.
2. If there is no oscillation, do nothing.
3. In case of oscillations (the start of oscillation is defined as the moment at which the rate of frequency change is greater than 100 mHz/sec), do the following:
4. The setting-less protection detects the faulted zones and determines the protection actions (trip breaker X at time t1, do not trip, etc.). If a trip decision is made, then send the new topology to the stability monitoring method.
5. The topology and model of the substation from (4) is used to calculate the new CoOs locations and construct the new equivalent n-generator system in an automatic way.

The model from (4) is used to perform the stability monitoring as described in the report. Note that this system is real-time and continuously updates itself as more information is coming from the data acquisition and the relay decisions.

3.4 Summary

The proposed PMU-based stability monitoring approach was introduced in chapter 2. It utilizes the frequency or phase angle at buses in the substation and neighboring substations to calculate the system Center of Oscillations (CoOs) whenever the system is in oscillating mode. Based on the CoO locations, the rest of the system beyond the CoOs is replaced with an equivalent system, which is a mirror image system of the substation with respect to the CoOs. Therefore, a simplified equivalent two-generator system is obtained and it is used to calculate the potential energy and kinetic energy for the generators in the substation. At the last step, system stability is determined via

Lyapunov's direct method. All the details and a sample system illustration are shown in the May's report.

Although the proposed approach works great with the help of PMU data, it still has the limitation that it may not predict the accurate stability when the system topology changes under the post-fault scenario. We posed the following questions: (a) what is the system stability after fault clearing? What system topology changes occur after fault initiation? How is the stability monitoring scheme works under system topology changes? To answer all these important questions, a setting-less protection method is introduced to coordinate with the stability monitoring approach. This method is called setting-less protection by EPRI because only simplified settings are needed. The setting-less protection can provide real time validated model of each power apparatus connected to the interested substation, in which the stability monitoring scheme is installed. For example, the real time model of a transmission line includes the information as the voltage frequencies at the two ends of a transmission line, whether the transmission line has a fault and whether it is tripped or it will be tripped, etc. Based on the provided real time validated model of each power apparatus, at the substation level, the system model and topology of the related substations are synthesized automatically and this provides the stability monitoring scheme all the necessary information for the calculation of the up-to-date simplified two-generator equivalent system.

4. Illustrative Examples

4.1 Summary Description of Examples

In this chapter, demonstrating results on the transient stability monitoring and generator out-of-step protection scheme are presented. Initially, the method is demonstrated on a simple, two-machine system which is used as a proof-of-concept test case. In this system, results are presented assuming that information is available from both substations, but also for the case where only information from the substation of interest is used, in which case the concept of the calculation of the CoO is used.

4.2 Two-Machine System - Proof of Concept Test Case

In this section, the proposed transient stability is demonstrated on a two substation system with two generating units, two step-up transformers and two overhead transmission lines connected in parallel as is illustrated in Figure 4.1. The parameters of the system are presented in Table 4-1.

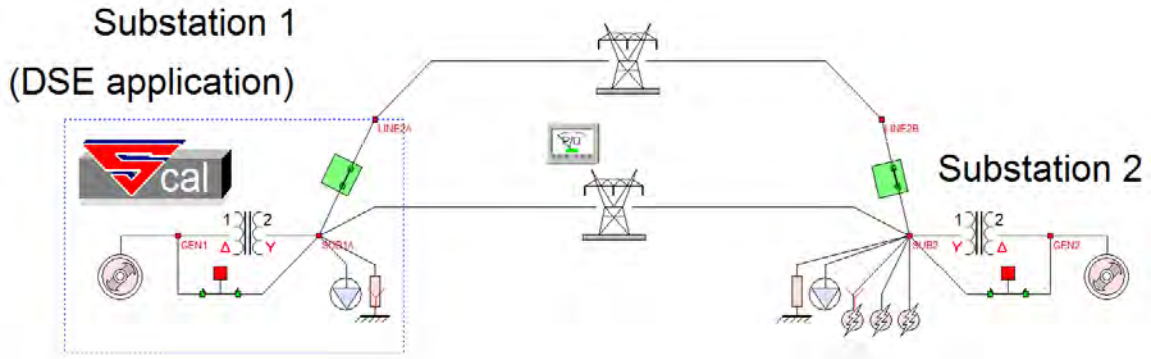

Figure 4.1 Single Line Diagram of the Two Generator System

Table 4-1 Test System Parameters

Gen1	100MVA	z= 0.001+j0.18 pu	H=2.5 sec	15 kV
Gen2	200MVA	z= 0.001+j0.18 pu	H= 3.0 sec	18 kV
XFMR1	100MVA	z=0.001+j0.07 pu	15 kV/115kV	
XFMR2	200MVA	z=0.001+j0.08 pu	115 kV/18kV	
Transmission Line 1		z=0.028+0.2698 pu	115 kV	50 miles
Transmission Line 2		z=0.028+0.2698 pu	115 kV	50 miles
Load 1		S=0.4+j0.1 pu	115 kV	
Load 2		S=1.5+j0.2 pu	115 kV	
Common S_{base}=100 MVA				

Here the focus is on the stability monitoring and out-of-step protection of the generator in the first substation, which is the substation of interest. The fault scenario that is examined

is a three-phase fault at the terminal of the second substation. The system is simulated in WinIGS.

4.2.1 Using Data from Both Substations

In this section, the energy based transient stability monitoring of the system is demonstrated assuming that the required information (generator's torque angle and speed) is available from both substations.

In particular, a single machine equivalent is derived using the equations presented in section 2.3.2. For this test system, the equilibrium point of the post fault system is computed to be at:

$$\delta_s = \delta_{s1} - \delta_{s2} = 18.17^0 - 5.03^0 = 13.14^0$$

Two test cases have been simulated. The first one corresponds to a three-phase fault that resulted in a stable system, and the second case corresponds to a three-phase fault that resulted in an unstable case. The fault is initiated at t=1 sec. The duration of the fault was 0.3 sec in the stable case and 0.4 sec in the unstable one. The fault is cleared by disconnecting the second (upper) transmission line. In Table 4-2 and Table 4-3 the generators' torque angles and speeds at the fault clearing time are given.

Table 4-2 Torque Angle & Frequency at Fault Clearing Time – Stable Scenario

Generator 1	**Generator 2**
δ_1=154.3 deg	δ_2=80.7 deg
f_1=62.57 Hz	f_2=61.4 Hz

Table 4-3 Torque Angle & Frequency at Fault Clearing Time – Unstable Scenario

Generator 1	**Generator 2**
δ_1=262.2 deg	δ_2=139.1 deg
f_1=63.41 Hz	f_2=61.85 Hz

The total energy (sum of potential and kinetic energy) of the system is computed next using equations 2.17-2.22. Figure 4.2 illustrates the total energy of the system superposed on the corresponding potential energy function for the stable case at the time when the fault was cleared (t=1.3 sec). It is clear in this case that the total energy is below the highest value of the potential energy, thus indicating a stable system.

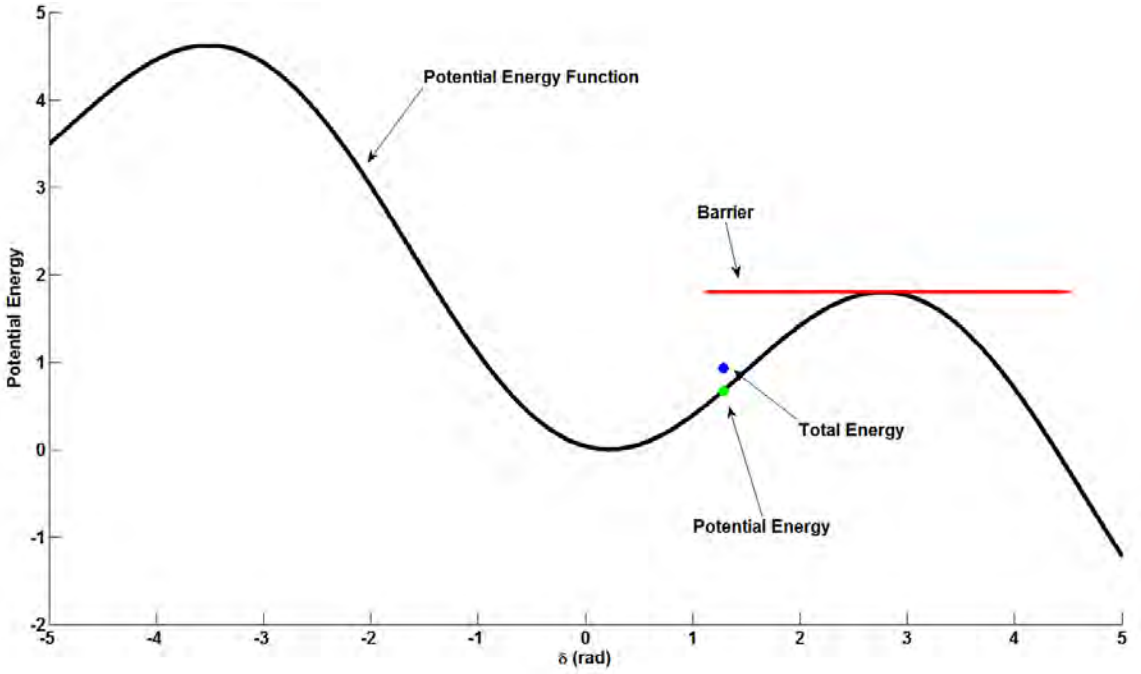

Figure 4.2 Total and Potential System Energy - Stable Case

In Figure 4.3 the unstable case is depicted. Note that in this case, the total energy at the fault clearing time (t=1.4 sec) exceeds the highest value of the potential energy function, thus indicating an unstable system.

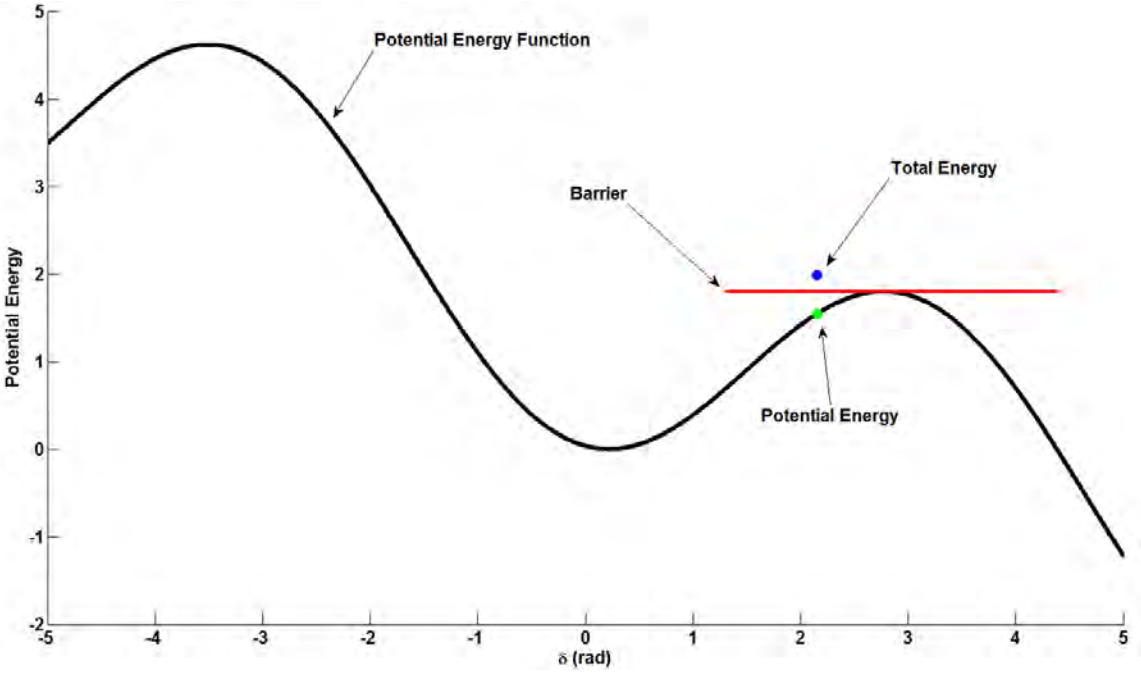

Figure 4.3 Total and Potential System Energy - Unstable Case

Next, it is illustrated how the proposed out-of-step protection scheme can predict instability before its occurrence for the unstable scenario described before. In particular, Figure 4.4 illustrates the trajectory of the potential and total energy of the generator for the unstable scenario. The total energy is continuously monitored and compared to the peak (barrier) value of the potential energy. When the total energy becomes higher than the barrier value, this indicates instability and a trip signal is issued to the generator. Note that this is a totally predictive out-of-step scheme that is taking place in real time. Specifically, in the described unstable scenario the fault is cleared at t=1.4 sec (0.4 sec after its initiation). Visualization of the total energy trajectory as illustrated in Figure 4.4 verifies that instability is asserted when δ=109.5 degrees at t=1.37 seconds.

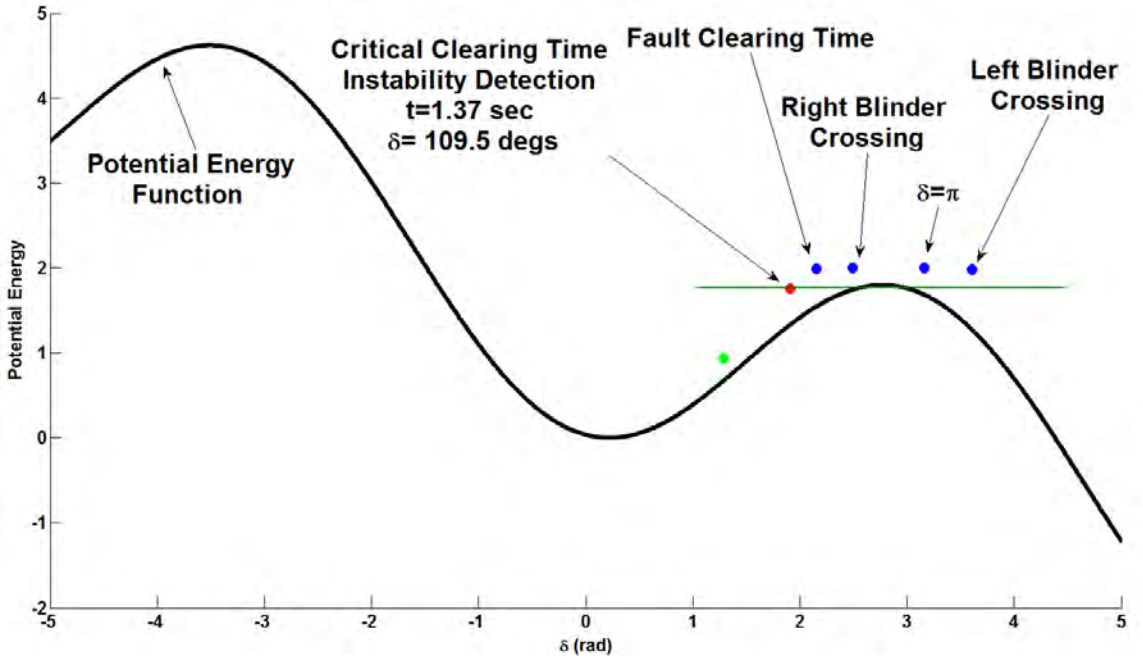

Figure 4.4 Total and Potential System Energy Trajectory

Next, the energy based scheme for stability monitoring and out-of-step protection is compared with the single blinder out-of-step protection method. In order to perform the comparison, the out-of-step function of the impedance relay is simulated for the same unstable scenario. Observing Figure 4.5, it is evaluated that the impedance trajectory crosses the right blinder at t=1.44 seconds. The left blinder is crossed at t=1.58 seconds. Additional delay is needed before generator tripping is issued. As a result the proposed approach and the generator total energy visualization predicted instability 0.21 seconds before the impedance relay, without considering additional delay of the impedance relay tripping due to the high value of the angle when the instability is detected. Note that comparison of Figure 4.4 and Figure 4.5 illustrates that in the developed scheme, instability detection was achieved before the fault clearing time, when the impedance was still between the two blinders (Figure 4.5 - During Fault point).

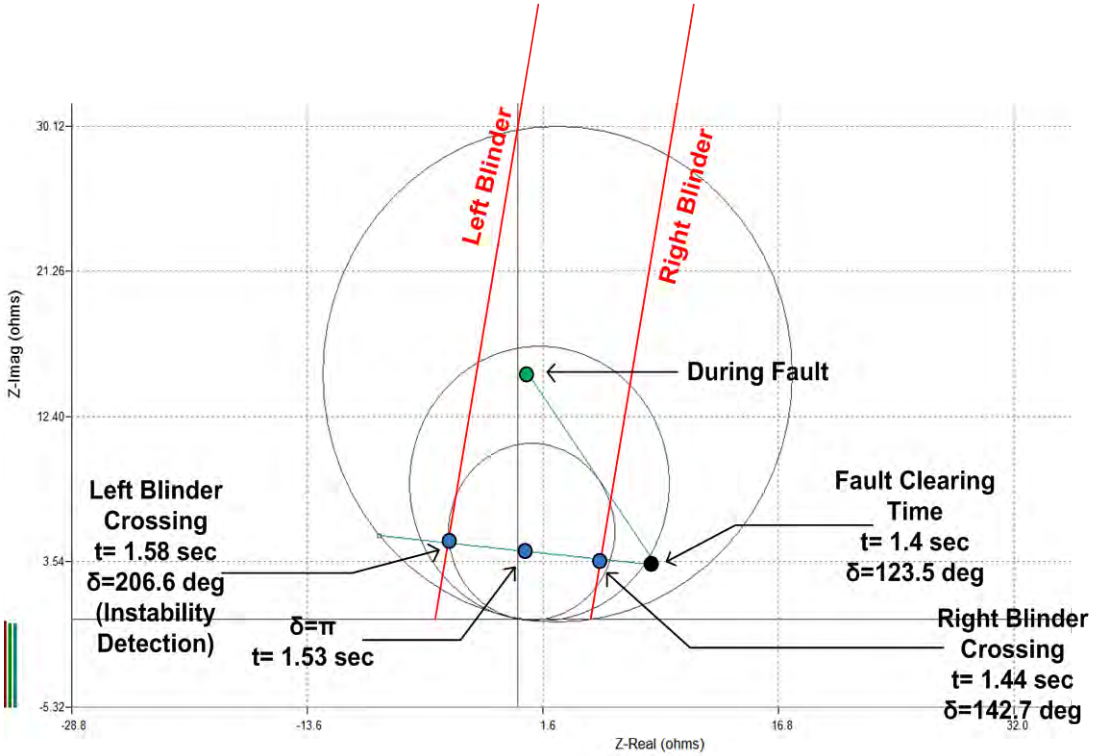

Figure 4.5 Impedance Trajectory Monitoring

4.2.2 Using Data Only from the Substation of Interest

The same test case is presented here, with the difference that now it is assumed that only information from the DSE that is performed at the substation of interest is available. In this case, which is the general case since for the developed scheme only information from the substation of interest is utilized, the potential energy function and the total energy of the generator of interest are computed in real time, in terms of the CoO as described in section 2.3.

The energy of the system is computed next for two time instants, t=1.25 sec and t=1.37 sec. In particular, the energy of the system is computed at time t=1.25 sec. Assuming that this is the fault clearing time, after a few cycles simulation of the system, the frequency at the two ends of the line that connects the two substations is given in Figure 4.6. Given the frequency at the two terminals of the line it is concluded that the CoO is within this line and it is evaluated by the optimization method described in section 2.3.1. The results are summarized in Table 4-4.

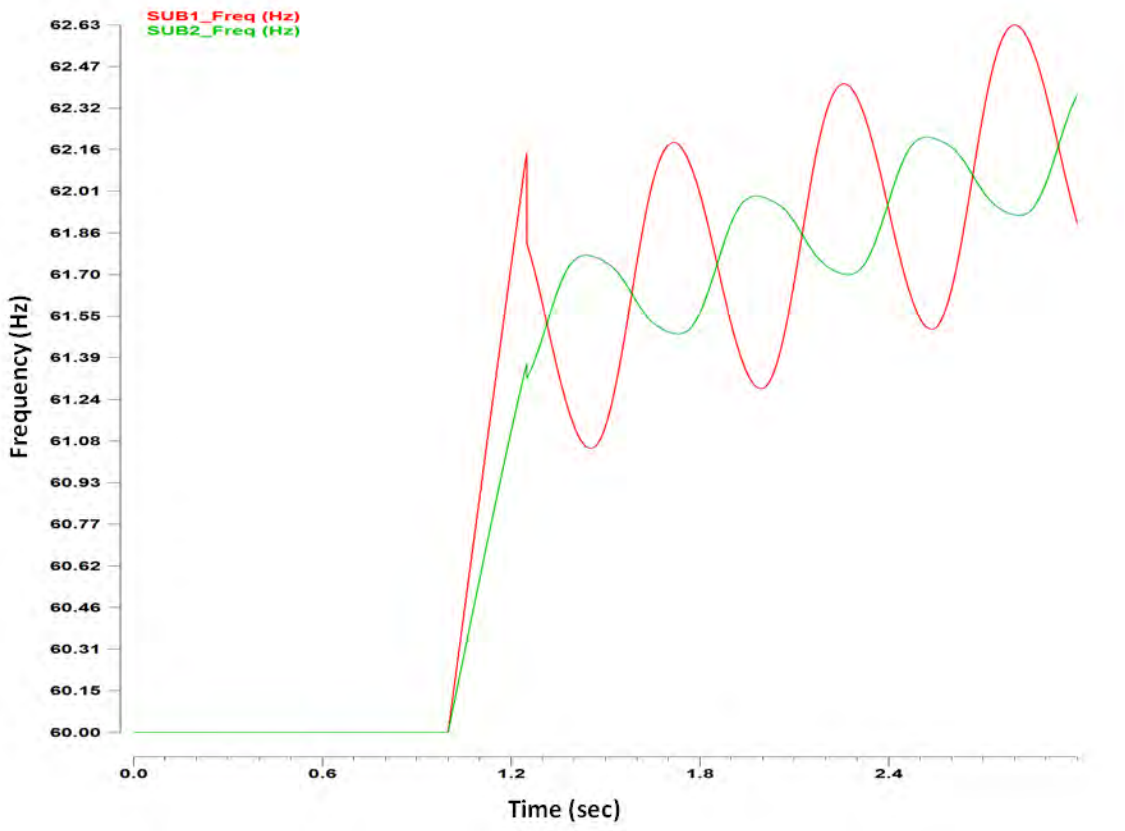

Figure 4.6 Frequency at the Terminals of the Line - Fault Clearing Time t=1.25 sec

Table 4-4 CoO Calculation Results - Fault Clearing Time t=1.25 sec

Line	α	b	c	CoO Length (miles)(away from Sub1)	Line Length (miles)	Coo Frequency Equation
SUB1-SUB2	0.36	61.49	0.42	32.0	50.0	$f_{CoO}(t) = 61.49 + 0.42 \cdot t$

The frequency at the two terminals of the line, along with the simulated frequency at the CoO and the equation of the frequency of the CoO are shown in Figure 4.7. Note that the simulated frequency at the CoO is well approximated by the computed CoO frequency.

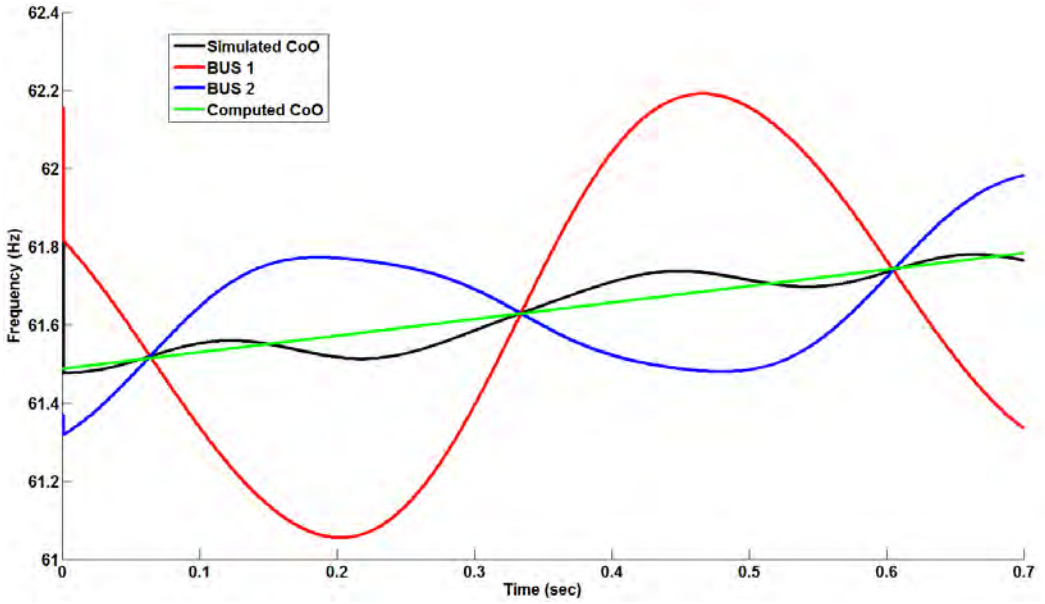

Figure 4.7 Comparison of Simulated and Computed CoO Frequency - Fault Clearing Time t=1.25 sec

Once the CoO is computed, a two generator equivalent was built as explained in section 2.3.2. The equivalent is shown in Figure 4.8.

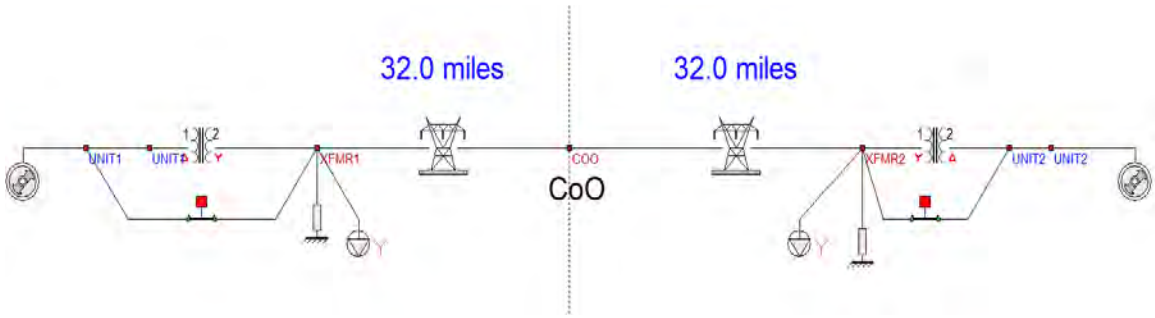

Figure 4.8 Equivalent System - Fault Clearing Time t=1.25 sec

In order to evaluate the accuracy of the equivalent model, the dynamics of the original system and the equivalent system are compared. In particular, the initial conditions (torque angle and speed) of the generator in the substation of interest were set to the values that the system had at the assumed fault clearing time. The initial conditions (torque angle and speed) of the generator in the second substation (mirror image part of the system) were set to be symmetric to the initial conditions of the first generator in terms of the CoO, as explained in section 2.3.2. The initial conditions at the equivalent system are given in Table 4-5.

Table 4-5 Torque Angle & Frequency - Fault Clearing Time t=1.25 sec

Generator 1	CoO	Generator 2
δ_1=113.3 deg	δ_{CoO}=68.0 deg	δ_2=22.6 deg
f_1=62.2 Hz	f_{CoO}=61.52 Hz	f_2=60.82 Hz

The torque angle and frequency of the generator of interest, the CoO phase angle and the relative angle between the generator's torque angle and the CoO phase angle are compared between the original and the equivalent system in Figure 4.9. As expected, the dynamics of the equivalent system are very close to the dynamics of the original system.

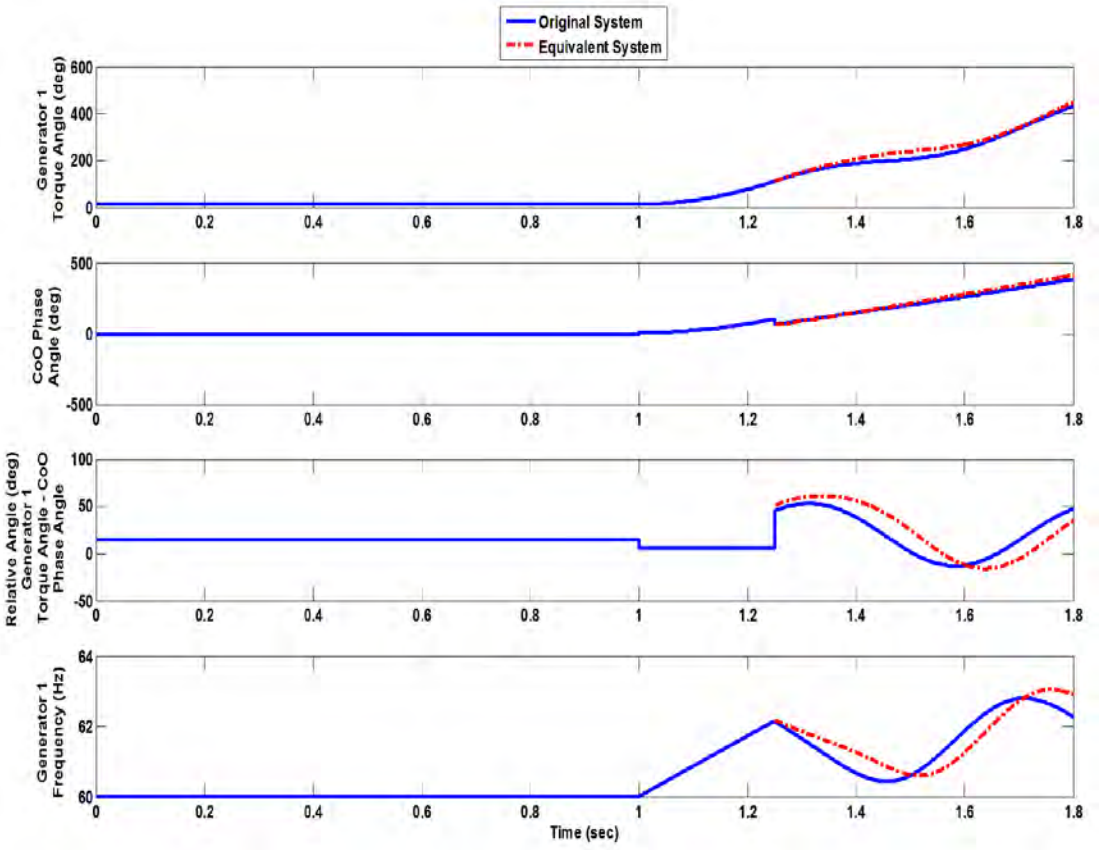

Figure 4.9 Comparison of Original and Equivalent System Dynamics - Fault Clearing Time t=1.25 sec

In order to evaluate the stability of the system for this assumed fault clearing time, the potential energy function of the equivalent system was evaluated. The total energy of the system is also computed and it is superposed on the corresponding potential energy function, as illustrated in Figure 4.10. For this computation the torque angle and the frequency of the two generators of the equivalent system at the assumed clearing time (Table 4-5) are used. Note that the total energy is below the barrier, thus indicating that the system is stable.

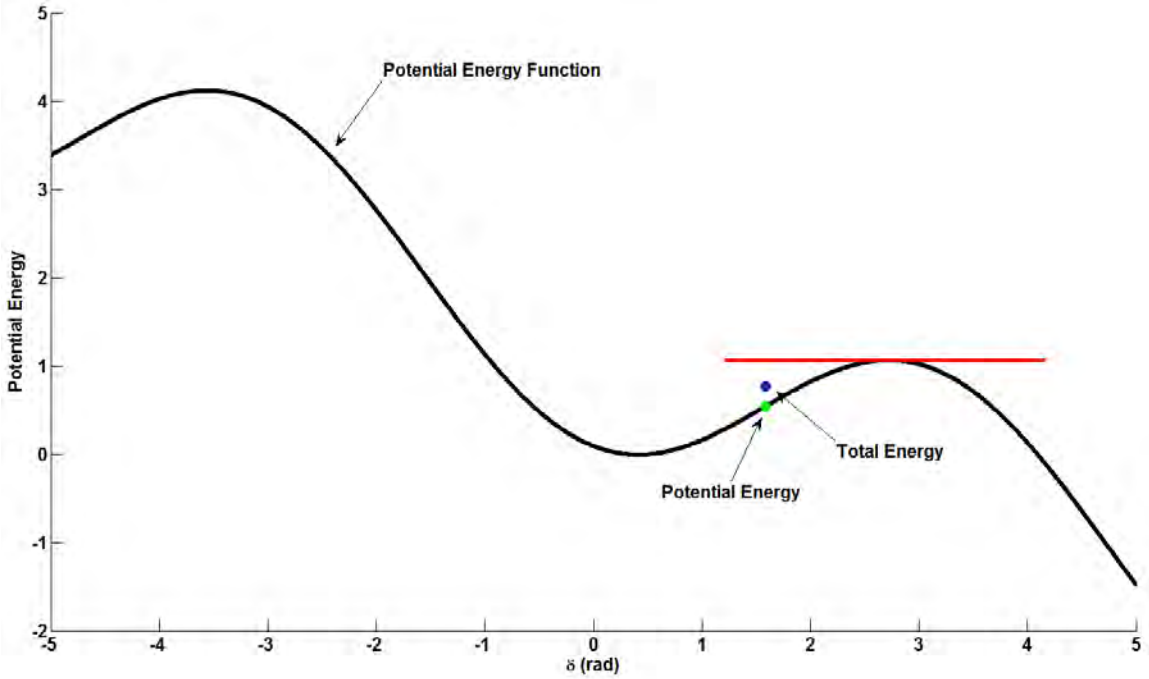

Figure 4.10 System Total Energy Evaluation and Stability Characterization - Fault Clearing Time t=1.25 sec

The same steps as before are followed again for the time instant t=1.37 sec. In particular, assuming that this is the fault clearing time, the frequency at the two ends of the line is simulated for a few cycles as shown in Figure 4.11. Given the frequency at the two terminals of the line, the CoO is computed to be within this line, as shown in the results in Table 4-6.

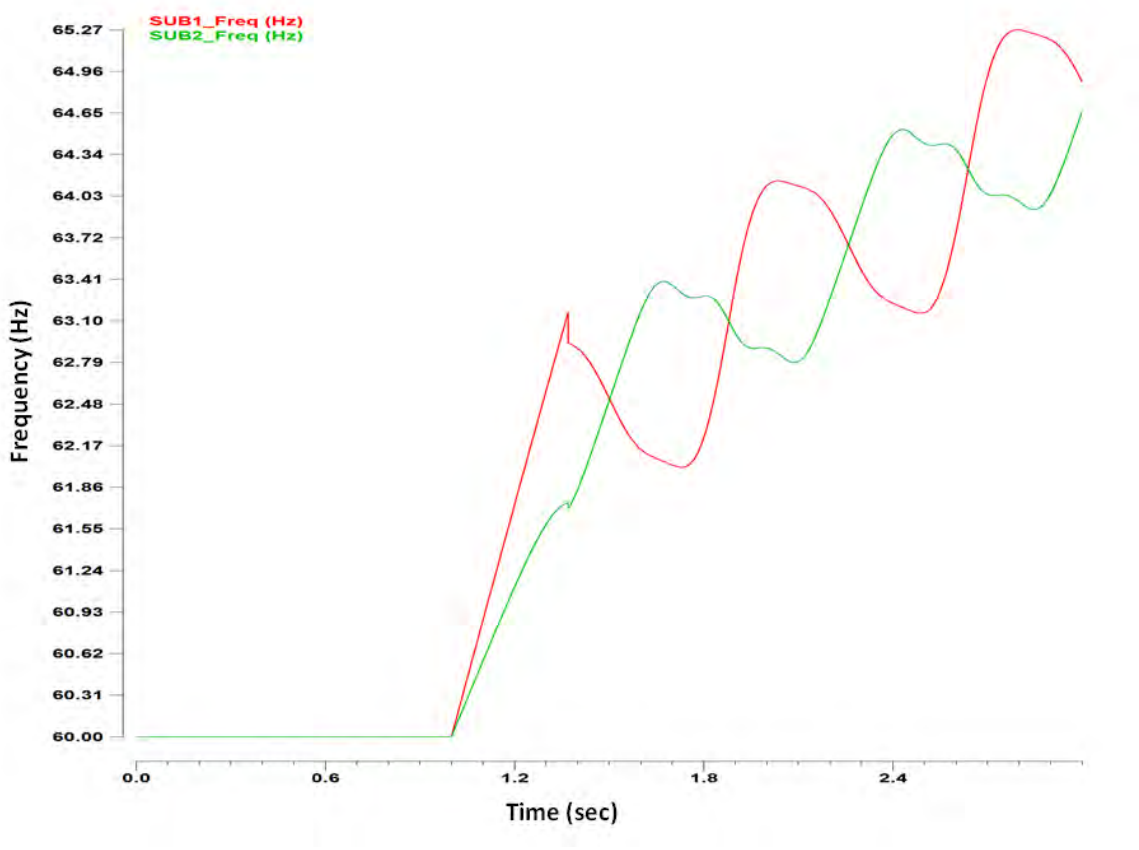

Figure 4.11 Frequency at the Terminals of the Line - Fault Clearing Time t=1.37 sec

Table 4-6 CoO Calculation Results - Fault Clearing Time t=1.37 sec

Line	α	b	c	CoO Length (miles)(away from Sub1)	Line Length (miles)	Coo Frequency Equation
SUB1-SUB2	0.72	62.28	1.63	14.0	50.0	$f_{CoO}(t) = 62.28 + 1.63 \cdot t$

The frequency at the two terminals of the line, along with the simulated frequency at the CoO is computed and the equation of the frequency of the CoO are shown in Figure 4.12. Note that the simulated frequency at the CoO is well approximated by the computed CoO frequency. However the accuracy is decreased compared with the previous case since the system approaches the instability region.

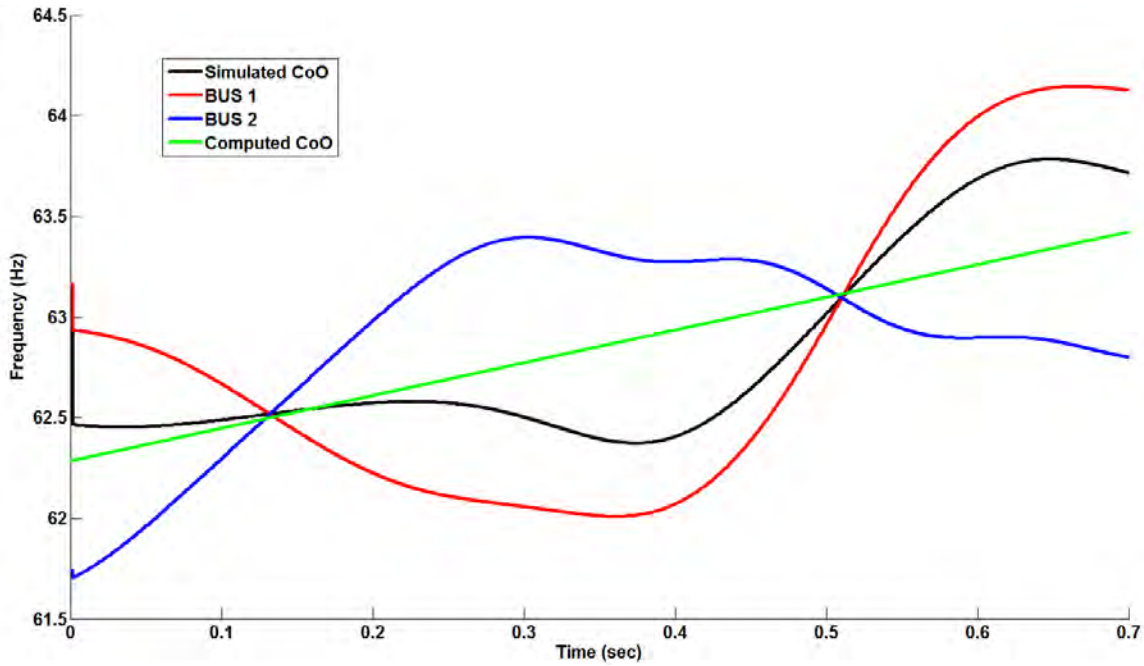

Figure 4.12 Comparison of Simulated and Computed CoO Frequency - Fault Clearing Time t=1.37 sec

Once the CoO is computed, a two generator equivalent was built as shown in Figure 4.13.

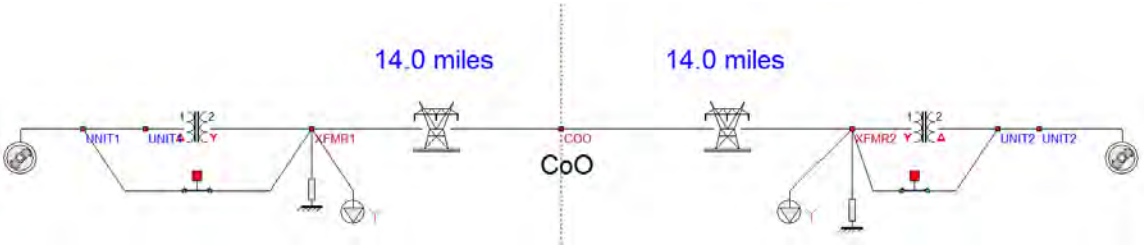

Figure 4.13 Equivalent System - Fault Clearing Time t=1.37 sec

The accuracy of the equivalent model is evaluated by comparing the dynamics of the original system and the equivalent system, as shown in Figure 4.14. The initial conditions of the equivalent system, calculated based on the generator of interest torque angle and speed along with the CoO phase angle and frequency, given in real time by the DSE that is performed at the substation of interest are given in Table 4-7.

Table 4-7 CoO Generators' Torque Angle & Frequency - Fault Clearing Time t=1.37 sec

Generator 1	CoO	Generator 2
δ_1=227.0 deg	δ_{CoO}=164.5 deg	δ_2=102.0 deg
f_1=63.1 Hz	f_{CoO}=62.43 Hz	f_2=61.75 Hz

As expected, the dynamics of the equivalent system are very close to the dynamics of the original system.

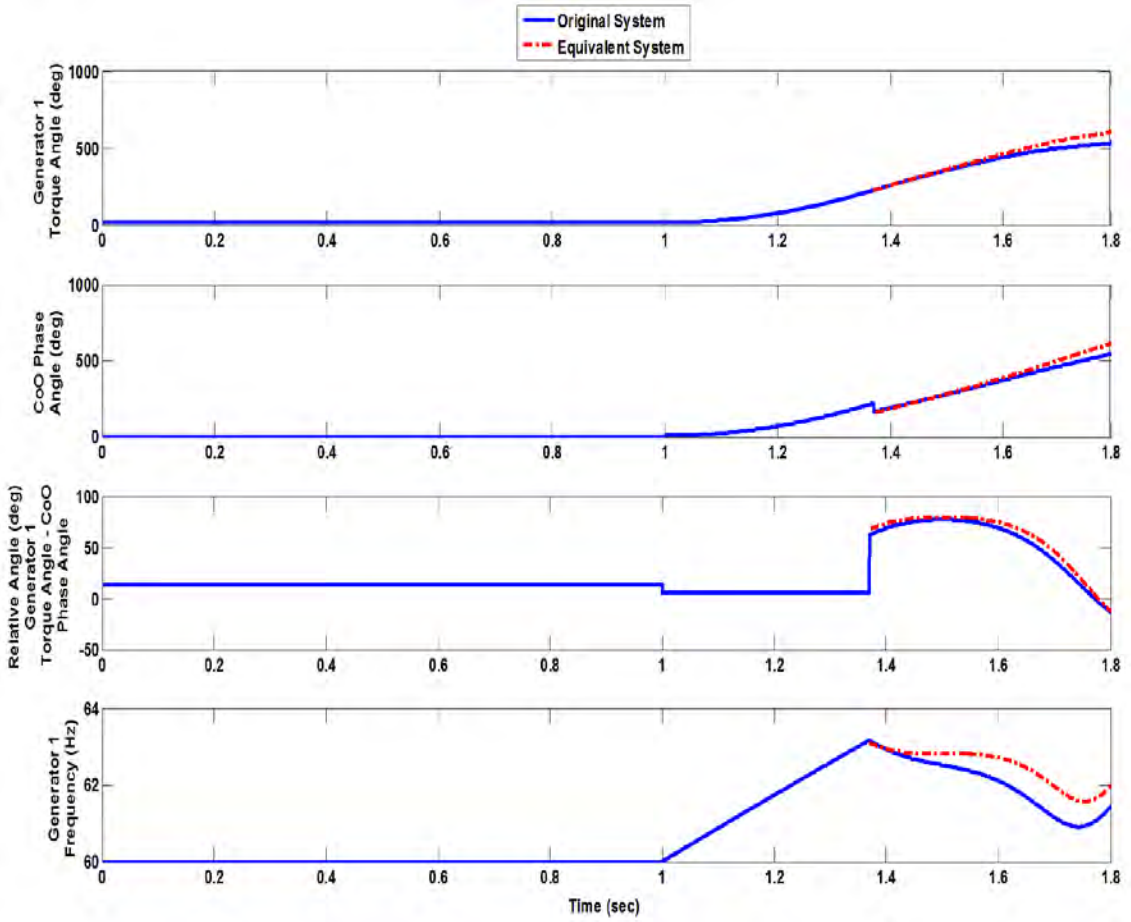

Figure 4.14 Comparison of Original and Equivalent System Dynamics - Fault Clearing Time t=1.37 sec

For this assumed fault clearing time, the stability of the system is evaluated by computing the potential energy function and the total energy of the system. The total energy of the system superposed on the corresponding potential energy function is shown in Figure 4.15. The total energy is equal to the barrier value of the energy, thus indicating that t=1.37 sec is the critical clearing time for the system and for the specific fault. Note that the total energy is computed given the torque angle and the frequency of the two generators of the equivalent system at the assumed clearing time (Table 4-7). Note also that, as expected, this is the same clearing time that was evaluated in section 4.2.1.

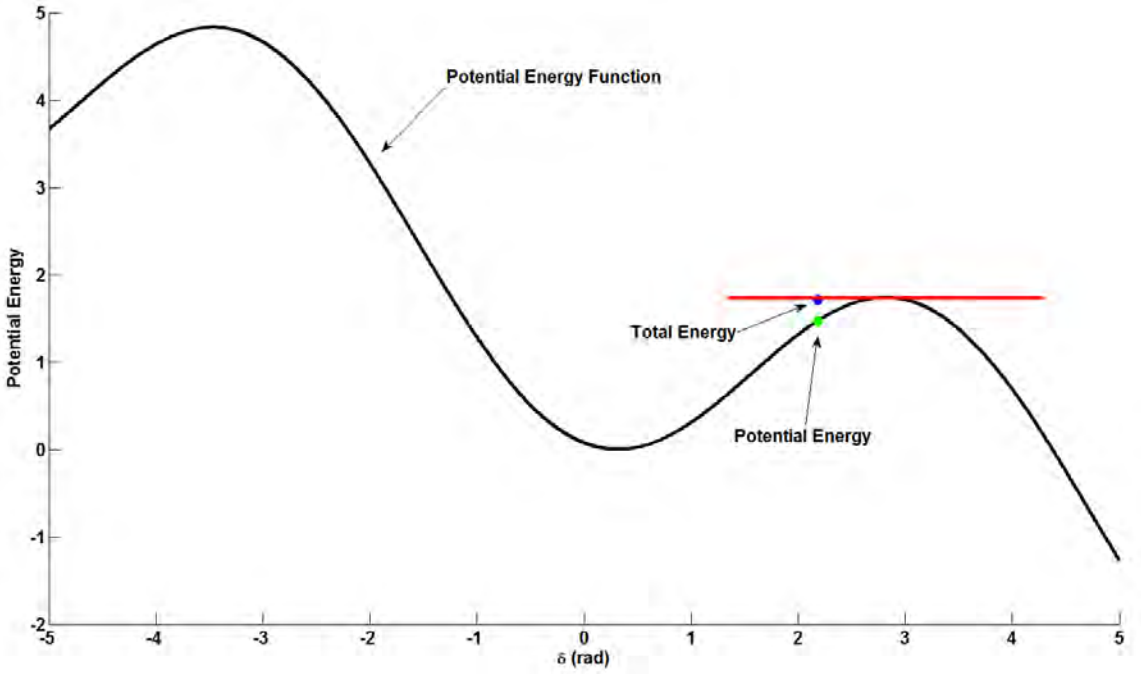

Figure 4.15 System Total Energy Evaluation and Stability Characterization - Fault Clearing Time t=1.37 sec

4.3 Coordination between Stability Monitoring and Setting-Less Protection

In this section, the coordination between the proposed transient stability monitoring approach and setting-less protection approach is demonstrated on a three substation system with three generating units, three step-up transformers and five overhead transmission lines connected in the system as is illustrated in Figure 4.16.

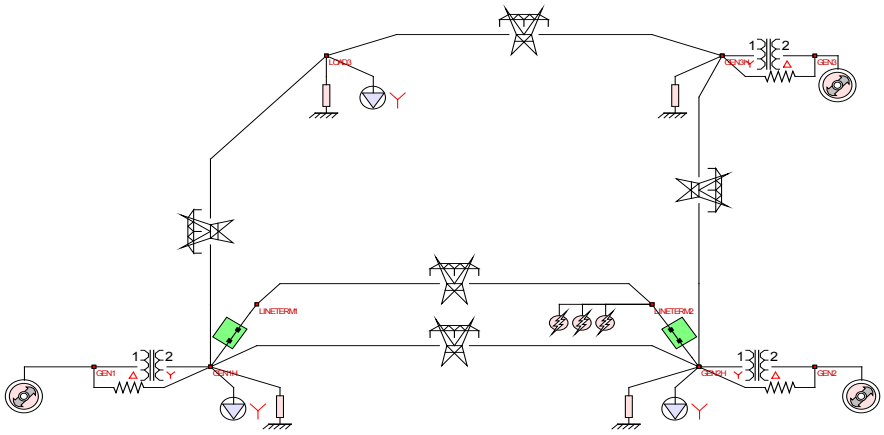

Figure 4.16 Original Test System

When a three phase to ground happens to the top line of the parallel lines and it is tripped by the breakers at the both sides of the line, the system starts to oscillate. According to

our proposed stability monitoring algorithm, an equivalent mirror system should be created at this point which is shown in Figure 4.17.

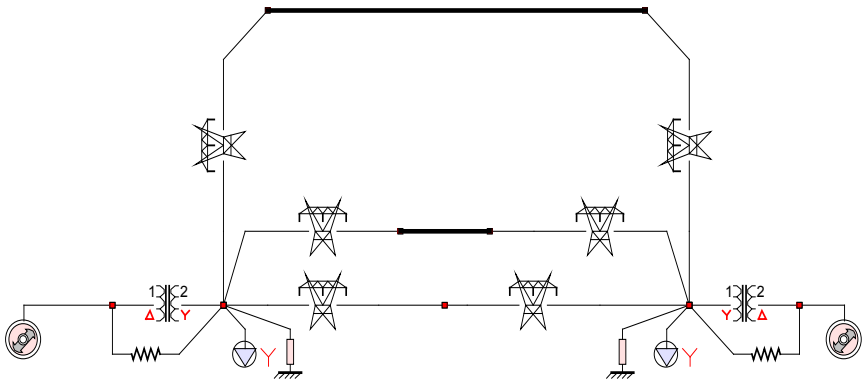

Figure 4.17 Two-generator Equivalent System

But obviously, this equivalent system is not accurate because the top parallel line has been tripped and our post fault equivalent system should not contain this line. To improve the accuracy of the stability monitoring approach, the setting-less protection should provide this system topology evolution.

When the fault happens on the line, the setting-less protection detects this fault and trips the line by opening the breakers. The new system topology is illustrated in Figure 4.18.

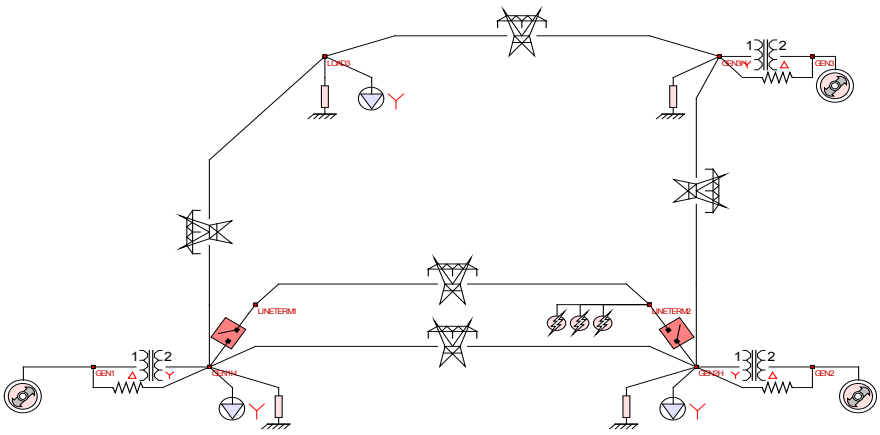

Figure 4.18 New System with Topology Change

The breaker operation sequence is transmitted to the stability monitoring algorithm so that the new equivalent system is created based on the new system topology. The new equivalent system is shown in Figure 4.19.

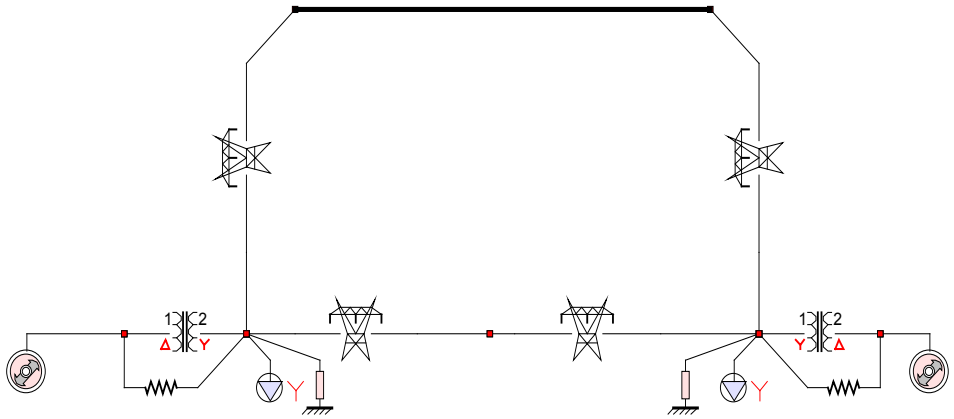

Figure 4.19 New Equivalent System

Since the new equivalent system is obtained, the proposed stability monitoring algorithm can compute the potential energy, kinetic energy and the barrier respectively so that it could predict the system stability accurately.

4.4 Out-of-Step Generator Protection

In this section, demonstrating results of the proposed generator out-of-step protection scheme are presented. The method is presented on two systems, one with a single CoO point and one with multiple CoO points in the system. In addition the developed scheme is compared with the commonly used impedance monitoring based out-of-step detection scheme.

4.4.1 Single CoO Case

The test system consists of five substations, three of which are generating substations, as is illustrated in Figure 4.20. The substation of interest, with the generator on which the predictive out-of-step protection scheme is applied, is substation 1. The parameters of the system can be found in the companion paper. A three-phase fault on the line between substations 1 and 4 and near the substation 1 terminal occurs at t=1 sec and is cleared by disconnecting the line.

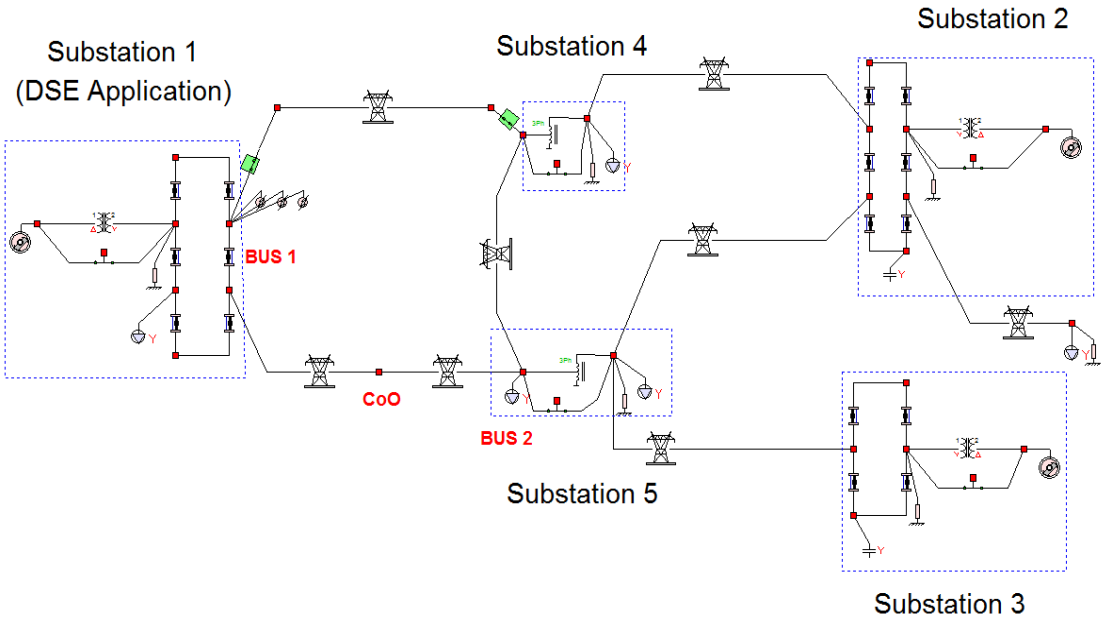

Figure 4.20 Test System – Single CoO Case

For the demonstration of the scheme we consider two subcases, a stable one in which the fault is cleared at 1.1 seconds and an unstable one in which the fault is cleared at 1.25 seconds. Note that for this system the critical fault clearing time has been computed and it is 1.2 seconds. In both subcases the out-of-step protection scheme monitors in real time the total energy of the generator and evaluates its synchronism.

For the stable scenario, the potential energy function of the generator at the fault clearing time (t=1.1 sec), was evaluated and is illustrated in Figure 4.21. The total energy of the generator is also computed and it is superposed on the corresponding potential energy function. It is clear in this case that the total energy is below the barrier, thus indicating a stable case. At this point it is emphasized that the computation of the total energy of the generator is performed based on the methodology described in the companion paper, with the computation of the CoO of the system and the derivation of the two generator equivalent system.

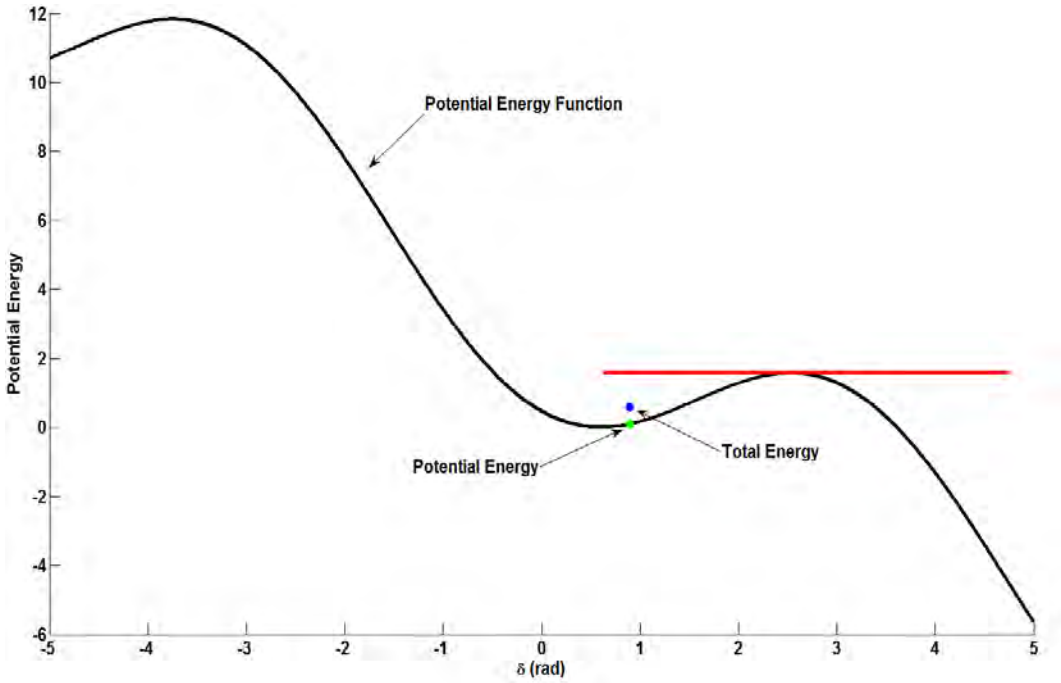

Figure 4.21 Single CoO Case - System Total Energy Evaluation and Stability Characterization – Stable Scenario

For the unstable scenario (fault clearing time t=1.25 sec), the total energy of the generator for the time instant t=1.2 sec is computed and superposed on the potential energy function, as shown in Figure 4.22. Note that at that time instant the total energy is equal to the barrier value of the energy, thus indicating that the generator will be driven in out-of-step condition. The proposed out-of-step protection scheme detects instability of the generator at this time instant and a trip signal can be sent to the generator. Note that the phase angle of the generator at this time instant is 82.7 deg, so there will be minimal overstress at the breaker and the generator can be disconnected.

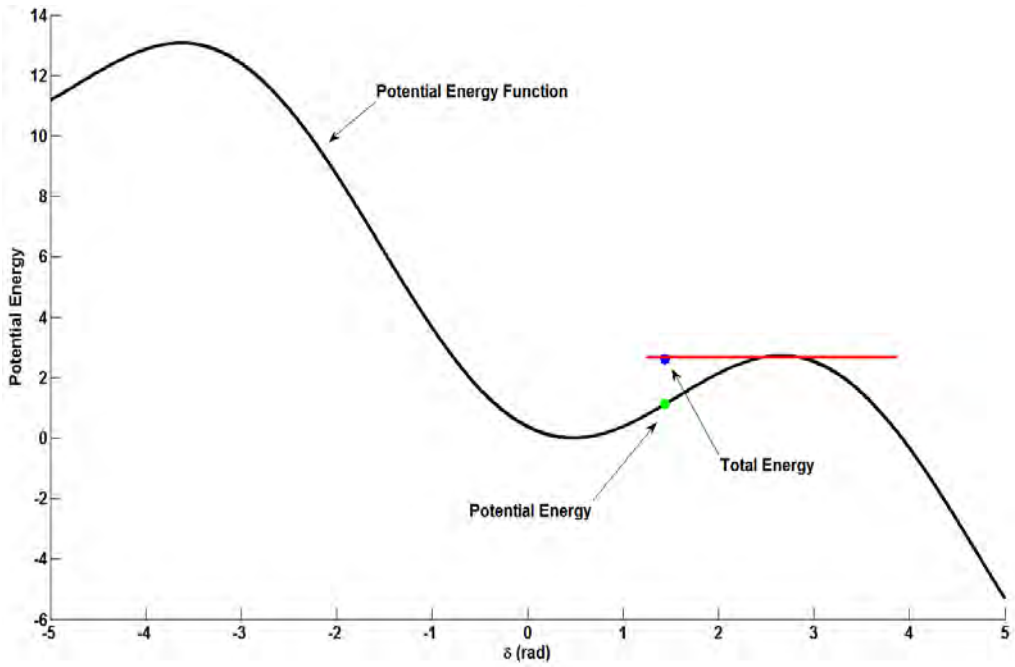

Figure 4.22 Single CoO Case - System Total Energy Evaluation and Stability Characterization – Unstable Scenario

Next, in order to illustrate the advantages of the developed out-of-step protection scheme compared to the state-of-the-art technology, the functionality of an impedance monitoring based, out-of-step relay is simulated and the instability detection time is evaluated for the same unstable scenario. The results are summarized in Figure 4.23. In particular, monitoring of the trajectory of the impedance at the terminals of the generator indicates that the right blinder and the left blinder are crossed at t=1.34 sec and t=1.51 sec respectively. As a result, the impedance based relay detected instability at t=1.51 sec, thus the developed method in this work predicted instability 0.31 sec before the conventional relay. The phase difference between the generator and system at 1.20 sec and 1.51 sec is 82.7 and 216.2 degrees respectively. In this case, the generator can be tripped at 1.2 sec (as indicated by the proposed scheme) when the angle is 82.7 degrees but it cannot be tripped at 1.51 sec because the breaker will be overstressed with transient recovery voltage. So, the tripping will be delayed until the angle returns to smaller values.

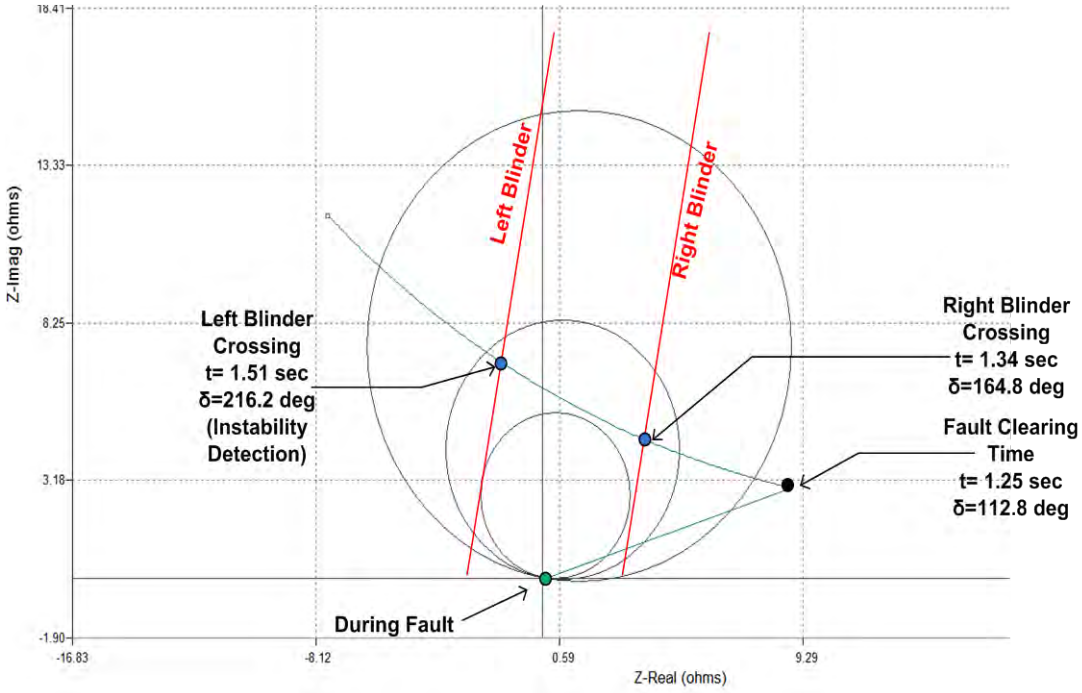

Figure 4.23 Impedance Trajectory Monitoring – Single CoO Case

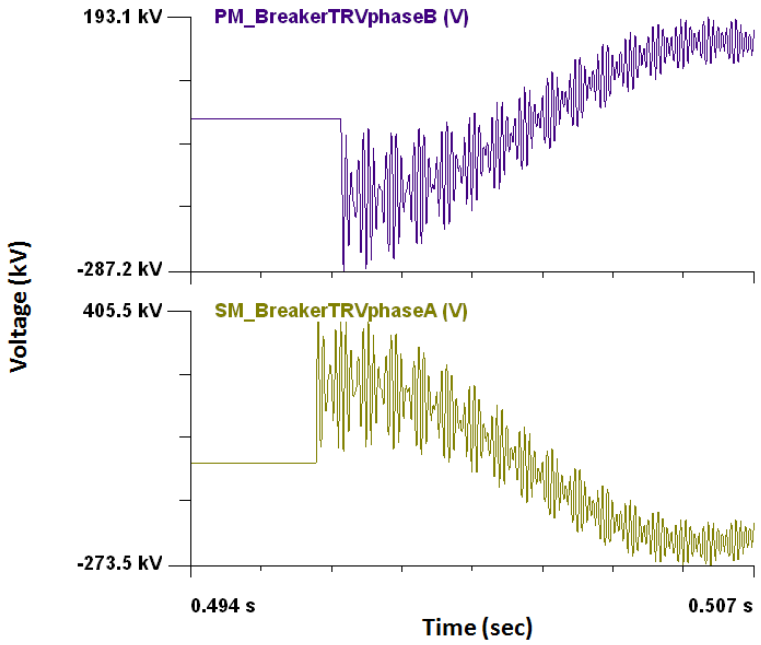

Figure 4.24 Worst Case TRV across the Breaker for the Proposed Method (top trace) and for the Standard Out-of-Step Protection (bottom trace)

The breaker transient recovery voltage is shown in Figure 4.24. The figure shows the transient recovery voltage for the worst case when the breaker is tripped with the propose

method (top trace) and the transient recovery voltage when the breaker is tripped when the standard out-of-step relay asserts instability (bottom trace). Note that the highest TRV occurs at different phases for the two cases. Also note that the highest TRV is 287 kV and 405 kV for the two cases respectively or 2.54 pu and 3.59 pu respectively.

4.4.2 Multiple CoO Case

In this section the generator out-of-step protection scheme is demonstrated on a three substation system with two CoO points, shown in Figure 4.25. Substation 2 is the substation of interest with the generator under protection. It is assumed that a three-phase fault occurs at the terminal of the second substation which causes the trip of one of the two parallel transmission lines that connect the first with the second substation. The fault initiates at t=1 sec. The parameters of the system can be found in the companion paper.

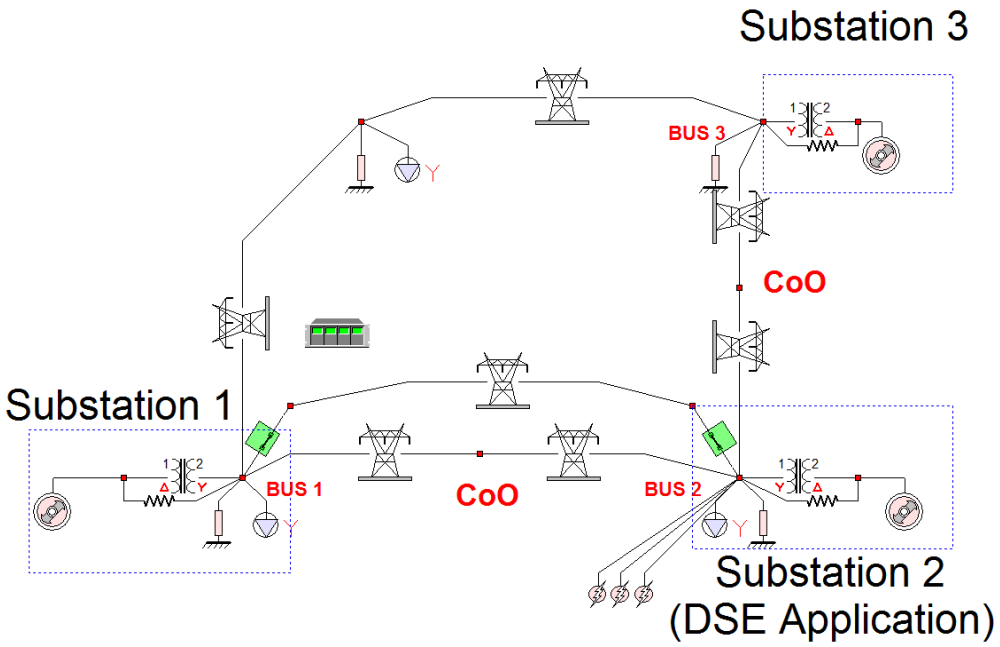

Figure 4.25 Test System – Multiple CoO Case

A stable and an unstable scenario are demonstrated. The fault clearing time at the stable case is 1.2 sec while for the unstable case is 1.4 sec. For this system the critical fault clearing time has been computed and it is 1.38 seconds. Based on the developed out-of-step protection scheme the energy of the generator is continuously monitored and its stability is assessed.

At the stable scenario, the potential energy function of the generator at the fault clearing time (t=1.2 sec) was evaluated. The total energy of the system is also computed and it is superposed on the corresponding potential energy function, as illustrated in Figure 4.26.

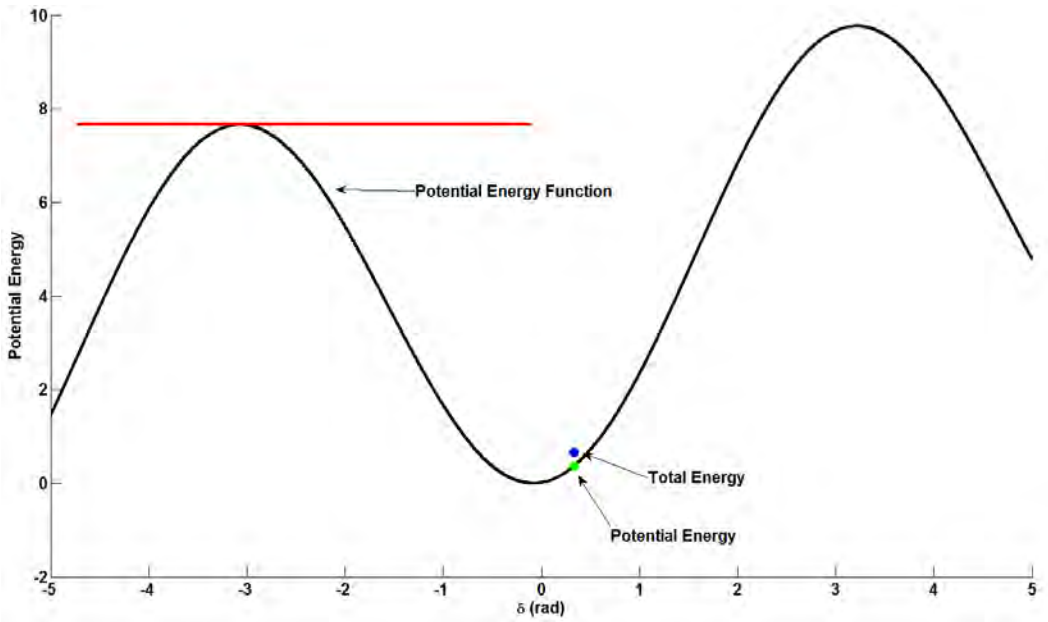

Figure 4.26 Multiple CoO Case - System Total Energy Evaluation and Stability Characterization – Stable Scenario

It is clear in this case that the total energy is below the barrier, thus indicating a stable system. Note that the barrier value is the smallest value among the potential energy value of the unstable equilibrium points that surround a stable equilibrium point.

At the unstable scenario, the total energy of the generator at the time instant t=1.38 sec is computed and superposed on the potential energy function as illustrated in Figure 4.27. At that time instant the total energy is equal to the barrier value of the energy, thus indicating that the generator will become unstable. As a result at this time instant a trip signal is sent to the generator to disconnect it before losing its synchronism. The phase angle of the generator at this time instant is 103.8 deg, thus there will be minimal overstress at the breaker.

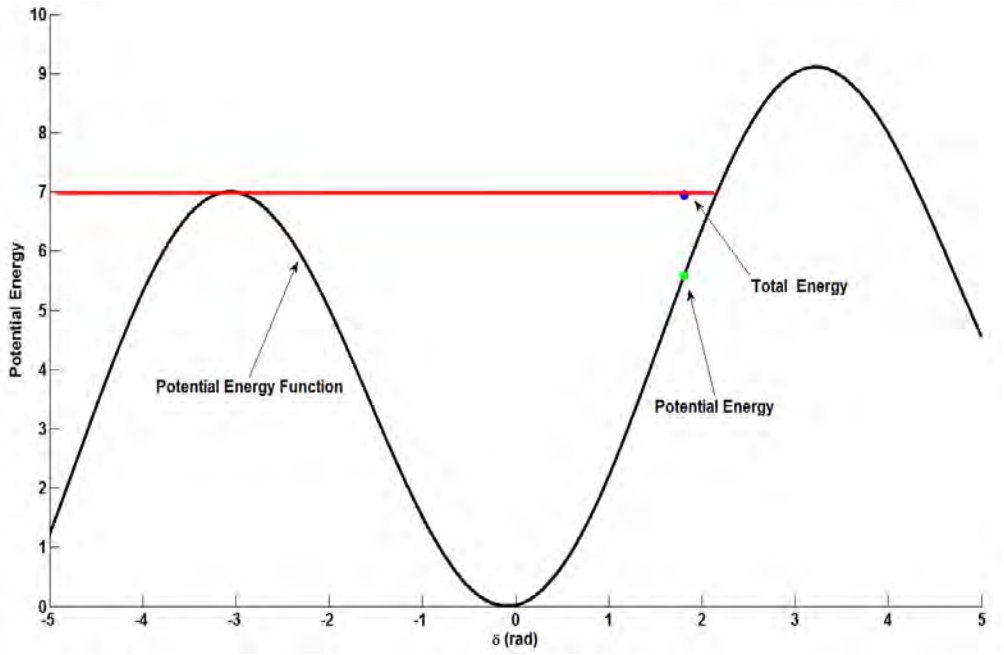

Figure 4.27 Multiple CoO Case - System Total Energy Evaluation and Stability Characterization – Unstable Scenario

Comparison between the developed out-of-step protection scheme and the response of a conventional, impedance monitoring based, out-of-step relay is performed next with the response of the impedance monitoring out-of-step relay simulated for the same unstable scenario. The results are summarized in Figure 4.28. In particular, monitoring of the trajectory of the impedance at the terminals of the generator indicates that the left blinder and the right blinder are crossed at t=1.43 sec and t=1.64 sec respectively. As a result, the impedance based relay detected instability at t=1.64 sec. Thus, it is concluded that the developed method predicted instability 0.26 sec before the conventional relay. The phase difference between the generator and system at 1.38 sec and 1.64 sec is 103.8 and 210.8 degrees respectively. In this case, the generator can be tripped at 1.38 sec (as indicated by the proposed scheme) when the angle is 103.8 degrees but it cannot be tripped at 1.64 sec because the breaker will be overstressed with transient recovery voltage. So, the tripping will be delayed until the angle returns to smaller values.

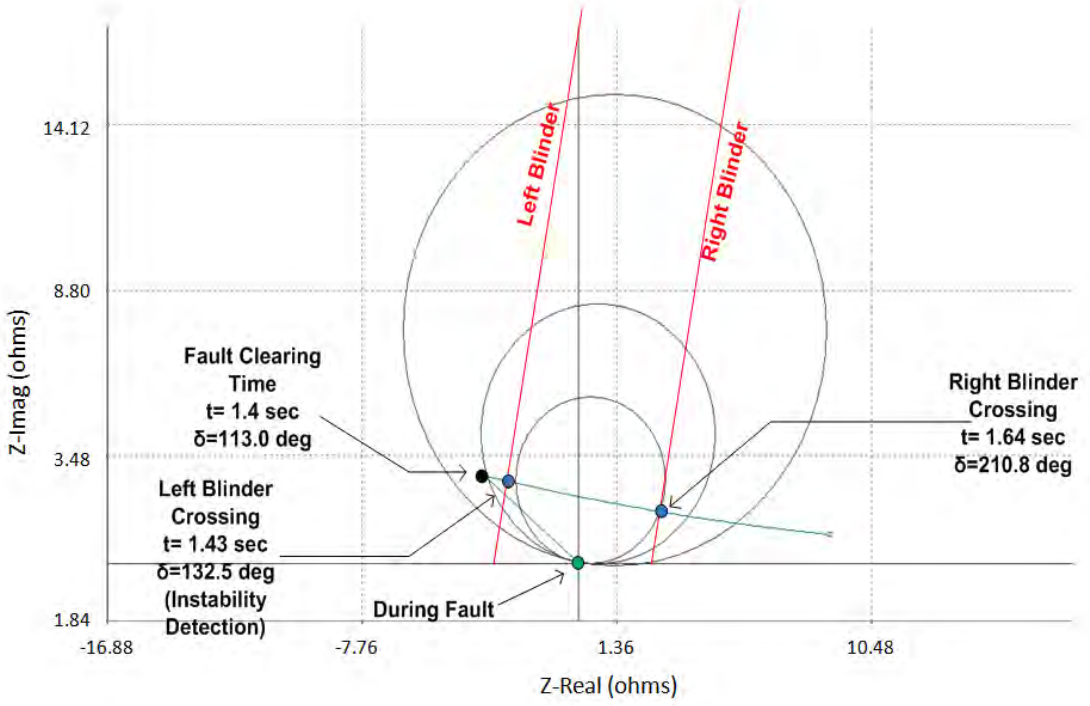

Figure 4.28 Impedance Trajectory Monitoring – Multiple CoO Case

The breaker transient recovery voltage is shown in Figure 4.29. The figure shows the transient recovery voltage for the worst case when the breaker is tripped with the propose method (top trace) and the transient recovery voltage when the breaker is tripped when the standard out-of-step relay asserts instability (bottom trace). Note that the highest TRV occurs at different phases for the two cases. Also note that the highest TRV is 334 kV and 422 kV for the two cases respectively or 2.96 pu and 3.74 pu respectively.

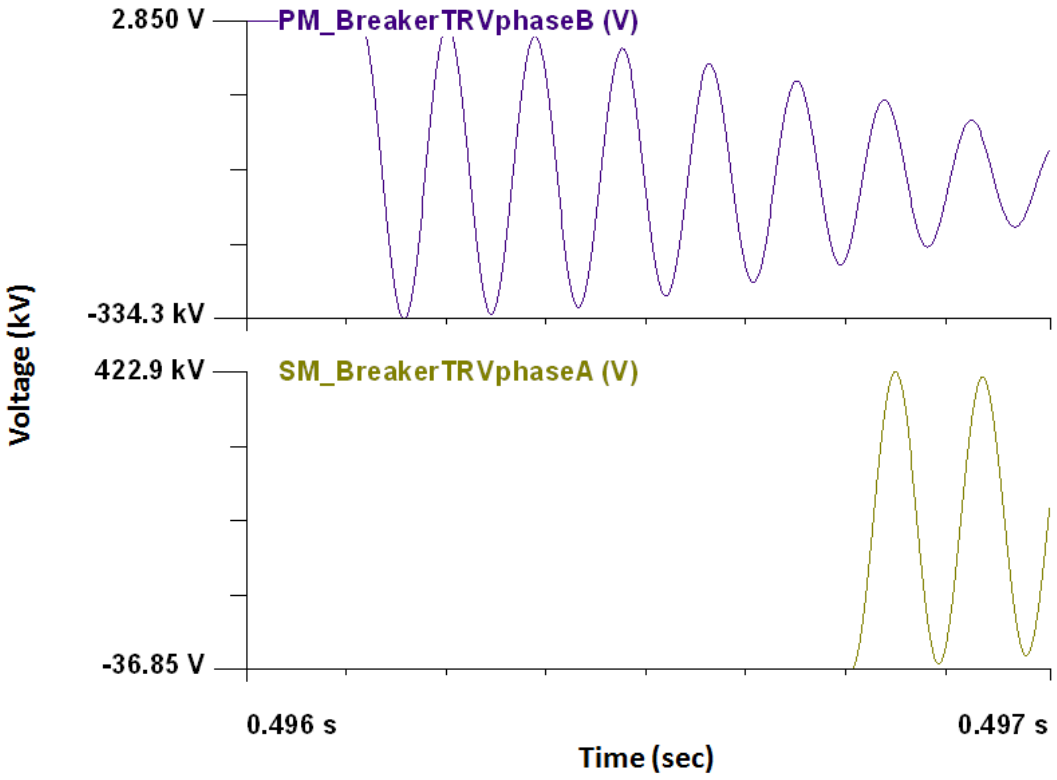

Figure 4.29 Impedance Worst Case TRV across the Breaker for the Proposed Method (top trace) and for the Standard Out-of-Step Protection (bottom trace)

5. Conclusions

The presented research work consists mainly of two parts: (a) a predictive, energy-based, transient stability monitoring scheme that is enabled by the dynamic state estimator and characterizes in real time the stability of the system and (b) a setting-less protection algorithm that protects the power components in real time and provides the evolution of the system topology. As an application of the transient stability monitoring scheme, a predictive generator out-of-step protection scheme that can protect a generator from a potential loss of synchronism has also been developed.

In particular, an energy-based transient stability monitoring scheme is presented first in this work. The scheme is enabled by the dynamic state estimator since it utilizes the estimated state of the substation, monitors in real-time the transient swings of the system and characterizes the stability of the system. In particular, the real-time dynamic model of the system, as given by the DSE, is utilized to evaluate the system's energy function based on Lyapunov's direct method and extract stability properties from the energy function. The two major components of the scheme are a) the calculation of the center of oscillations of the system and b) the derivation of an equivalent, reduced sized model which is used for the calculation of the potential and kinetic energy of the system based on which the stability of the system is determined. The mathematical formulation for the calculation of the center of oscillations and the methodology for the equivalent derivation are presented in detail. The overall algorithm of the stability monitoring scheme and in particular how the information given by the dynamic state estimation is used for the real-time characterization of the stability of the system, are also given.

To provide the system topology evolution to the purposed transient stability monitoring approach, a setting-less protection algorithm is also presented in the work. Whenever a fault happens, the setting-less protection relays will determine which and when breakers will trip which will change the system topology. The principle of the proposed setting-less protection scheme is that it monitors the health status of the device under protection by fitting the real-time measurements to the device model. If the real-time measurements fit the model it means the device operation corresponds to the model of the device in its normal mode. If there are any internal faults or abnormal conditions that change the model of the device, there will be mismatches between the measurements and the device model. In this case the relay decides to trip breakers to isolate the faulty device at specific times. The breaker trips change the network topology. The topology change information together with the time of occurrence is sent to the stability monitoring algorithm. In summary, the DSE-based protection approach provides the following:

1. Real-time dynamic state of the system
2. Health status of power apparatus
3. Up-to date network topology
4. Bad data identification ability

5. Model validation capability
6. Other

Finally an application of these two schemes, which is a novel, predictive, generator out-of-step protection scheme is described. Given the DSE results, the energy of the generator is computed and continuously monitored and if it exceeds a predefined threshold then instability is asserted and a trip signal can be sent to the generator. The schemes have been demonstrated on various test systems in order to demonstrate their efficiency and accuracy along with comparison with the state-of-the art technology for generator out-of-step protection in order to demonstrate the superiority of the developed method. The major advantage of the scheme is that the out-of-step condition is predicted before its occurrence and therefore relays can act much faster than today's technology. It is concluded that the scheme can predict the generator's instability much earlier than traditional methods such as present day out-of-step relays. The prediction time is of such magnitude that the generating unit can be tripped before it actually slips a pole as it is the case with present out of step relaying systems.

References

[1] E. Farantatos, "A Predictive Out-Of-Step Protection Scheme Based On PMU Enabled Distributed Dynamic State Estimation", PhD Thesis, Georgia Institute of Technology, 2012

[2] PSERC, "Real Time Security Assessment of Angle Stability Through Synchrophasor," May 2010.

[3] P. Kundur, "Power System Stability and Control," McGraw-Hill, 1994.

[4] M. Anderson and A. A. Fouad, "Power System Control and Stability", 2nd edition. New York: Wiley, 2003.

[5] M. Pavella and P. G. Murthy, "Transient Stability of Power Systems, Theory and Practice", John Wiley & Sons Publications.

[6] M. Pavella, D. Ernst, and D. Ruiz-Vega, "Transient Stability of Power Systems: A Unified Approach to Assessment and Control", Kluwer's Power Electronics and Power Systems Series.

[7] H. D. Chiang, "Direct Methods for Stability Analysis of Electric Power System", Wiley Publications.

[8] V. Vittal, S. Rajagopal, A. A. Fouad, M. A. El-Kady, E. Vaahedi and V. F. Carvalho, "Transient stability analysis of stressed power systems using the energy function method," IEEE Trans. Power Systems, vol. 3, pp. 400-412, May 1988.

[9] M. A. El-Kady, C. K Tang, V. F. Carvalho, A. A. Fouad and V. Vittal "Dynamic Security Assessment Utilizing the Transient Energy Function Method," IEEE Trans. Power Systems, vol. 1, issue 3, pp. 284-291, Aug. 1986.

[10] A. Michel, A. A. Fouad and V. Vittal, "Power system transient stability using individual machine energy functions," IEEE Trans. Circuits and Systems, vol. CAS-30, issue 5, pp. 266-276, May 1983.

[11] L. Wang, M. Klein, S. Yirga and P. Kundur, "Dynamic reductions of large power systems for stability studies", IEEE Trans. Power Syst., 1997, 12, (2), pp. 889–895

[12] J. H. Chow, R. Galarza, P. Accari and W. W. Price, "Inertial and slow coherency aggregation algorithms for power system dynamic model reduction", IEEE Trans. Power Syst., 1995, 10, (2), pp. 680–685.

[13] S. K. Joo, C. C. Liu, L. E. Jones and J. W. Choe, "Coherency and Aggregation Techniques Incorporating Rotor and Voltage Dynamics," IEEE Trans. Power Systems, vol. 19, no. 2, pp. 1068-1075, 2004.

[14] M. L. Ourari, L. A. Dessaint, and V. Q. Do, "Dynamic equivalent modeling of large power systems using structure preservation technique," IEEE Trans. Power Systems, vol. 21 (3), pp.1284- 1295, Aug. 2006.

[15] F. Ma, X. Luo, and V. Vittal, "Application of Dynamic Equivalencing in Large-scale Power Systems," in Proc. 2011 PES General Meeting, Detroit, MI, July 24-29 2011.

[16] A. B. Almeida, R. Reginatto, Rui. J and G. C. da Silva "A software tool for the determination of dynamic equivalents of power systems ", IREP Symposium 2010, Bulk Power System Dynamics and Control VIII, August 1-6, 2010

[17] A. Chakrabortty, J. H. Chow and A. Salazar, "A Measurement-based Framework for Dynamic Equivalencing of Power Systems using Wide- Area Phasor Measurements," IEEE Trans. on Smart Grid, vol. 1(2), 2011.

[18] A. P. S. Meliopoulos, G. J. Cokkinides, F. Galvan, B. Fardanesh and P. Myrda, "Delivering Accurate and Timely Data to All: Model Based Substation Automation Applications for Advanced Data Availability", IEEE Power & Energy Magazine, Volume 5, No: 3, pp 74-86, May/June 2007.

[19] J. Berdy, "Out-of-Step Protection for Generators," GE Publication No. GER-3179.

[20] M. A. Pai, Power Systems Stability, North Holland Publishing Co., New York, 1981.

[21] P. Kundur, Power System Stability and Control. New York: McGraw-Hill, 1994.

[22] P. W. Sauer, M. A. Pai, Power System Dynamics and Stability.

[23] P. M. Anderson, A. A. Fouad, Power System Control and Stability, IEEE Press, 2003.

[24] M. Pavella, P.G. Murthy, Transient Stability of Power Systems, Theory and Practice, John Wiley & Sons Publications.

[25] Mania Pavella, Damien Ernst, and Daniel Ruiz-Vega, *Transient Stability of Power Systems: A Unified Approach to Assessment and Control*, Kluwer's Power Electronics and Power Systems Series.

[26] P. C. Mangusson, "Transient energy method of calculating stability," AIEE Trans., vol. 66, pp. 747-755, 1947.

[27] P. D. Aylett, "The energy-integral criterion of transient stability limits of power systems," Proc. of the IEEE, vol. 105C, 8, Sept. 1958, pp. 257-536.

[28] V. Vittal, S. Rajagopal, A. A. Fouad, M. A. El-Kady, E. Vaahedi and V. F. Carvalho, "Transient stability analysis of stressed power systems using the energy function method," IEEE Trans. Power Systems, vol. 3, pp. 400-412, May 1988.

[29] V. Vittal, N. Bhatia, A. A. Fouad, G. A. Maria and H. M. Z. El-Din "Incorporation of nonlinear load models in the transient energy function method," IEEE Trans. Power Systems, vol. 4, pp. 1031-1-36, Aug. 1989.

[30] M. A. El-Kady, C. K Tang, V. F. Carvalho, A. A. Fouad, V. Vittal "Dynamic Security Assessment Utilizing the Transient Energy Function Method," IEEE Trans. Power Systems, vol. 1, issue 3, pp. 284-291, Aug. 1986.

[31] A. A. Fouad, V. Vittal, S. Rajagopal, V. F. Carvalho, M. A. El-Kady, C. K. Tang, J. V. Mitsche, M. V. Pereira, "Direct Transient Stability Analysis Using Energy Functions Application to Large Power Networks," IEEE Trans. Power Systems, vol. 2, issue 1, pp. 37-43, Feb. 1987.

[32] A. Michel, A Fouad, V. Vittal, "Power system transient stability using individual machine energy functions," IEEE Trans. Circuits and Systems, vol. CAS-30, issue 5, pp. 266-276, May 1983.

[33] Y. Xue, T. Van Cutsem and M. Ribbens-Pavella, "A simple direct method for fast transient stability assessment of large power systems," IEEE Trans. Power Systems, vol. 3, pp. 400-412, May 1988.

[34] I. A. Hiskens and D. J. Hill, "Energy functions, transient stability and voltage behaviour in power systems with nonlinear loads," IEEE Trans. Power Systems, vol. 4, pp. 1525-1533, Nov. 1989.

[35] H. D. Chiang and J. S. Thorp, "The closest unstable equilibrium point method for power system dynamic security assessment," IEEE Trans. Circuits and Systems, vol. 36, pp. 1187-1200, Sept. 1989.

[36] T. S. Chung and D. Z. Fang, "Corrected transient energy function and transient stability limit assessment," in Proc. 2000 IEEE Power Engineering Society Winter Meeting, 23-27, vol. 1, pp. 72-77, Jan. 2000.

[37] F. A. Rahimi, M. G. Lauby, J. N. Wrubel and K. L. Lee, "Evaluation of the transient energy function method for on-line dynamic security analysis," IEEE Trans. Power Systems, vol. 8, pp. 497-507, May 1993.

[38] Y. Z. Sun, X. Li and Y. H. Song, "A new Lyapunov function for transient stability analysis of controlled power systems," in Proc. 2000 IEEE Power Engineering Society Winter Meeting, vol. 2, pp. 1325-1330, Jan. 2000.

[39] A. P. Sakis Meliopoulos, G. J. Cokkinides, "Power System Relaying, Theory and Applications," Georgia Institute of Technology Course Notes.

[40] M. Pavella, P.G. Murthy, *Transient Stability of Power Systems, Theory and Practice*, John Wiley & Sons Publications.

Appendix A: Overall Design of the Setting-Less Relay

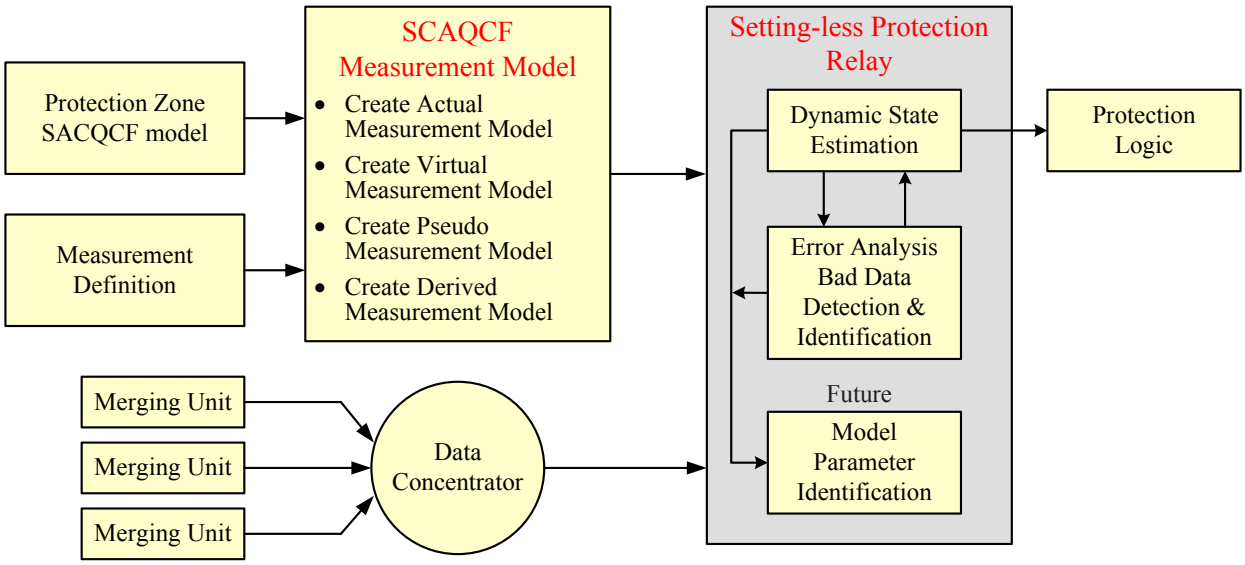

Figure A.1 Overall Design of Setting-less Protection Relay

Figure A.1 illustrates the overall design of setting-less protection relay. The algorithms for the setting-less protection have been streamlined for the purpose of increasing efficiency. An object-oriented approach for the DSE based protection algorithm is developed by utilizing the State and Control Algebraic Quadratic Companion Form (SCAQCF). All the mathematical models of the protection zones in the power system are written in SCAQCF format so that the DSE based protection algorithm could be applied to any device. The setting-less protection relay has two kinds of input data. One of the input data is the measurement model in the SCAQCF syntax and the other one is the real-time measurements data coming from the data concentrator. The measurement model in SCAQCF syntax is created by using the measurement pointers defined in the measurement definition file and getting the mathematical formulas for the measurements from the corresponding SCAQCF device model file, which describes the mathematical model of the protection zone. The details of how to formulate the SCAQCF measurement model can be found in Appendix B. There is a possibility that the real-time measurement data comes from multiple merging units, and a data concentrator is provided in the overall approach to align all data from different merging units with the same time stamp and feed them as one-way streaming data to the setting-less protection relay. The output of the setting-less protection relay is the protection logic, which determines the protection action according to the following criteria: if the real-time measurements fit the device measurement model well (the dynamic state estimation shows a high confidence level), then the protection zone is in a healthy status; otherwise, some abnormalities inside the

protection zone have occurred, protection action should be acted. Note that the protection zone SCAQCF model and the measurement definition is automatically generated by the software WinIGS.

Inside the setting-less protection relay, dynamic state estimation performs whenever the data comes in. At the same time, error analysis and bad data detection are simultaneously operating in case there is some bad data or computation error which could both bring the incorrect protection results. In the near future, model parameter identification function will be added so that it can modify the protection zone model provide that the device parameters are changed.

Appendix B: Object-Oriented Implementation

B.1 Time Domain SCAQCF Device Model Description

Each device mathematical model should be expressed in the generalized State and Control Algebraic Quadratic Companion Form (SCAQCF) so that each model is in the object-oriented manner. Most devices in the power system are nonlinear and for the differential equation, the quadratic integration method could be utilized to make each device model in quadratic form. The standard SCAQCF model is shown below:

$$\begin{Bmatrix} I(\mathbf{x},\mathbf{u}) \\ \vdots \\ 0 \\ \vdots \end{Bmatrix} = Y_{eqx}\mathbf{x} + \begin{Bmatrix} \vdots \\ \mathbf{x}^T F_{eqx}^i \mathbf{x} \\ \vdots \end{Bmatrix} + Y_{equ}\mathbf{u} + \begin{Bmatrix} \vdots \\ \mathbf{u}^T F_{equ}^i \mathbf{u} \\ \vdots \end{Bmatrix} + \begin{Bmatrix} \vdots \\ \mathbf{x}^T F_{eqxu}^i \mathbf{u} \\ \vdots \end{Bmatrix} - B_{eq}$$

$$B_{eq} = -N_{eqx}\mathbf{x}(t-h) - N_{equ}\mathbf{u}(t-h) - M_{eq}I(t-h) - K_{eq}$$

$$\mathbf{h}(\mathbf{x},\mathbf{u}) = Y_{opx}\mathbf{x} + Y_{opu}\mathbf{u} + \begin{Bmatrix} \vdots \\ \mathbf{x}^T F_{opx}^i \mathbf{x} \\ \vdots \end{Bmatrix} + \begin{Bmatrix} \vdots \\ \mathbf{u}^T F_{opu}^i \mathbf{u} \\ \vdots \end{Bmatrix} + \begin{Bmatrix} \vdots \\ \mathbf{x}^T F_{opxu}^i \mathbf{u} \\ \vdots \end{Bmatrix} - B_{op}$$

Scaling factors: *Iscale*, *Xscale and Uscale*

Connectivity: *TerminalNodeName*

$$\textit{subject to}: \quad \mathbf{h}_{\min} \le \mathbf{h}(\mathbf{x},\mathbf{u}) \le \mathbf{h}_{\max}$$

$$\mathbf{u}_{\min} \le \mathbf{u} \le \mathbf{u}_{\max}$$

where:

$I(\mathbf{x},\mathbf{u})$: the through variables of the device model, $I = [I(t), I(t_m)]$

$\mathbf{x}$: external and internal state variables of the device model, $\mathbf{x} = [\mathbf{x}(t), \mathbf{x}(t_m)]$

$\mathbf{u}$: control variables of the device model, i.e. transformer tap, etc. $\mathbf{u} = [\mathbf{u}(t), \mathbf{u}(t_m)]$

Y_{eqx}: matrix defining the linear part for state variables,

F_{eqx}: matrices defining the quadratic part for state variables,

Y_{equ}: matrix defining the linear part for control variables,

F_{equ}: matrices defining the quadratic part for control variables,

F_{eqxu}: matrices defining the quadratic part for the product of state and control variables,

B_{eq}: history dependent vector of the device model,

N_{eqx}: matrix defining the last integration step state variables part,

N_{equ}: matrix defining the last integration step control variables part,

M_{eq}: matrix defining the last integration step through variables part,

K_{eq} : constant vector of the device model,

$Iscale$: scaling factors for the through variables and zeros on the left side of the equations,

$Xscale$: scaling factors for the state variables $\mathbf{x}$,

$Uscale$: scaling factors for the control variables $\mathbf{u}$,

$TerminalNodeName$: terminal names defining the connectivity of the device model,

$\mathbf{h}_{\min} \le \mathbf{h}(\mathbf{x},\mathbf{u}) \le \mathbf{h}_{\max}$: operating constraints,

$\mathbf{u}_{\min}, \mathbf{u}_{\max}$: lower and upper bounds for the control variables.

Y_{opx} : constraint matrix defining the linear part for state variables,

F_{opx} : constraint matrices defining the quadratic part for state variables,

Y_{opu} : constraint matrix defining the linear part for control variables,

F_{opu} : constraint matrices defining the quadratic part for control variables,

F_{opxu} : constraint matrices defining the quadratic part for the product of state and control variables,

B_{op} : constraint history dependent vector of the device model.

B.2 Time Domain SCAQCF Measurement Model Description

The measurement model is derived from the above SCAQCF device model. The primary data that define a measurement are pointers and the measurement error. Specifically a measurement is defined as follows:

Measurement type: number 14 stands for actual TORQUE measurement;
number 15 stands for actual SPEED measurement;
number 16 stands for actual VOLTAGE measurement;
number 17 stands for actual CURRENT measurement;
number 24 stands for the virtual measurement;
number 25 stands for voltage pseudo measurement;
number 27 stands for current pseudo measurement;
number 28 stands for voltage derived measurement;
number 29 stands for current derived measurement;
Measurement standard deviation: standard deviation in metric unit
Measurement Terminal: the terminal numbers where this measurement comes from

For derived measurements, the following three definitions are required:
Measurement Ratio: the ratio of the derived measurement to the actual measurement
Measurement Number: from which actual measurement this derived measurement can be derived

All details about the measurement definition are shown in the next section.

From the above definition and the SCAQCF the measurement model is extracted in the following form. All the measurements from the device are listed on the left side of the equations.

$$\mathbf{y}(\mathbf{x},\mathbf{u}) = Y_{m,x}\mathbf{x} + \begin{Bmatrix} \vdots \\ \mathbf{x}^T F^i_{m,x}\mathbf{x} \\ \vdots \end{Bmatrix} + Y_{m,u}\mathbf{u} + \begin{Bmatrix} \vdots \\ \mathbf{u}^T F^i_{m,u}\mathbf{u} \\ \vdots \end{Bmatrix} + \begin{Bmatrix} \vdots \\ \mathbf{x}^T F^i_{m,xu}\mathbf{u} \\ \vdots \end{Bmatrix} + C_m$$

$$C_m = N_{m,x}\mathbf{x}(t-h) + N_{m,u}\mathbf{u}(t-h) + M_m I(t-h) + K_m$$

Measurement standard deviation: *sigma* (metric unit)

where:

$\mathbf{y}(\mathbf{x},\mathbf{u})$: measurement variables at both time t and time t_m, $\mathbf{y} = [\mathbf{y}(t), \mathbf{y}(t_m)]$

$\mathbf{x}$: external and internal state variables of the measurement model, $\mathbf{x} = [\mathbf{x}(t), \mathbf{x}(t_m)]$

$\mathbf{u}$: control variables of the measurement model, i.e. transformer tap, etc. $\mathbf{u} = [\mathbf{u}(t), \mathbf{u}(t_m)]$

$Y_{m,x}$: matrix defining the linear part for state variables,

$F_{m,x}$: matrices defining the quadratic part for state variables,

$Y_{m,u}$: matrix defining the linear part for control variables,

$F_{m,u}$: matrices defining the quadratic part for control variables,

$F_{m,xu}$: matrices defining the quadratic part for the product of state and control variables,

C_m : history dependent vector of the measurement model,

$N_{m,x}$: matrix defining the last integration step state variables part,

$N_{m,u}$: matrix defining the last integration step control variables part,

M_m : matrix defining the last integration step through variables part,

K_m : constant vector of the measurement model,

sigma : matrix defining the standard deviation in metric unit.

The measurement model should be constructed from the device model and the definition of the measurements. The measurements include actual measurements, pseudo measurements, virtual measurements and derived measurements. The definition of all the measurements are shown in the next section and the creation of the SCAQCF time domain measurement model of different devices are presented in the following Appendices.

B.3 Measurement Definition

This section shows how measurements are defined for the setting-less protection algorithm. There are four types of measurements: (1) actual measurement; (2) pseudo measurement; (3) virtual measurement and (4) derived measurement.

B.3.1 Actual Measurement

Actual measurements are the measurements which can be actually measured. For each actual measurement, the following information is provided:

Measurement type: number 14 stands for TORQUE measurement; number 15 stands for SPEED measurement; number 16 stands for VOLTAGE measurement; number 17 stands for CURRENT measurement
Measurement standard deviation: standard deviation in metric unit
Measurement Terminal: the terminal numbers where this measurement comes from

MeasurementType, 16
MeasStdDev, 600
MeasTerminal, 2, 3
MeasurementEnd
MeasurementType, 17
MeasStdDev, 5
MeasTerminal, 0
MeasurementEnd

Some typical actual measurements are given above. From the measurement type it is easy to know the first measurement is a voltage actual measurement. Its standard deviation is 600V. The voltage is measured between device terminal 2 and 3, i.e. $v_{meas} = v_2 - v_3$.

The second measurement is a current actual measurement. Its standard deviation is 5A. The current is measurement at device terminal 0, i.e. $i_{meas} = i_0$. The expression of i_0 could be obtained from the SCAQCF device model.

B.3.2 Virtual Measurement

Virtual measurements present the zeros on the left side of the internal equations. For each virtual measurement, the following information is provided:

Measurement type: number 24 stands for the virtual measurement
Measurement standard deviation: standard deviation in metric unit
Measurement Terminal: the device equation number where this measurement comes from

MeasurementType, 24
MeasStdDev, 0.0010000

MeasTerminal, 4
MeasurementEnd

A typical virtual measurement is given above. From the measurement type it is easy to know this measurement is a virtual measurement. Its standard deviation is 0.001. The value of this measurement is 0.0 and it is used for the 4thequation (start from 0th) of the device model.

B.3.3 Pseudo Measurement

Pseudo measurements are the measurements which are normally not measured, like the voltage or current at the neutral terminal. For each pseudo measurement, the following information is provided:

Measurement type: number 25 stands for voltage pseudo measurement; number 27 stands for current pseudo measurement
Measurement standard deviation: standard deviation in metric unit
Measurement Terminal: the terminal number where this measurement comes from

MeasurementType, 25
MeasStdDev, 0.10000
MeasTerminal, 3
MeasurementEnd
MeasurementType, 27
MeasStdDev, 0.10000
MeasTerminal, 3
MeasurementEnd

Some typical pseudo measurements are given above. From the measurement type it is easy to know the first measurement is a voltage pseudo measurement. Its standard deviation is 0.1V. The pseudo measurement is for the voltage at device terminal 3, i.e. $0 = v_3$.

The second measurement is a current pseudo measurement. Its standard deviation is 0.1A. The pseudo measurement is for the current at device terminal 3, i.e. $0 = i_3$. The expression of i_0 could be obtained from the SCAQCF device model.

B.3.4 Derived Measurement

Derived measurements are the measurements which can be derived from the actual measurements. For each derived measurement, the following information is provided:

Measurement type: number 28 stands for voltage derived measurement; number 29 stands for current derived measurement
Measurement standard deviation: standard deviation in metric unit
Measurement Terminal: the terminal numbers where this measurement comes from

Measurement Ratio: the ratio of the derived measurement to the actual measurement
Measurement Number: from which actual measurement this derived measurement can be derived

MeasurementType, 28
MeasStdDev, 600
MeasTerminal, 2, 3
MeasRatio, 1.0
MeasNumber, 0
MeasurementEnd
MeasurementType, 29
MeasStdDev, 5
MeasTerminal, 0
MeasRatio, 1.0
MeasNumber, 1
MeasurementEnd

Since the derived measurements come from the actual measurements, the standard deviation and the terminal information should be the same as the original measurement.

Some typical actual measurements are given above. From the measurement type it is easy to know the first measurement is a voltage derived measurement. Its standard deviation is 600V. This derived voltage measurement has the same value as the voltage measured between device terminal 2 and 3, i.e. $v_{dereived} = v_2 - v_3$.

The second measurement is a current derived measurement. Its standard deviation is 5A. This derived current measurement has the same value as the current measured at device terminal 0, i.e. $i_{derived} = i_0$. The expression of i_0 could be obtained from the SCAQCF device model.

B.4 Sparsity Based State Estimation Algorithm

Given the SCAQCF measurement model and input matrices, the next step is the formation of the system Jacobian matrix and measurement vectors. A suitable sparse matrix library is used in order to store sparse matrices and execute sparse matrix operations.

The estimation algorithm is based on the Gauss-Newton iterative algorithm.

$$X^{\upsilon+1} = X^{\upsilon} - \left(H^T W H\right)^{-1} H^T W \left(h(X^{\upsilon}) - Z\right)$$

At each time step of the estimation algorithm, the contributions of each measurement to the information matrix $H^T WH$ and the vector $H^T W(h(X^{\nu}) - Z)$ are computed. For example assuming that the ith measurement has the following generic form:

$$z_i = c_i + a_{i1} \cdot x_{i1} + a_{i2} \cdot x_{i2} \cdot x_{i3} + \eta_i$$

Then the Jacobian matrix's ith row will be:

$$\begin{bmatrix} 0 & \cdots & a_{i1} & \cdots & a_{i2}\cdot x_{i2} & \cdots & a_{i2}\cdot x_{i3} & \cdots & 0 \end{bmatrix}$$

The contribution of this row to the information matrix $H^T WH$ is the following:

$$\begin{bmatrix} 0 & \cdots & 0 & \cdots & 0 & \cdots & 0 & \cdots & 0 \\ \vdots & & \vdots & & \vdots & & \vdots & & \vdots \\ 0 & \cdots & w_i a_{i1} a_{i1} & \cdots & w_i a_{i1} a_{i2} x_{i2} & \cdots & w_i a_{i1} a_{i2}\cdot x_{i3} & \cdots & 0 \\ \vdots & & \vdots & & \vdots & & \vdots & & \vdots \\ 0 & \cdots & w_i a_{i1} a_{i2}\cdot x_{i2} & \cdots & w_i \left(a_{i2}\cdot x_{i2}\right)^2 & \cdots & w_i a_{i2}^2\cdot x_{i2} x_{i3} & \cdots & 0 \\ \vdots & & \vdots & & \vdots & & \vdots & & \vdots \\ 0 & \cdots & w_i a_{i1} a_{i2}\cdot x_{i3} & \cdots & w_i a_{i2}^2\cdot x_{i2} x_{i3} & \cdots & w_i \left(a_{i2}\cdot x_{i3}\right)^2 & \cdots & 0 \\ \vdots & & \vdots & & \vdots & & \vdots & & \vdots \\ 0 & \cdots & 0 & \cdots & 0 & \cdots & 0 & \cdots & 0 \end{bmatrix}$$

The contribution of the measurement to the vector $H^T W(h(X^\nu) - Z)$ is the following:

$$\begin{bmatrix} 0 \\ \vdots \\ w_i a_{i1} b_i \\ \vdots \\ w_i a_{i2}\cdot x_{i2} b_i \\ \vdots \\ w_i a_{i2}\cdot x_{i3} b_i \\ \vdots \\ 0 \end{bmatrix}, \quad where \quad b_i = c_i + a_{i1}\cdot x_{i1} + a_{i2}\cdot x_{i2}\cdot x_{i3} - z_i$$

Based on the above formulas, it's possible to calculate the non-zero contributions of each measurement formula and insert the contributions to the information matrix $H^T WH$ and the vector $H^T W(h(X^\nu) - Z)$ .Once the reading of all the measurements is completed and their contribution is added to the corresponding matrix and vector, the formation of the information matrix $H^T WH$ and the vector $H^T W\left(h(X^\upsilon) - Z\right)$ is completed and stored in sparse form using a suitable Spartrix Library.

The flow chart of object-oriented setting-less protection is shown in Figure B1 and Figure B2. All the SCAQCF component models are stored in the standard matrices which are introduced in section 3. In the initialization step, the program reads all the matrices,

calculates the linear part of the Jacobian matrix H and prepares the output COMTRADE channels. After the initialization, the dynamic station estimation based setting-less protection algorithm starts to check the health status of the component under protection. It performs the Chi-square test based on the calculated measurements from state estimation and the original measurements from the COMTRADE file. Meanwhile, bad data identification and operation limit monitoring are also done during the state estimation procedure. According to the result of Chi-square test, the protection logic decides the protection action for the component. The entire algorithm is real time and it iterates until no more measurements are available.

It is important to notice that most of device models are nonlinear, which means the Jacobian matrix needs to be updated at each iteration. To increase the speed, the linear part of matrix H can be pre-calculated at the SE initialization procedure. The program will identify whether the device model is linear or nonlinear. If the model is linear, then the Jacobian matrix H will stay constant. Otherwise, the program will only update the nonlinear part of H to minimize the calculation. The sparsity based state estimation algorithm mentioned before is applied and only the non-zero data will contribute to the information matrix $H^T WH$ and the vector $H^T W\left(h(X^\upsilon)-Z\right)$.

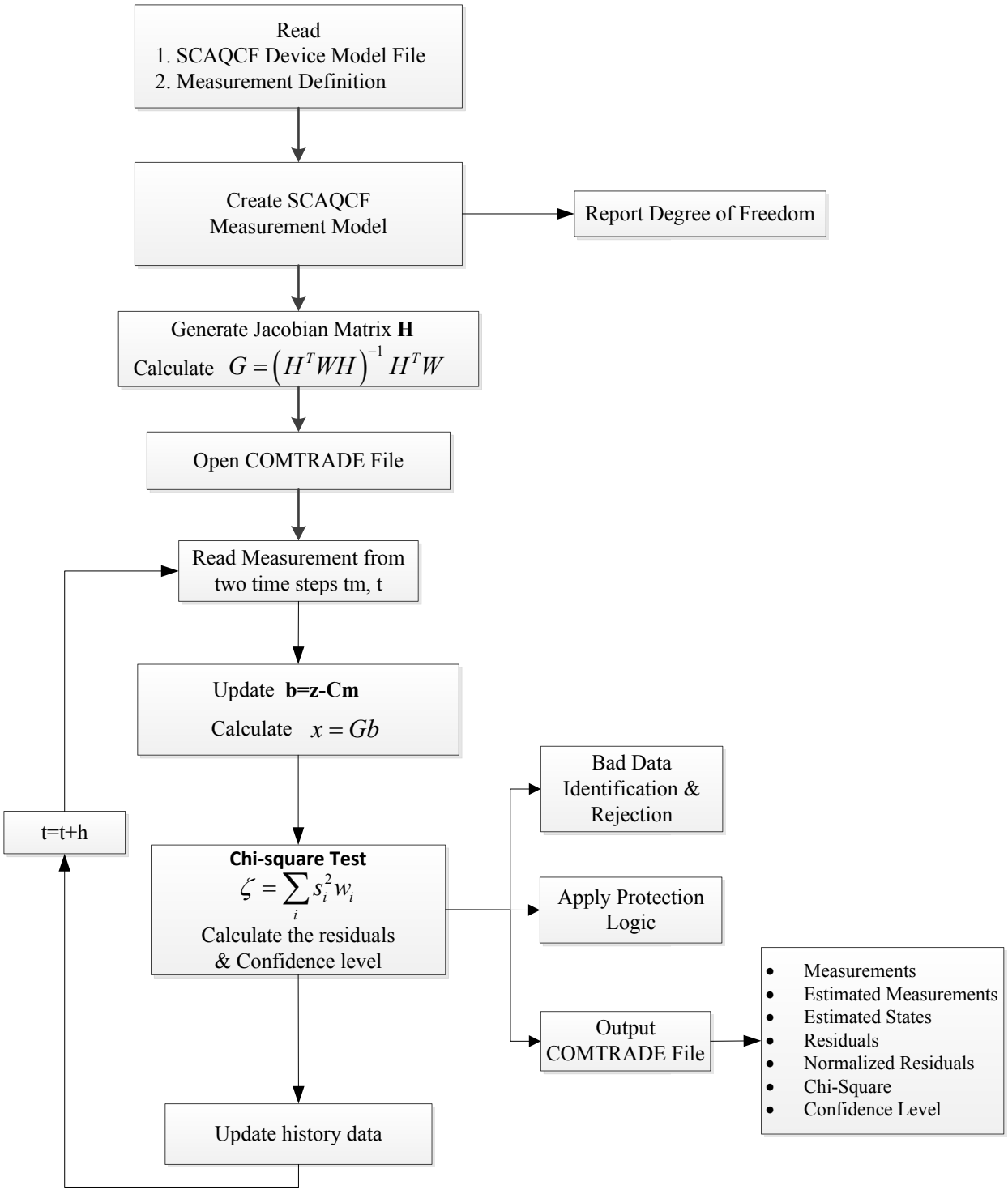

Figure B.2 Overall Flow Chart of Setting-Less Protection for Linear Case

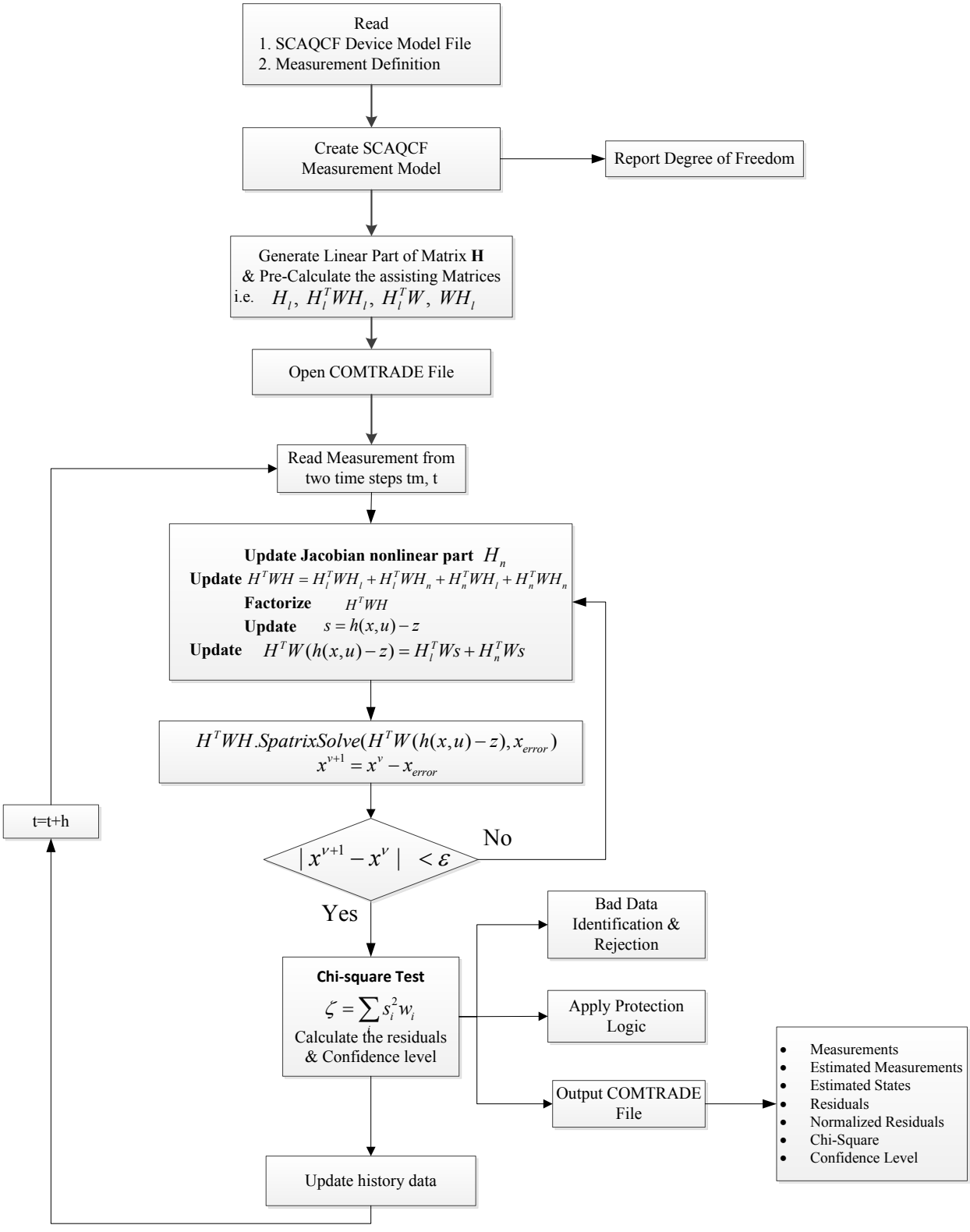

Figure B.3 Overall Flow Chart of Setting-Less Protection for Nonlinear Case

B.5 Frequency Domain SCAQCF Device Model Description

The frequency domain device model should be expressed in the generalized State and Control Algebraic Quadratic Companion Form (SCAQCF) as well. Compared with the time domain model, the frequency domain SCAQCF device model only has the states and control variables in the steady state. States in the frequency domain is usually expressed in the phasor format. Here in the SCAQCF model, each phasor is separated into real and imaginary parts for computation simplification. The frequency domain standard SCAQCF model is shown below:

$$\begin{Bmatrix} \mathbf{I} \\ \vdots \\ 0 \\ \vdots \end{Bmatrix} = Y_{eqx}\mathbf{X} + \begin{Bmatrix} \vdots \\ \mathbf{X}^T F_{eqx}^i \mathbf{X} \\ \vdots \end{Bmatrix} + Y_{equ}\mathbf{U} + \begin{Bmatrix} \vdots \\ \mathbf{U}^T F_{equ}^i \mathbf{U} \\ \vdots \end{Bmatrix} + \begin{Bmatrix} \vdots \\ \mathbf{X}^T F_{eqxu}^i \mathbf{U} \\ \vdots \end{Bmatrix} - B_{eq}$$

$$\mathbf{h}(\mathbf{X},\mathbf{U}) = Y_{opx}\mathbf{X} + Y_{opu}\mathbf{U} + \begin{Bmatrix} \vdots \\ \mathbf{X}^T F_{opx}^i \mathbf{X} \\ \vdots \end{Bmatrix} + \begin{Bmatrix} \vdots \\ \mathbf{U}^T F_{opu}^i \mathbf{U} \\ \vdots \end{Bmatrix} + \begin{Bmatrix} \vdots \\ \mathbf{X}^T F_{opxu}^i \mathbf{U} \\ \vdots \end{Bmatrix} - B_{op}$$

Scaling factors: *Iscale*, *Xscale and Uscale*

Connectivity: *TerminalNodeName*

$$subject\ to: \quad \mathbf{h}_{\min} \le \mathbf{h}(\mathbf{X},\mathbf{U}) \le \mathbf{h}_{\max}$$

$$\mathbf{U}_{\min} \le \mathbf{U} \le \mathbf{U}_{\max}$$

where:

$\mathbf{I}$: the through variables of the device model,

$\mathbf{X}$: external and internal state variables of the device model,

$\mathbf{U}$: control variables of the device model, i.e. transformer tap, etc.

Y_{eqx} : matrix defining the linear part for state variables,

F_{eqx} : matrices defining the quadratic part for state variables,

Y_{equ} : matrix defining the linear part for control variables,

F_{equ} : matrices defining the quadratic part for control variables,

F_{eqxu} : matrices defining the quadratic part for the product of state and control variables,

B_{eq} : constant vector of the device model,

Iscale : scaling factors for the through variables and zeros on the left side of the equations,

Xscale : scaling factors for the state variables $\mathbf{X}$,

Uscale : scaling factors for the control variables $\mathbf{U}$,

TerminalNodeName : terminal names defining the connectivity of the device model

$\mathbf{h}_{\min} \le \mathbf{h}(\mathbf{X},\mathbf{U}) \le \mathbf{h}_{\max}$: operating constraints,

$\mathbf{U}_{\min}, \mathbf{U}_{\max}$: lower and upper bounds for the control variables.

Y_{opx} : constraint matrix defining the linear part for state variables,

F_{opx} : constraint matrices defining the quadratic part for state variables,

Y_{opu} : constraint matrix defining the linear part for control variables,

F_{opu} : constraint matrices defining the quadratic part for control variables,

F_{opxu} : constraint matrices defining the quadratic part for the product of state and control variables,

B_{op} : constraint history dependent vector of the device model.

B.6 Frequency Domain SCAQCF Measurement Model Description

The frequency domain measurement model is derived from the above frequency domain SCAQCF device model. The primary data that define a measurement are pointers and the measurement error. Specifically a measurement is defined as follows:

Measurement type: number 14 stands for actual TORQUE measurement;
number 15 stands for actual SPEED measurement;
number 16 stands for actual VOLTAGE measurement;
number 17 stands for actual CURRENT measurement
number 24 stands for the virtual measurement;
number 25 stands for voltage pseudo measurement;
number 27 stands for current pseudo measurement;
number 28 stands for voltage derived measurement;
number 29 stands for current derived measurement
Measurement standard deviation: standard deviation in metric unit
Measurement Terminal: the terminal numbers where this measurement comes from

For derived measurements, the following three definitions are required:
Measurement Ratio: the ratio of the derived measurement to the actual measurement
Measurement Number: from which actual measurement this derived measurement can be derived

All details about the measurement definition are shown in the next section.

All the measurements from the device are listed on the left side of the equations.

$$\mathbf{Y} = Y_{mx}\mathbf{X} + \left\{ \begin{array}{c} \vdots \\ \mathbf{X}^T F_{mx}^i \mathbf{X} \\ \vdots \end{array} \right\} + Y_{mu}\mathbf{U} + \left\{ \begin{array}{c} \vdots \\ \mathbf{U}^T F_{mu}^i \mathbf{U} \\ \vdots \end{array} \right\} + \left\{ \begin{array}{c} \vdots \\ \mathbf{X}^T F_{mxu}^i \mathbf{U} \\ \vdots \end{array} \right\} + C_m$$

Measurement standard deviation: *sigma* (metric unit)

where:
$\mathbf{Y}$: measurement variables in the steady state,
$\mathbf{X}$: external and internal state variables of the component model,
$\mathbf{U}$: control variables of the component model, i.e. transformer tap, etc.

Y_{mx} : matrix defining the linear part for state variables,

F_{mx} : matrices defining the quadratic part for state variables,

Y_{mu} : matrix defining the linear part for control variables,

F_{mu} : matrices defining the quadratic part for control variables,

F_{mxu} : matrices defining the quadratic part for the product of state and control variables,

C_m : history dependent vector of the measurement model.

$sigma$: matrix defining the standard deviation in metric unit.

The frequency domain measurement model should be constructed from the frequency domain device model and the definition of the measurements. The measurements include actual measurements, pseudo measurements, virtual measurements and derived measurements. The definition of each measurement has already shown in Chapter 3.The creation of the frequency domain SCAQCF time domain measurement model are presented in Appendix B.

Appendix C: Multi-Machine System Potential Energy Computation

In this section, the methodology for deriving the expression of the power output of the generators in a multi-machine power system as a function of the units' rotor position δ is described. For the derivation, the following assumptions are made:

- The positive sequence model of the multi-machine power system will be used.
- The machines are represented by a constant voltage $E_i \angle \delta_i$ behind the generator impedance
- The loads in the system are represented as constant admittance loads

Consider the multi-machine power system in Figure C.1 with m buses, n of which represent generator buses.

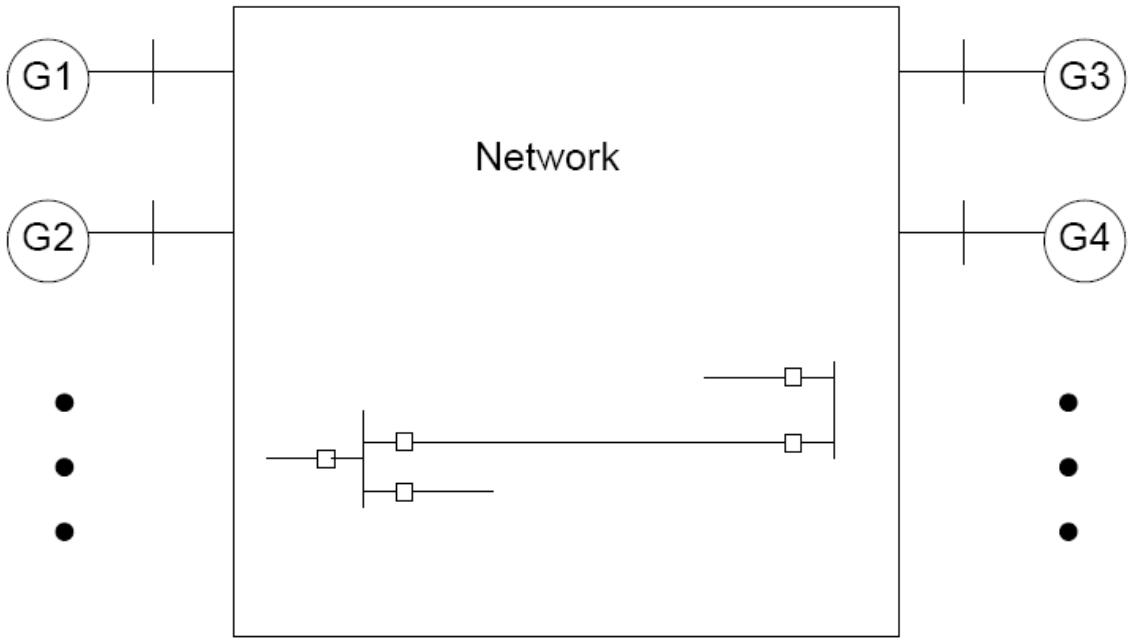

Figure C.4 Multi-Machine Power System

Upon converting the voltage sources into current sources and applying nodal analysis it holds that:

$$\begin{bmatrix} \frac{E_1 \cdot e^{\delta_1}}{j \cdot x'_{d1}} \\ \vdots \\ \frac{E_n \cdot e^{\delta_n}}{j \cdot x'_{dn}} \\ 0 \\ \vdots \\ 0 \end{bmatrix} = \begin{bmatrix} Y_{11} & \cdots & Y_{1n} & \cdots & Y_{1m} \\ \vdots & \ddots & \vdots & \ddots & \vdots \\ Y_{n1} & \cdots & Y_{nn} & \cdots & Y_{nm} \\ \vdots & \ddots & \vdots & \ddots & \vdots \\ Y_{m1} & \cdots & Y_{mn} & \cdots & Y_{mm} \end{bmatrix} \cdot \begin{bmatrix} \widetilde{V}_1 \\ \widetilde{V}_2 \\ \vdots \\ \widetilde{V}_m \end{bmatrix}$$

where Y is the admittance matrix of the system, that is the diagonal terms Y_{ii} are the self admittance terms, equal to the sum of the admittances of all devices incident to bus i, while the off-diagonal terms, Y_{ij}, are equal to the negative of the sum of the admittances connecting the two buses i and j.

The nodal equations can be written in compact form as follows:

$$\begin{bmatrix} I_G \\ 0 \end{bmatrix} = \begin{bmatrix} Y_{GG} & Y_{GN} \\ Y_{NG} & Y_{NN} \end{bmatrix} \cdot \begin{bmatrix} V_G \\ V_N \end{bmatrix}$$

where $I_G = \begin{bmatrix} \frac{E_1 \cdot e^{\delta_1}}{j \cdot x'_{d1}} & \cdots & \frac{E_n \cdot e^{\delta_n}}{j \cdot x'_{dn}} \end{bmatrix}^T$, $V_G = \begin{bmatrix} V_{G,1} & \cdots & V_{G,n} \end{bmatrix}^T$, $V_N = \begin{bmatrix} V_{N,(n+1)} & \cdots & V_{N,m} \end{bmatrix}^T$.

Expanding the matrix equations it holds that:

$$I_G = Y_{GG} \cdot V_G + Y_{GN} \cdot V_N$$
$$0 = Y_{NG} \cdot V_G + Y_{NN} \cdot V_N$$

The second equation can be solved for V_N yielding:

$$V_N = -Y_{NN}^{-1} \cdot Y_{NG} \cdot V_G$$

Substitution in the first equation and upon solution for V_G yields:

$$V_G = (Y_{GG} - Y_{GN} \cdot Y_{NN}^{-1} \cdot Y_{NG})^{-1} \cdot I_G$$

or equivalently:

$$\widetilde{V}_1 = \widetilde{a}_{11} \cdot e^{\delta_1} + \cdots + \widetilde{a}_{1n} \cdot e^{\delta_n}$$
$$\vdots$$
$$\widetilde{V}_n = \widetilde{a}_{n1} \cdot e^{\delta_1} + \cdots + \widetilde{a}_{nn} \cdot e^{\delta_n}$$

From the computed voltages the electric power can be computed as:

$$P_{e1} = \mathrm{Re}\left[\widetilde{V}_1 \cdot \left(\frac{E_1 \cdot e^{\delta_1}}{j \cdot x'_{d1}}\right)^*\right] = f_1(e^{\delta_2-\delta_1}, \cdots, e^{\delta_n-\delta_1}) =$$

$$A_1 + B_{1,2} \cdot \cos(\delta_2 - \delta_1) + C_{1,2} \cdot \sin(\delta_2 - \delta_1) + \cdots + B_{1,n} \cdot \cos(\delta_n - \delta_1) + C_{1,n} \cdot \sin(\delta_n - \delta_1)$$

$$\vdots$$

$$P_{en} = \mathrm{Re}\left[\widetilde{V}_n \cdot \left(\frac{E_n \cdot e^{\delta_n}}{j \cdot x'_{dn}}\right)^*\right] = f_n(e^{\delta_1-\delta_n}, \cdots, e^{\delta_{n-1}-\delta_n}) =$$

$$A_n + B_{1,n} \cdot \cos(\delta_1 - \delta_n) + C_{1,n} \cdot \sin(\delta_1 - \delta_n) + \cdots + B_{n-1,n} \cdot \cos(\delta_{n-1} - \delta_n) + C_{n-1,n} \cdot \sin(\delta_{n-1} - \delta_n)$$

A simple example of a two generator system shown in Figure C.2 follows next.

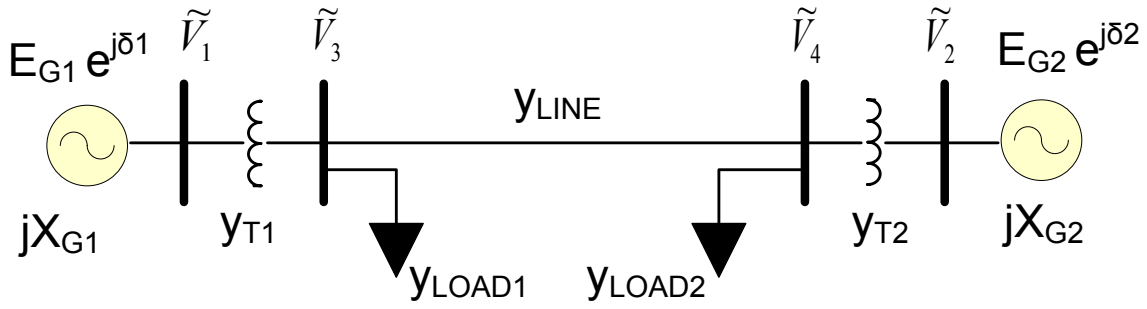

Figure C.5 Two Generator System - Potential Energy Computation Example

The nodal equations can be written in compact form as follows:

$$\begin{bmatrix} I_G \\ 0 \end{bmatrix} = \begin{bmatrix} Y_{GG} & Y_{GN} \\ Y_{NG} & Y_{NN} \end{bmatrix} \cdot \begin{bmatrix} V_G \\ V_N \end{bmatrix}$$

where: $I_G = \begin{bmatrix} \frac{E_1 \cdot e^{\delta_1}}{j \cdot x'_{d1}} & \frac{E_2 \cdot e^{\delta_2}}{j \cdot x'_{d2}} \end{bmatrix}^T$, $V_G = \begin{bmatrix} \widetilde{V}_1 & \widetilde{V}_2 \end{bmatrix}^T$, $V_N = \begin{bmatrix} \widetilde{V}_3 & \widetilde{V}_4 \end{bmatrix}^T$,

$$Y_{GG} = \begin{bmatrix} y_{G1} + y_{T1} & 0 \\ 0 & y_{G2} + y_{T2} \end{bmatrix}, \qquad Y_{GN} = Y_{NG} = \begin{bmatrix} -y_{T1} & 0 \\ 0 & -y_{T2} \end{bmatrix},$$

$$Y_{NN} = \begin{bmatrix} y_{T1} + y_{LINE} + y_{LOAD1} & -y_{LINE} \\ -y_{LINE} & y_{T2} + y_{LINE} + y_{LOAD2} \end{bmatrix}.$$

The voltages at the terminals of the generators are computed to be:

$$\widetilde{V}_1 = Y_{inv}(1,1) \cdot \frac{E_1 \cdot e^{\delta_1}}{j \cdot x'_{d1}} + Y_{inv}(1,2) \cdot \frac{E_2 \cdot e^{\delta_2}}{j \cdot x'_{d2}}$$

$$\widetilde{V}_2 = Y_{inv}(2,1) \cdot \frac{E_1 \cdot e^{\delta_1}}{j \cdot x'_{d1}} + Y_{inv}(2,2) \cdot \frac{E_2 \cdot e^{\delta_2}}{j \cdot x'_{d2}}$$

where $Y_{inv} = (Y_{GG} - Y_{GN} \cdot Y_{NN}^{-1} \cdot Y_{NG})^{-1}$

From the computed voltages the electric power can be computed as:

$$P_{e1} = \mathrm{Re}\left[\widetilde{V}_1 \cdot \left(\frac{E_1 \cdot e^{\delta_1}}{j \cdot x'_{d1}}\right)^*\right] = A_1 + B_{1,2} \cdot \cos(\delta_2 - \delta_1) + C_{1,2} \cdot \sin(\delta_2 - \delta_1)$$

$$P_{e2} = \mathrm{Re}\left[\widetilde{V}_2 \cdot \left(\frac{E_2 \cdot e^{\delta_2}}{j \cdot x'_{d2}}\right)^*\right] = A_2 + B_{2,1} \cdot \cos(\delta_1 - \delta_2) + C_{2,1} \cdot \sin(\delta_1 - \delta_2)$$